Author:
Barden, Lucy A

Title:
Synthesis and application of porous organic polymers for removal of pollutants from wastewater

Synthesis and application of porous organic polymers for removal of pollutants from wastewater

Lucy Barden

Supervisor

Professor Charl F. J. Faul

A dissertation submitted to the University of Bristol in accordance with the requirements for award of the degree of Master of Science by Research in the Faculty of Science

Submitted: 16/11/23

Word count: 26252

Acknowledgements

I'd like to thank Prof. Charl Faul for the opportunity to join his research group and undertake a project which has allowed me to gain valuable skills for my future career. I'd also like to say thank you to Charl for the continuous support, advice and, guidance given throughout this project.

I'd like to thank Dr. Ben Baker for all of his suggestions, help and optimistic encouragement throughout my research as well as providing many signatures for safety forms.

The entire Faul research group have been an enormous help to me during my research, from helping with problems in the lab to giving constructive criticism during presentations. But most of all being so welcoming and making coming into the lab a joy.

I'd like to thank my friends and family for their love and support throughout this process, without which I would be lost.

Authors declaration

I declare that the work in this dissertation was carried out in accordance with the requirements of the University's *Regulations and Code of Practice for Research Degree Programmes* and that it has not been submitted for any other academic award. Except where indicated by specific reference in the text, the work is the candidate's own work. Work done in collaboration with, or with the assistance of, others, is indicated as such. Any views expressed in the dissertation are those of the author

Signed: LABarden Date: 31/08/23

Abstract

Organic dyes and heavy metals, as waste products from industries such as: textile, leather, paper, pharmaceutical and food, can cause significant damage to the environment and human health through water pollution. Many developing countries rely on the textile industry for income and have little ability to combat those responsible for releasing toxic chemicals into the environment. Thus, there is a great need for a sustainable and economic solution for capturing water-based pollutants.

Adsorption has been shown to be an effective way of removing water-based contaminants due to the re-usability, high removal efficiency and low cost of adsorbents. Porous organic polymers (POPs) are a class of materials that typically possess high surface areas, chemical and thermal stability. The structures of POPs can be fine-tuned, which is why they have been so popular in a wide range of applications including water treatment, CO_2 capture and conversion, hydrogen storage and catalysis. Triazine-based POPs have been investigated and found to have favorable properties for the adsorption of water-based contaminants as the abundance of nitrogen atoms inherent in their structure can act as binding sites for target pollutants.

In this work triazine-based POPs have been synthesized and applied to the adsorption of organic dyes and heavy metals. Two synthetic routes have been explored using Buchwald-Hartwig cross-coupling and condensation polymerization reactions to yield porous materials with a high nitrogen content. Polymers were synthesized using different triazine cores and a comparison between the triazine-based POPs was made. An investigation into the hydrophilicity of the materials was undertaken to ensure effective interactions with the water-based pollutants were possible. Adsorption studies using a range of organic dyes and heavy metals were conducted and the adsorption mechanisms were deduced. The results of this work are promising for the adsorption of water-based pollutants produced by the textile industry.

List of Figures

Schemes

List of Tables

List of equations

List of abbreviations

United Nations (UN)

Sustainable development goal (SDG)

Chemical oxygen demand (COD)

Biological oxygen demand (BOD)

International Union of Pure and Applied Chemistry (IUPAC)

World Health Organisation (WHO)

Environmental Protection Agency (EPA)

United States (US)

Activated carbon (AC)

porous organic polymers (POPs)

Conjugated microporous polymers (CMPs)

Polymers of intrinsic microporosity (PIMs)

Porous aromatic frameworks (PAFs)

Covalent organic frameworks (COFs)

Covalent triazine frameworks (CTFs)

Brunaur-Emmett-Teller (BET)

Buchwald Hartwig cross coupling (BH coupling)

Bristol–Xi'an Jiaotong (BXJ)

Carbon dioxide (CO_2)

4,4',4''-(1,3,5-triazine-2,4,6-triyl)trianiline (TAPT)

5,5',5''-(1,3,5-triazine-2,4,6-triyl)tris(pyridine-2-amine) (TAPT-N)

Fourier-transform infrared (FTIR)

Ultraviolet-visible light (UV-Vis)

X-ray power diffraction (XRD)

Scanning electron microscopy (SEM)

Dibenzylideneacetone (dba)

2-dicyclohexylphosphino-2',4',6'-triisopropylbiphenyl (XPhos)

Dimethylformamide (DMF)

Sodium tert-butoxide (NaO*t*-Bu)

Trifluoromethanesulfonic acid (triflic acid)

Dimethyl sulfoxide (DMSO)

Tetrahydrofuran (THF)

Nuclear magnetic resonance (NMR)

Highest occupied molecular orbital (HOMO)

Lowest occupied molecular orbital (LUMO)

Methyl orange (MO)

Acid violet 7 (AV7)

Congo red (CR)

Methylene blue (MB)

Mass adsorbed per unit mass of adsorbent at equilibrium (q_e)

Acid dissociation constants (pKa)

Isoelectric point (IEP)

Contents

1 Introduction

1.1 Water pollution

Water is one of the most essential components of life on earth. We need water for hydration, sanitation, growth of crops and livestock. Additionally, water is vital for the sustainment of almost all ecosystems on the planet. The effects of growing population, urbanization, agriculture and, industry has caused immense stress on our water sources.[1] It is no surprise that the pollution of our waterways is a major concern, with over 1000 people dying every day as a result of unsafe drinking water.[2] The United Nations (UN) has set out 17 sustainable development goals (SDGs) to address global issues such as poverty, education and hunger. Clean water and sanitation is number 6 of the 17 goals indicating water pollution is one of the most important environmental issues we face in the 21st century.[3] Water pollution is the release of substances into our waterways; rivers, lakes, oceans, estuaries and subsurface groundwater to the extent that these substances interfere negatively with the ecosystems and the use of such water.[4] The contamination of our waterways from pollutants such as oil, radioactive waste, toxic chemicals, organic waste, fertilizers, biological contaminants, plastics and other solid waste can have drastic consequences for all those using the contaminated water.[5,6] Water pollution may come

Figure 1: Sources of water pollution. [2,4]

from a point source in which the origin of the pollutants can be identified as originating from a single point of discharge, such as a pipe from a factory.[7] Pollution may also come from a wide and undefined area, a non-point source, for instance when it rains there is water runoff from roads containing oil, tire rubber particles and dog waste that may enter sewage systems, rivers, lakes and seas.[8] It is perhaps predictable that it is easier to control wastewater coming from a point source as a filtration or other treatment system may be put in place to remove pollutants. On the other hand, a dispersed source of pollution is much harder to control and treat in the correct way as the polluted water may come from a variety of sources and enter waterways at different points. Figure 1 identifies different origins of point and dispersed source pollution.

The UN SDG 6.3 aims to "improve water quality by reducing pollution, eliminating dumping and minimizing release of hazardous chemicals and materials, halving the proportion of untreated wastewater and substantially increasing recycling and safe reuse globally".[9] In 2020, 5.8 billion people used safely managed drinking services, where water is available when needed on premises and is free of faecal matter and chemicals. Out of the remaining 2 billion, 368 million people were taking water from unprotected springs and wells, whilst 122 million people were collecting untreated groundwater from rivers, lakes, streams and ponds.[10] Evidently there is still a significant amount of work to be done to ensure safe drinking water universally. These differences in clean water accessibility are often attributed to social and economic differences and typically less economically developed countries have less access to safely managed drinking services.[11,12]

Contamination of water can also come from natural sources. The natural weathering of rocks and volcanic activity releases species that have been trapped in the earth's crust into waterways.[13,14] Inorganic species such as Ca^{2+}, F^- and SO_4^{2-} occur naturally, though human activity such as burning coal, use of road salts and release of sewage can increase their concentrations in the environment.[15–17] Some organic contaminants are biodegradable and can be broken down by microorganisms, these contaminants often originate from fats, proteins, carbohydrates and oils. [18] The process of breaking down these contaminants requires oxygen to be available for the microorganisms to respire,[19] thus depleting the levels of oxygen in the water and reducing the amount of oxygen available to ecosystems.

1.1.1 Dye pollution in water

Water pollution from industries such as textiles, tanning, printing, food and, pharmaceuticals cause a variety of organic dyes to be released into our waterways. It has been reported that the textile industry is the 3rd largest user of fresh water in the world, with 100 tons/year of dyes and pigments released into waste streams, requiring treatment before being released into the environment.[20–22] There are many types of dyes used in these industries for a variety of different purposes and they can be classified based on their structure and applications, summarized in Table 1.

Table 1: Types of dyes used in the textile industry.[23,24]

Dye type	**Structural features**	**Properties**
Direct	Sodium salts of sulfuric or carboxylic acids. Chromophore group is azobenzene.	Water soluble, anionic, dying process requires electrolysis and alkaline conditions, mostly used to dye cellulose.
Reactive	Typically contain azo unit. Halogen reactive group responsible for forming covalent bonds with dyestuff.	Bind to textiles using covalent bonds. Water soluble, anionic, dying process requires electrolysis and alkaline conditions, used to dye cotton.
Acid	Sulfuric or carboxylic salts, anionic group responsible for colour.	Very water soluble, anionic, acidic conditions needed, used to dye protein fibers.
Basic	Salts of organic bases, cationic group responsible for colour.	Cationic, soluble in alcohol not water, weakly acidic conditions needed, used to dye jute and acrylic.
Vat	Structure consists of keto group.	Natural colouring, made water soluble by vatting, vatting needs alkaline conditions, used for dying denim.
Sulphur	Similar to vat dyes, contains a disulfide linkage.	Reducing agents needed to make water soluble, alkaline conditions and oxidation needed, used to dye cotton black and brown colours.
Disperse	Mostly substituted azo, diphenylamine or anthraquinone compounds. Low molecular weight, non-ionic.	Only slightly water soluble, used as a dispersing agent for dying man made hydrophobic thermoplastic fibers.
Azoic	Mono or bis azo compounds.	Water insoluble, to produce colour they need coupling compounds, coupling compounds and azo group defines colour.
Mordant	Inorganic metal present in structure, mainly chromium.	Soluble in cold water, produce dark colours, no preference for specific materials.

Due to the sheer mass of water needed in the dying process, it is no wonder that the textile industry is a main contributor of effluent wastewater. The World Bank has estimated 17-20% of industrial wastewater is generated from dyeing and finishing treatments given to fabrics.[25]

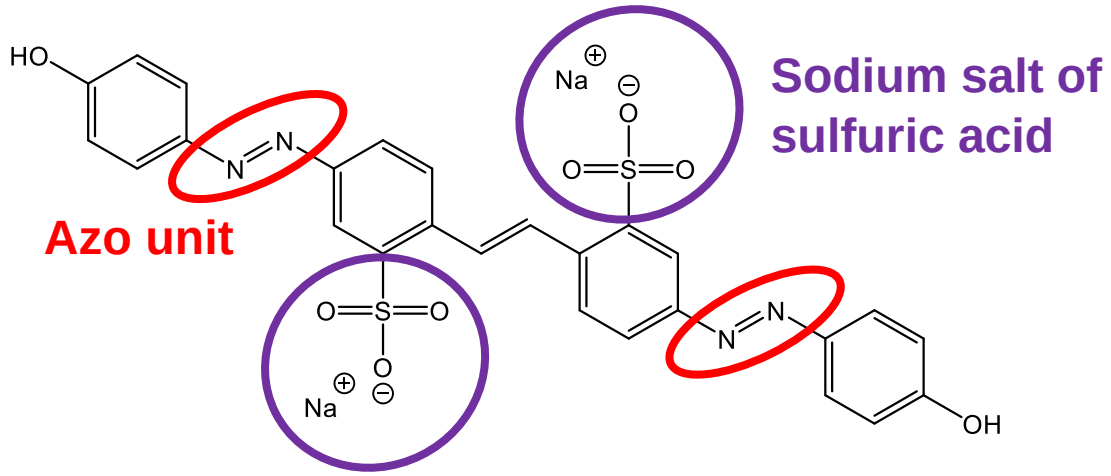

Figure 2: Brilliant yellow dye structure.[225]

Azobenzene dyes have vivid colour and are some of the most important and widely used dyes in industry, making up 60-70% of all dyes used.[23,26] The structure of these dyes can vary greatly; containing single or multiple azo units as well as the ability to alter the structures with amino-, chloro-, nitro-, carboxyl- and, hydroxyl groups. [27] Figure 2 shows the structure of a typical azo dye: Brilliant yellow. Generally, azo dyes have a chemical structure of R-N=N-R' with the R groups representing phenyl or naphthyl rings usually in combination with sodium salts of carboxylic or sulfuric acids.[28] Broadly used as they are cheaply and easily synthesized, are chemically stable and have long shelf lives.[29] However, this class of dye can have severe effects on both humans and aquatic life if released into the environment as they are not biodegradable.[30] Many azo dyes are toxic, carcinogenic and mutagenic, furthermore, the products from the dyes breaking down, such as aromatic amines, can be just as harmful if not more so.[31] The dyes can absorb light whilst in water severely reducing light available to ecosystems and inhibiting the photosynthesis of plants.[32] Additionally, the toxic chemicals may build up in fish and other marine life, further polluting ecosystems and the food chain.[33] Polluted water may be used for irrigation of farmland spreading toxicities

to crops and livestock.[34] Consequently, human and animal consumption of toxic chemicals increases and can cause severe health problems.[35]

Figure 3: River in Bangladesh polluted from dye wastewater. [36]

In 2019 three rivers were declared biologically dead in Bangladesh due to wastewater from textile factories being released into the rivers without proper treatment; an example can be seen in Figure 3. [36] The sources of water for the local people have become too polluted to drink or use in any way, but for many these rivers are the only source of water available. Bangladesh is one of the world's largest producers of clothing, second to China, thus the industry is a main source of income for the country contributing over 80% of export revenue.[37,38] However, the pollution produced by the dyeing of fabrics must be addressed for the survival of the people who live there. Textile industries have been declared as "red industries" by environmental governing bodies in Bangladesh, meaning waste produced must be monitored and correctly treated.[39] Unfortunately, lack of proper enforcement and high costs of waste treatment has meant these regulations have not had the desired impact on the industry and the waste it produces.[40]

In addition to the dye pigments being released into waterways, many other harmful species are released by the textile industry as part of the wastewater streams. Typical wastewater may be of high pH and salinity and contain suspended solids, heavy metals, species of high chemical oxygen demand (COD) and biological oxygen demand (BOD).[41] These additional pollutants in the wastewater are responsible for further negative impacts on the environment. Release of heavy metals into the environment poses a significant threat due to their high toxicity and ability to be absorbed by soil thus, posing serious health concerns to humans and wildlife.[42]

1.1.2 Metal pollution in water

Metals occur naturally as part of the earth's crust and do not biodegrade. Metals are therefore present in soil and water, and we are exposed to them through consumption of food and water. Metals such as zinc and magnesium are essential trace elements in the body. It's important to have the right levels of these metals otherwise health issues such as stunted growth may and neurological disorders may occur.[43] However, consuming too high a concentration of metals, in particular heavy metals, can cause severe health problems as described in Table 2. The International Union of Pure and Applied Chemistry (IUPAC) have questioned the meaningfulness of the term 'heavy metal' as it has been vastly overused in both literature and legislative policy describing metals or metalloids as having high atomic density and toxicity, however, not all are toxic and some that are toxic do not have high atomic densities. Consequently, many different elements and compounds can fall into this category and the term has little real meaning.[44] However, for the purpose of this study we can define heavy metals as metals or metalloids with relatively high atomic weight and densities that are capable of causing toxicity in the environment.[45,46] These include but are not limited to: chromium, mercury, lead, cadmium and, arsenic. The metals listed are some of the most toxic and dangerous metal ions as they can cause detrimental impact to our ecosystems, cause serious damage to human health and in some cases death.[47,48] Table 2 gives a range of heavy metals, their effects on humans and, their exposure limit.

Table 2: Examples of heavy metals and their effects on humans.[46,49,50]

Metal	**Source**	**Effects on humans**	**Exposure limits**
Chromium	**Food:** Meats, vegetables, grains, fruits, shellfish. **Other:** Tanning and textile industry, metal production, electroplating, tobacco smoke.	Oral intake of Cr (VI): nausea, diarrhea, liver damage, gastrointestinal ulcerations, death (1-3 g consumed). Inhalation of Cr (VI) can lead to more severe effects: cancer, bronchitis, liver and kidney disease, chrome holes.	**WHO:** 0.05 mg/L drinking water quality guidelines for total chromium. **EPA:** 0.1 mg/L maximum contaminant level for total chromium.
Manganese	**Food:** Spinach, herbs, nuts, olive oil, rice, grains, oysters. **Other:** Mining,	Adverse effects on the nervous system. Symptoms similar to Parkinson's disease: tremors, anxiety,	**WHO:** 0.4 mg/L drinking water quality guidelines. **EPA:** 1 mg/L over 1-10 day period, should not

	agriculture, soil, fertilizer, dump sites.	dystonia, discoordination of movement.	exceed 0.3 mg/L over lifetime.
Cobalt	**Food:** Cheese, chocolate, butter, meat. **Other:** Paint manufacturing, mining, tanning, nuclear power plant, electroplating.	Skin and respiratory issues, congestion, pneumonia, nausea and vomiting, liver disorders. Most adverse effects from inhalation.	**WHO:** no data given. **EPA:** 1.3 mg/L limit for safe drinking water.
Nickel	**Food:** Beans, cocoa, tea, oats, rye, peas, nuts, lentils, soy products. **Other:** Battery production, alloys, nickel planting.	Asthma, heart disorders, increases possibilities of cancer, allergic reaction.	**WHO:** 0.02 mg/L drinking water quality guidelines. **EPA:** 0.1 mg/L drinking water threshold.
Copper	**Food:** Liver, dark chocolate, leafy greens, seeds, nuts, lobster. **Other:** Pipe erosion, battery production.	Wilson's disease, metal fever, kidney disease, anxiety, restlessness, death.	**WHO:** 1.3 mg/L limit for drinking water consumed. **EPA:** 1.3 mg/L drinking water threshold.
Arsenic	**Food:** Cereals, meat, fish, poultry, dairy products. **Other:** Volcanic activity, drugs, mining, textiles, paints, agriculture.	Nerve damage, brain damage, lung irritation, damage to DNA, infertility.	**WHO:** 0.01 mg/L drinking water threshold. **EPA:** 0.05 mg/L drinking water threshold.
Cadmium	**Food:** Mushrooms, shrimp, dried seaweed, shellfish, liver. **Other:** Alloys, paints, batteries, metal smelting, fertilizers.	Psychological disorders, cancer, impairment of DNA, gastrointestinal disorders infertility.	**WHO:** 0.003 mg/L drinking water quality guidelines. **EPA:** 0.04 mg/L over 10 days (in youths), 0.005 mg/L over a lifetime.
Mercury	**Food:** Mushrooms, seafood. **Other:** Mining, volcanic activity, tanning, electroplating.	Damage to DNA, Down's syndrome, damage to reproductive system, Minamata disease.	**WHO:** 0.001 mg/L drinking water quality guidelines for all forms of mercury. **EPA:** 0.002 mg/L drinking water threshold for inorganic mercury.
Lead	**Food:** Red meat, fruit, red wine, vegetables, grains, seafood. **Other:** Batteries, cable covers, paint, glass, lead extraction, wielding.	Miscarriages, nerve damage, iron deficiency, stillbirths, sperm damage, altered brain development in children.	**WHO:** 0.01 mg/L drinking water quality guidelines. **EPA:** 0.015 mg/L drinking water action level.

Heavy metal pollution can come from a range of industries such as mining, dyeing and, agriculture.[51,52] Heavy metals such as chromium, zinc, nickel, copper and, lead are used to produce colour pigments in textile dyes.[53] The United States (US) Environmental Protection

Agency (EPA) has listed these metals along with mercury and lead as priority pollutants.[54] In addition, metals such as iron, cadmium and, manganese have also been found in textile effluents in China, Pakistan, Ethiopia and Bangladesh.[54]

Similar to the dye pollution discussed in Section 1.1.1, these non-biodegradable substances remain in the environment for long periods of time and can cause waterways to become polluted, in turn polluting aquatic life, soil, plants, crops and, livestock. Once again, poverty in combination with legislative and enforcement issues are at the heart of the problem. Therefore, a solution needs to be found: one that is effective, affordable and easily applied under local conditions.

1.1.3 Methods for treating textile wastewater

There are many methods used to treat textile effluents for pollutants: in industry there is usually a long treatment process involving multiple steps. These steps involve the removal of solids, suspended solids, dissolved solids, organic matter, microorganisms, species of BOD along with heavy metals, nitrogen and phosphorous.[55] This lengthy process produces sludge containing heavy metals amongst other pollutants that then require further treatment before it can safely be released.[56]

Coloured dyes and pigments are not treated effectively by conventional methods thus, biological, chemical and physical processes are used to remove the colour from textile effluents.[57]

Biological treatment involves the use of microorganisms such as algae, fungi, yeast, and other bacteria to decolour textile waste by biochemical and biosorption processes.[58] These methods are seen as eco-friendly having benefits such as lower cost and reduced production of sludge and hazardous waste.[59] A wide range of microorganisms can process dyes such as rhodamine B, reactive red 120, orange G and more through biosorption or biodegradation.[60–62] However, bacterial degradation and the conditions needed for the microorganisms to function limit the application of biological treatments. [63] Factors affecting bacterial degradation include pH, temperature, oxygen, concentration of nitrogen and carbon, dye concentration and structure.[64]

A variety of chemical techniques can also be used to treat textile wastewaters: oxidation, ozonation, electrochemical and, photochemical, to name a few.[65] Broadly, these methods work to cleave the bonds in the dye structure to produce either carbon dioxide and water or small organic molecules that can be further processed. [66] Though effective, most chemical methods are costly, require specialist equipment and high energy.[67]

Physical processes are widely used methods to treat textile effluents. A variety of membrane filtration processes can be used depending on the nature of the wastewater. These methods include nanofiltration, reverse osmosis, microfiltration and ultrafiltration.[68] Though these filtration methods can be effective, waste material builds up on the surface requiring removal and they can be prone to blockage from species present in the wastewater.[69] In recent years, adsorption has been recognized for its effectiveness in

removing a wide range of contaminants, and the ability of adsorbents to be reusable and of low cost.[70] Adsorption is a surface phenomenon based on the transfer of substances from liquid or gaseous phase onto a solid. The adsorption process is most commonly described as physisorption or chemisorption. Physisorption is a reversible process that involves weak forces of attraction between the adsorbent and adsorbate such as, hydrogen bonding, π-π stacking and dipole-dipole interactions. Chemisorption is an irreversible process involving valence forces and electronic orbitals and includes covalent bonding, complex formation, chelation and redox reactions.[71]

Many different materials can be used as adsorbents, both natural and manmade. Natural adsorbents like clay and zeolites are porous in nature and have surface properties capable of interacting and adsorbing dyes.[72] There has been much research into using agricultural/industrial waste as low cost adsorbents,[73] for instance, sawdust is readily available from the timber industry and has been found to remove dyes from textile waste.[74] Activated carbon (AC) is perhaps the most widely used adsorbent in the industry due to its high surface area and microporous nature.[75] Though commercially available, AC can be expensive; researchers are exploring low-cost AC that can be made from natural products such as banana pith, corn cobs and, orange peel.[76–78] Specifically, coconut shells have been utilized to produce AC and adsorb dyes from water.[79] However, unmodified AC has little selectivity towards target pollutants and possess problems with regeneration and disposal.[70,80] Synthetic porous organic polymers (POPs) have emerged as a new class of material that can be finely tuned for the adsorption of specific pollutants.[81] Many of these materials can adsorb and desorb their target pollutants from the surface making the materials re-usable and thus more sustainable.[82]

1.2 Porous polymers

1.2.1 Porous organic polymers

Porous materials have gained considerable interest over recent years owing to their exciting properties and range of applications. According to the IUPAC porous materials can be categorized based on their pore widths: micropore 2 nm or less, mesopore 2-50 nm and, macropore 50 nm or more.[83] Porous materials can be divided into three different categories as shown in Figure 4: organic porous materials, inorganic porous materials and hybrid porous materials. Organic porous materials have strong covalent bonds connecting organic building blocks creating complex 2D and 3D polymeric networks that may be amorphous or crystalline. By altering the starting materials, synthetic conditions and reaction types, these organic materials can be engineered to produce materials with different structural and porosity properties.[84] Inorganic porous materials include silica,[85] natural and synthetic zeolites,[86] and clays[87] and are used in size-exclusion filtration and catalysis as well as adsorption. The materials often have high surface areas and contain a variety of cations and anions including but not limited to Si^{4+}, AL^{3+}, O^{2-}. Though inorganic porous materials are generally cheap and readily available, it is difficult to alter their structural and chemical properties for specific applications. Activated carbon (AC) can also be classed as an inorganic porous material. AC is an amorphous material often with very high surface areas and is sourced from coal, wood and coconut shells. Because of its high surface area, AC is classed as an excellent adsorbent and is used in many water and air filtration systems.[88] Though AC is widely used, there are issues with the selectivity, re-usability and disposal of the material. Hybrid porous materials are composed of both organic and inorganic species to create a porous network. Metal organic frameworks (MOFs) contain metal centers connected by organic ligands to create these hybrid porous materials. Physical and chemical properties of MOFs may be modified by using different metal centers and organic ligands. Though MOFs are known for their high surface areas and tunability, they have issues with stability and may use expensive and toxic metals.[89]

This work will focus on organic porous materials also referred to as porous organic polymers (POPs). Generally, POPs are porous in nature with high surface areas, are tunable, chemically and thermally stable and, contain light atoms (O, C, H, N).[90] Types of POPs can be categorized based on their surface properties as well as their physical and chemical

composition: conjugated microporous polymers (CMPs),[91] polymers of intrinsic microporosity (PIMs),[92] porous aromatic frameworks (PAFs),[93] covalent organic frameworks (COFs) and covalent triazine frameworks (CTFs).[94] These types of materials can be tuned in the synthetic process to yield polymers capable of specific tasks including, water purification,[95] gas capture and conversion,[96] catalysis and energy storage.[97,98]

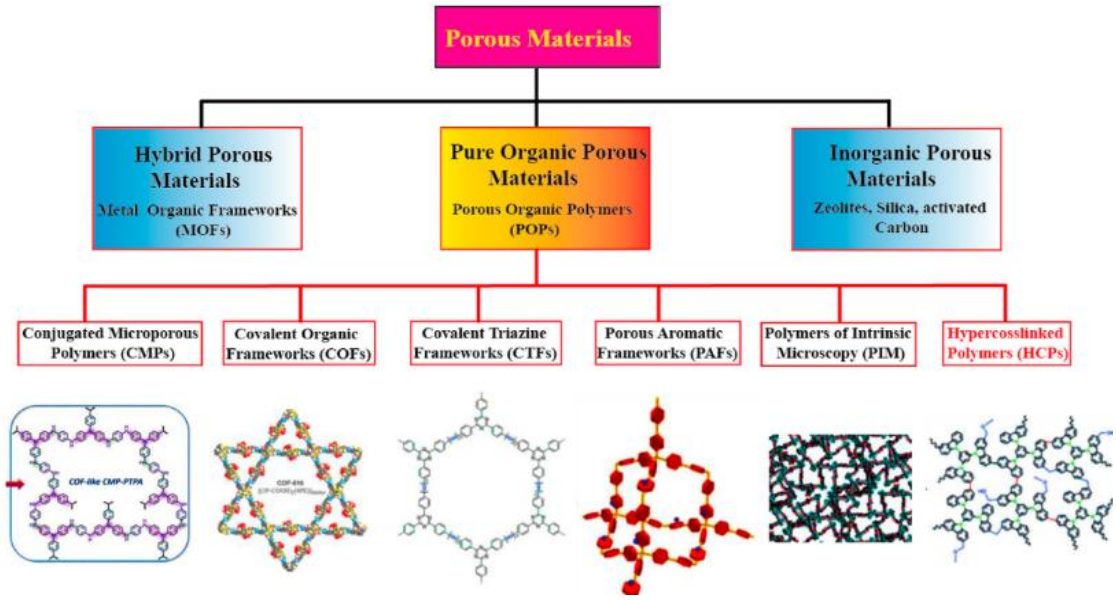

Figure 4: Types of porous materials. [226]

1.2.2 Conjugated microporous polymers

As the name suggests, CMPs are microporous in nature and have alternating double and single bonds to form their conjugated structures. The first CMP was reported in 2007 by Cooper et al. using a Sonogashira-Hagihara cross coupling reaction, achieving a Brunaur-Emmett-Teller (BET) surface area of 834 m^2 g^{-1}.[99] Since then CMPs have received increasing attention from researchers, producing materials with surface areas of over 1000 m^2 g^{-1}.[100] The ability to finely tune the porosity and functionality of these materials along with their conjugated properties makes CMPs incredibly important to the field of functional materials. There are many reactions that are capable of yielding CMPs including Buchwald Hartwig cross coupling (BH coupling),[101] Sonogashira-Hagihara cross coupling,[102] Suzuki coupling[103] and the Heck reaction to name a few. [104] Generally, a "core" molecule with C_3, C_4 or C_6 symmetry is reacted with a "linker" molecule with C_2, C_3 or C_4 symmetry to yield the corresponding 3D polymeric network.[105] Figure 5 gives an overview of the different synthetic routes capable of yielding CMPs.

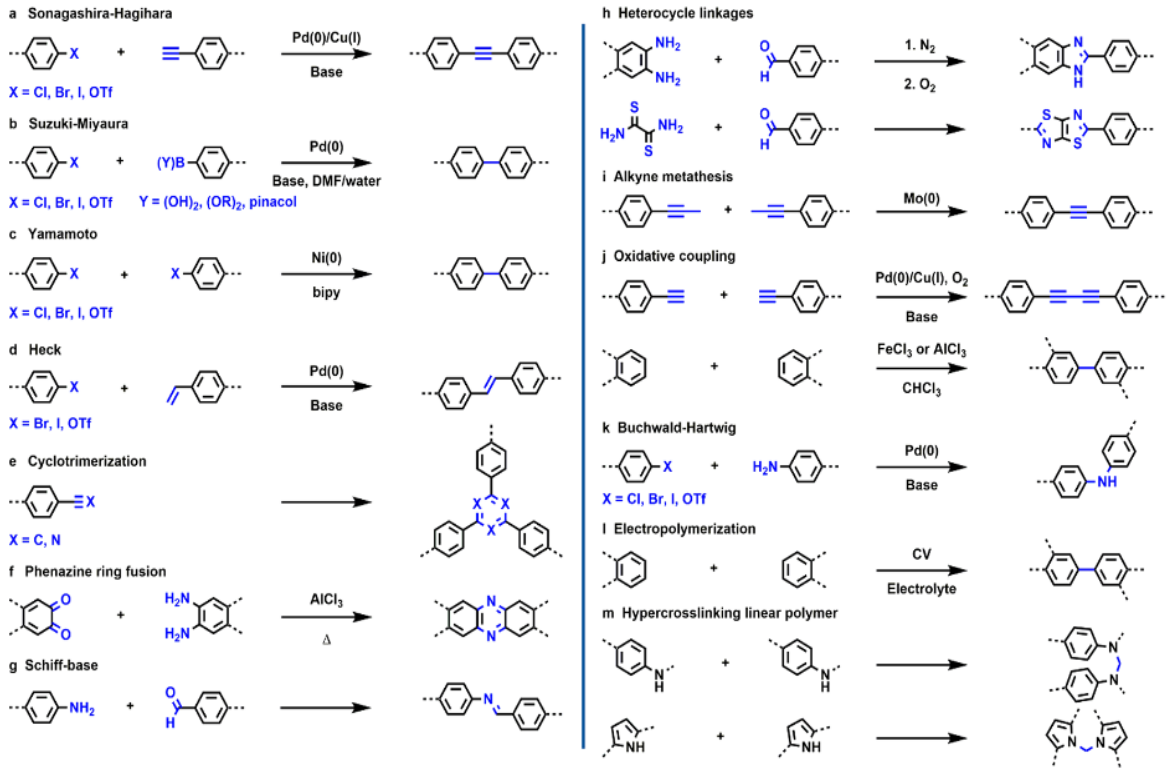

Figure 5: Different synthetic routes to yield CMPs. [227]

The vast possibilities of “core” and “linker” molecules that may be used to create CMPs is one reason why the structures of the polymers are highly tunable. Additionally, post-synthesis modification possibilities can bring new functional properties to the materials. In 2018 Liang et al. reported a charged polymer through post synthetic methylation of CMP-PM. Though this process reduced the BET surface area from 416 m^2g^{-1} to 241 m^2g^{-1}, the charged sites allowed the polymer to rapidly adsorb anionic dyes from water.[106] Porosity properties can be tuned by the monomers used, the monomer ratios and reaction conditions.[107,108] Work by Faul et al. has shown the ability to control porosity properties using the Bristol–Xi’an Jiaotong (BXJ) method. The BXJ method was introduced to tune and improve the surface areas and pore volumes of CMPs synthesized via BH coupling. The salts used in the BXJ method can tune the Hansen solubility parameters of the solvents used, potentially improving the ability of the solvent to interact with growing polymer structures (solute), leading to better control over the reaction.[109]

One of the most significant properties of CMPs is their conjugated backbone, responsible for the semi-conductive and luminescent properties they possess.[110,111] A high concentration of micropores and high chemical stability, means CMPs have a wide scope of applications, in particular: carbon dioxide (CO_2) capture and conversion,[112] photochemical and heterogeneous catalysis,[113,114] energy storage,[115] hydrogen evolution,[116] chemical capture and chemo-sensing.[117,118]

As CMPs are largely hydrophobic, due to their highly conjugated structures, the area of water treatment has received relatively little attention.[119] However, in recent years CMPs have been shown to remove both organic and inorganic pollutants from water. It has been shown that superhydrophobic CMPs are effective in removing other hydrophobic elements such as oil and organic solvents from water.[118] Deng et al. created a perfluorous CMP with a BET surface area of 901 m^2g^{-1} that demonstrated the ability to adsorb metal ions, dyes and, organic solvents from water.[120] It is evident that incorporating electronegative elements or charged sites into the structure of the materials can encourage interactions with target pollutants.[121,122]

1.2.3 Triazine-based polymers

Trimerization reactions have been used to create starting materials for the synthesis of porous materials as well as the synthesis of covalent triazine frameworks (CFTs) themselves.[123,124] The term CFT was first used by Thomas et al. in 2008 to describe CFT-1, a crystalline porous material with a surface area of 791 m^2/g, synthesized by the trimerization of aromatic nitriles under isothermal conditions. [125] Since then, CFTs have been synthesized by superacid catalyzed[126] and phosphorous pentoxide catalyzed synthesis methods,[127] Friedel-Craft coupling[128] and amidine-based polycondensation.[129] CFTs have characteristics of both CMPs and COFs, they are generally synthesized with the aim of having a crystalline structure. However, the reaction conditions used can often yield polymers with a more amorphous nature.[130] In addition, the nature of the monomers and the type of reaction often yields conjugated polymer networks. Usually CFTs have high surface areas, excellent thermal and chemical stability, with strong covalent C=N bonds and an inherently high nitrogen content.[131,132] Owing to these properties CTFs are advantageous in applications such as energy storage,[133] iodine capture[134] and H_2 storage.[135]

CTFs have excellent stability in water and have been used for water purification processes via adsorption to remove heavy metals,[136] organic dyes[137] and pharmaceutical waste.[138] The adsorption of these pollutants can also be enhance by photocatalytic properties of the CTF materials.[139] In particular, CFT-1 has been synthesized from 1,4-dicyanobenzene multiple times to explore its potential applications in water purification. In 2018 Ahmad and Iqbal et al. synthesized CFT-1 with a BET surface area of 490 m^2/g and showed its capacity to adsorb Cd^{2+} ions from water. The research highlights the importance of electrostatic interactions and external factors such as temperature in the adsorption process.[136] Zheng and Xu et al. synthesized CFT-1 and CFT_{DCBP} with BET surface areas of 782.44 m^2/g and 1745.45 m^2/g respectively. In 2017 the pair investigated the adsorption of antibiotics tylosin and sulfamethoxazole using CFT-1 and CFT_{DCBP}. The results indicated effective adsorption and selectivity due to π-π and Lewis acid-base interactions of the CFTs with the antibiotics. While the differences in size of the antibiotic molecules and the pore sizes of the CTFs are identified as important features in the selective adsorption of the antibiotics.[140] A few years later, in 2020 Zheng and Xu et al. investigated the removal of three different organic dyes (methylene blue, methyl orange and, chrysophenine G) using CTF-1 and CFT_{DCBP}. The study

found that cation-π, hydrogen bonding and, electrostatic interactions were responsible for the effective adsorption of the dyes from water. Once again the selective adsorption observed was accredited to the differences in pore size of the CFTs and size of the dye molecules.[137] Porous materials containing triazine units have also been synthesized and used for a variety of applications including heterogeneous catalysis,[141] CO_2 adsorption,[142] and hydrogen evolution.[143] Materials containing triazine units differ from CTFs as the bonds between the monomers are not formed through trimerization. Thus, these materials have the potential to fall into any of the categories of porous materials outlined in Section 1.2.1. It can be advantageous to have both the properties of the triazine unit in combination with those inherent of different porous materials.[134] For instance, Lui et al. incorporated triazine groups into the synthesis of siloxane cages to create highly porous materials with high capacity to adsorb organic dyes Congo red and rhodamine, as well as iodine detection and adsorption.[144] Triazine-based POPs have also been effective in removing heavy metals such as mercury,[145] copper,[146] and lead [147] from aqueous solution. Figure 6 demonstrates the potential interactions between a triazine-based covalent organic framework (T-COF) and mercury ions reported by Moradi et al. in 2020. The high surface areas of the materials in combination with strong chelating interactions between the metal ions and sites of electron density within the structure of the materials means they are effective at interacting with aqueous metal ions.[148]

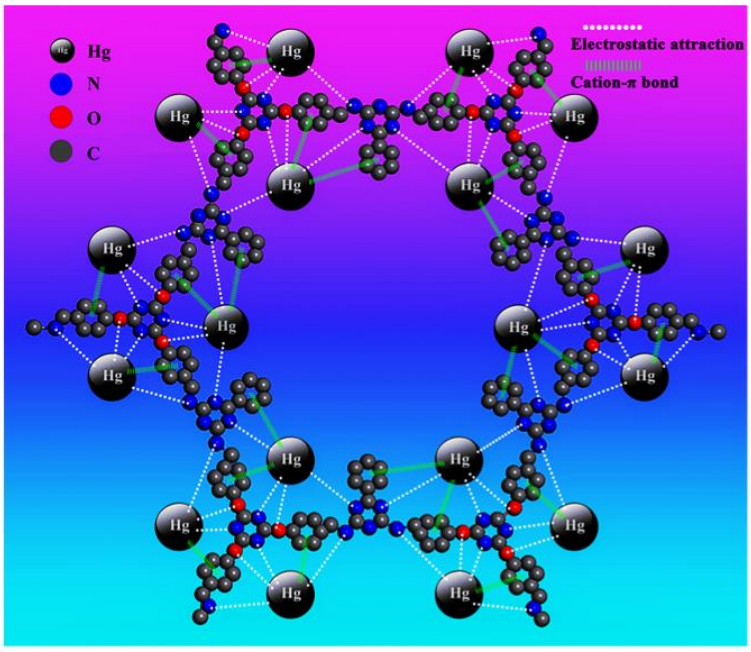

Figure 6: Possible chelating interactions between Hg^{2+} and T-COF. [145]

Triazine-based POPs are capable of adsorbing organic dyes through electrostatic interactions and intermolecular forces between the heteroatoms and functional groups within the materials.[149,150] Mokhtari et al. synthesized triazine-based POPs capable of interacting with organic dye Sky blue A through π-π interactions with triazine and phenol units and hydrogen bonding with the amide and imide functional groups present.[151] The incorporation of additional heteroatoms and functionalities such as: oxygen, fluorine, amides and imides are made easier by using triazine units as building blocks for the synthesis of porous materials. Incorporation of electron withdrawing triazine units to CMPs can be advantageous in terms of electron state manipulation and stability of the polymers.[152] Furthermore, the combination of the delocalized electronic structure and high nitrogen content of triazine containing CMPs enhance the properties of the materials giving a wider range of applications.[153]

1.3 Synthesis

In this work two synthetic routes (Buchwald Hartwig cross coupling and condensation polymerization) have been explored to yield porous materials. Additionally, trimerization reactions were undertaken for the preparation of two starting materials 4,4’,4’’-(1,3,5-triazine-2,4,6-triyl)trianiline (TAPT) and 5,5’,5’’-(1,3,5-triazine-2,4,6-triyl)tris(pyridine-2-amine) (TAPT-N). Due to the insolubility of the POP networks NMR and mass spectrometry characterization were not possible and access to solid-state NMR was not available. Thus, materials were characterized by Fourier-transform infrared (FTIR) spectroscopy, solid-state ultraviolet-visible light (UV-Vis) spectroscopy and X-ray power diffraction (XRD). Their porosity and surface properties were analyzed using Brunauer-Emmett-Teller (BET) analysis, scanning electron microscopy (SEM) images and contact angle measurements.

1.3.1 Buchwald Hartwig cross coupling

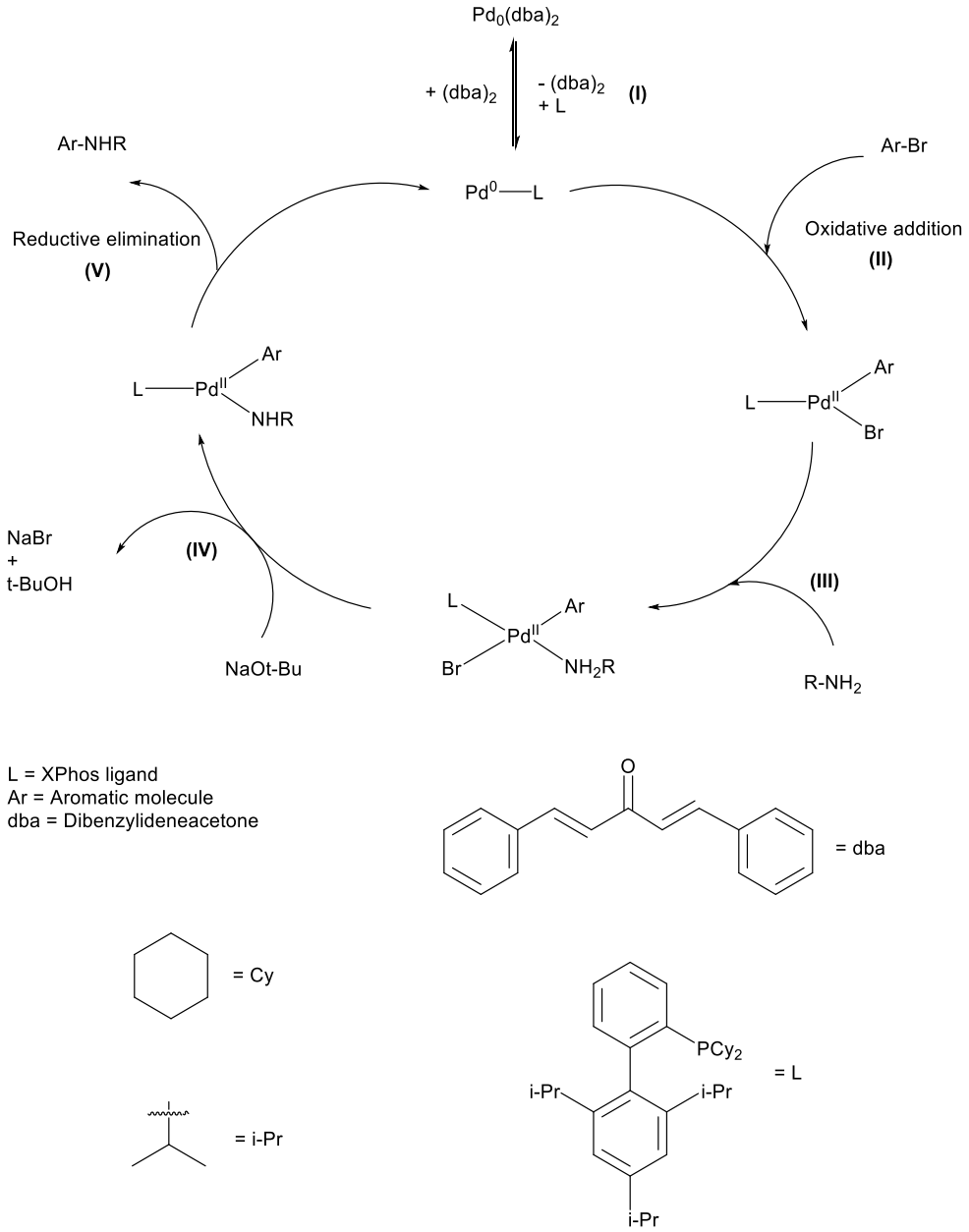

Scheme 1: Buchwald Hartwig catalytic cycle (used to synthesize POP 1-4). [155]

Buchwald Hartwig cross coupling (BH coupling) is a synthetic reaction that creates a C-N bond starting from an amine and an aryl halide using a palladium (Pd) catalyst (Scheme 1).[154] (Step I) The ligand on the Pd catalyst is substituted for a stronger bulky ligand. In this case, the dibenzylideneacetone (dba) ligand is replaced by the 2-dicyclohexylphosphino-2',4',6'-triisopropylbiphenyl (XPhos) ligand. The dba ligand is weak

and easily replaced by the XPhos ligand. XPhos is a monodentate ligand and has been shown to be an ideal catalyst in amination reactions due to its steric bulk and electron rich nature.[155] The electron withdrawing effect of the ligand activates the Pd catalyst whilst the second aryl ring induces stabilizing π-coordination. The bulky ligand ensures only one side of the catalyst is available for the subsequent steps in the reaction. (Step II) Following the activation of the catalyst, oxidative addition of the aryl halide to the metal center occurs, changing the oxidation state of Pd from 0 to +2. The biaryl ligand (XPhos) has a strong *trans* effect on the Pd(II) complex meaning the position *trans* to the aryl group is empty, allowing for the facile coordination of the amine to occur (Step III).[156,157] (Step IV) The halogen is removed from the Pd complex by the base creating a sodium salt and tert-butyl alcohol. (Step V) Finally reductive elimination occurs and the desired product is formed whilst the Pd is reduced and the catalyst regenerated.

The solubility of the reagents in the reacting medium is essential for a successful BH coupling reaction. Finding a suitable solvent that is capable of dissolving organic, inorganic and metallic reagents can prove to be difficult. Generally, non-polar and aromatic solvents are favored for BH coupling reactions of aryl amines. In 2014 Norrby et al. used theoretical and experimental studies to investigate the effects of different polarity solvents (toluene and DMF) on the role of the base (*t*-BuO^-) in BH coupling reactions.[156] When using a non-polar solvent such as toluene, the base removes the halogen from the Pd center and deprotonates the amine before it associates with the Pd avoiding the formation of a charged complex. Whereas, when using a polar aprotic solvent such as DMF, the halogen is easily dissociated from the Pd center whilst the base is inclined to act as a ligand forming charged complexes that inhibit the reaction.[158]

Choice of base also plays a role in the success of a BH coupling reaction. Generally, a strong base such as sodium tert-butoxide (NaO*t*-Bu) is used. Using NaO*t*-Bu gives faster reaction times and means less catalyst is needed however, can also produce undesirable side products.[154] On the other hand, weaker bases (such as Cs_2CO_3) are better at tolerating different functional groups that may be present in the starting materials, although give slower rates of reaction.[155]

The BH coupling reaction has been utilized to produce pharmaceuticals and new materials such as CMPs.[159] Over time the reaction has been optimized using many different catalysts,

ligands and, bases in the catalytic cycle to yield a range of products.[155] When using the BH coupling reaction to synthesize CMPs, nitrogen atoms are inherent in their structure. These nitrogen atoms can act as binding sites for certain pollutants.[160] Furthermore, the variety of monomers available for the BH coupling reaction allows for additional heteroatoms to be incorporated into the structure of the polymers with ease.

1.3.2 Condensation

Condensation reactions involve the removal of water from reactants. Usually, two small molecules react to produce a desired product and water as a by-product (Scheme 2).

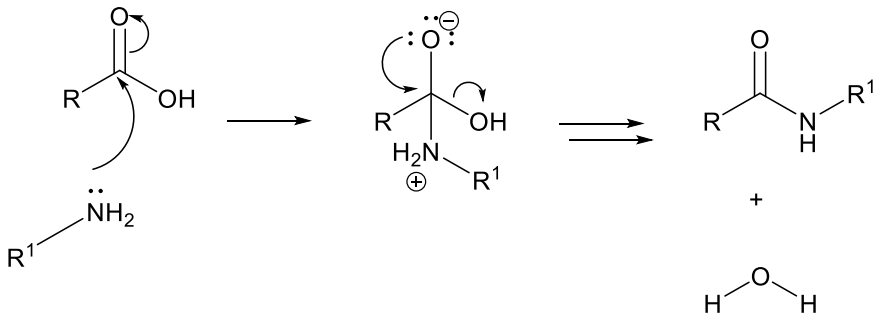

Scheme 2: Proposed mechanism for a condensation reaction.

In this work, aryl amines are reacted with aryl carboxylic acids to produce condensation polymers. The lone pair of electrons on the amide attacks the carbonyl carbon, which upon re-arrangement leads to loss of an OH^- ion. Removal of a proton from the amine finally produces an amide and water.

The products of the condensation polymerization reactions cannot strictly be classed as CMPs due to the lack of extended conjugation. However, many POPs have been successfully synthesized using this method.[161–163] Furthermore, using condensation reactions to produce POPs is a facile method of incorporating amide groups, and therefore additional heteroatoms (nitrogen and oxygen), into the materials structure. Work by Huang et al. demonstrated porous materials synthesized from melamine and trimesic acid were effective in adsorbing Hg^{2+} from solution.[162] With the aim of removing heavy metals from solution the synthesis described by Huang et al. was replicated and adapted in this work. A comparison of three condensation polymers using triazine-based cores (melamine, TAPT and TAPT-N) were explored for the adsorption of target pollutants.

1.3.3 Trimerization

The most common trimerization syntheses occur via a [2+2+2] cycloaddition reaction between aryl nitriles with the aid of high temperatures of 400 ℃ and Zn catalyst or a strong acid, trifluoromethanesulfonic acid (triflic acid).[164,165] Scheme 3 shows the proposed mechanism for the reaction using triflic acid.

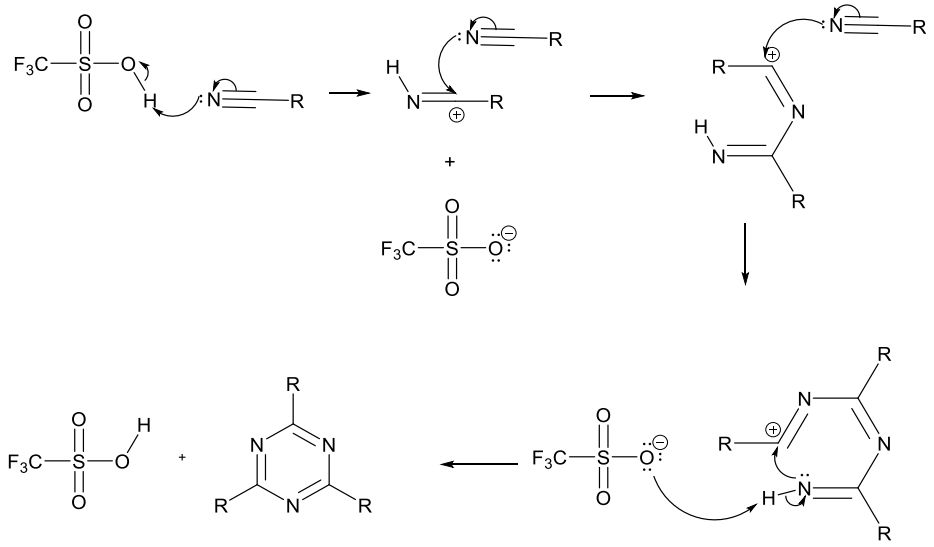

Scheme 3: Proposed trimerization mechanism of aryl nitriles using triflic acid. [228]

4-Aminobenzonitrile was used to create the starting material TAPT (Scheme 5) for the synthesis of POP-3, POP-4 and POP-6. Additionally, 6-aminonicotinonitrile has been used to create starting material TAPT-N (Scheme 9). It was found TAPT-N was insoluble in BH coupling solvents and could only be used in the condensation reaction explored in Section 2.5.

1.4 Conclusion

Wastewater released by the textile industry is a major environmental concern. The industry is responsible for the release of hazardous chemicals such as dyes and heavy metals into the environment. These chemicals are responsible for the destruction of eco systems, poisoning of flora, fauna and, humans alike. There are many different methods that may be used to treat wastewater for these pollutants however, adsorption is often preferred owing to the efficiency, cost-effectiveness and environmentally friendly nature. CMPs as a subclass of POPs have emerged in recent years as highly effective materials in the fields of gas capture, battery technology, catalysis, hydrogen evolution and chemo-sensing. However, there has been comparatively little research into CMPs as water-based adsorbents. This work will investigate triazine-based porous materials applied to the removal of toxic dyes and heavy metals from wastewater.

1.5 Aims and objectives

The aim of this project was to synthesize porous materials that were capable of removing water-based pollutants produced by the textile industry.

To achieve this aim, three main objectives were addressed:

- To synthesize porous materials containing a high concentration of heteroatoms.
- To evaluate the adsorption mechanisms and re-usability of materials synthesized.
- To test porous materials for their ability to adsorb pollutants under simulated wastewater conditions.

2 Results and discussion

2.1 POP-1 and POP-2

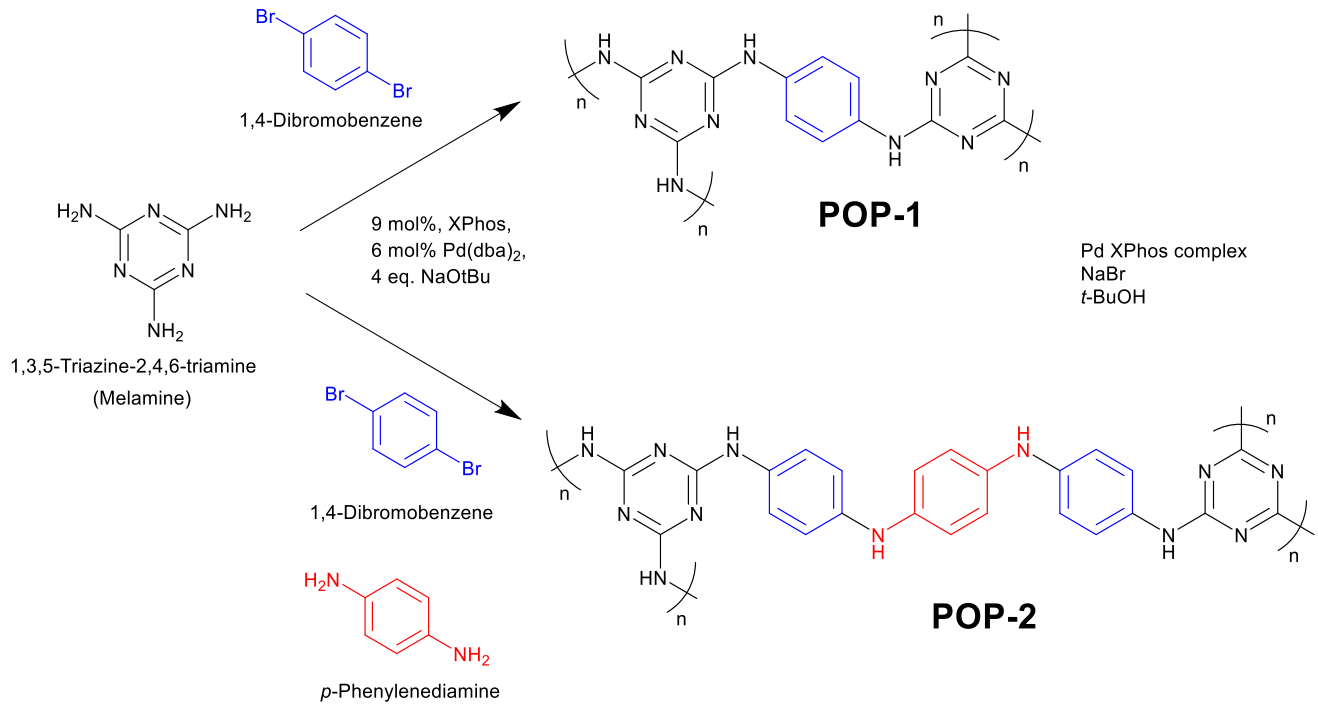

Scheme 4: Synthetic pathway of POP-1 and POP-2.

Scheme 4 depicts the syntheses of POP-1 and POP-2 conducted using the BH coupling procedure set out by Faul et al. in 2014.[166] To ensure interactions between the materials and target pollutants was achieved, the main aim of synthesizing materials with a high concentration of heteroatoms was explored. Melamine was chosen as a core and 1,4-dibromobenzene as a linker for the BH cross coupling reaction. In 2023, work by Faul et al. showed the synthesis of an extended CMP network with excellent adsorption capacity for organic dyes. As well as using the traditional two monomer approach, a third monomer was introduced to the BH coupling reaction to extend the polymeric network creating a CMP that showed better dispersion in water and a higher uptake of organic dyes.[167] Following these results, i.e. that an extended CMP network would allow for better dispersion in water and therefore better interactions with the target pollutants, *p*-phenylenediamine was used as a co-monomer in the synthesis of POP-2.

To the best of the authors knowledge these reactions have not been published. The monomers and reagents were heated for 72 h and the resulting polymer networks were

washed and dried, producing POP-1 and POP-2 in 4% and 1% yield, respectively. The low yields observed may be due to several reasons including solvent choice, steric hinderance and monomer ratios. DMSO was chosen as the solvent for the synthesis of POP-1 and POP-2 due the insolubility of melamine in less polar solvents such as THF and toluene. The choice of solvent itself may have hindered the reaction due to its polarity or the solubility of other reagents in the reaction mixture hindering bond formation. It was hypothesized that the size of the monomers along with the bulky ligand typical of this reaction caused too much steric hindrance around the reacting amine, preventing complete polymerization and crosslinking.[168] Thus, although a precipitate was observed, the vast majority of the product was soluble in the solvents used in the washing process.

FTIR spectroscopy was used to characterize the resulting materials (Section 7.1, Appendix). The N-H peak at 3469 cm^{-1} corresponding to the primary amine and the C-Br peak at 1064 cm^{-1}, typical for the starting materials were greatly diminished. The FTIR analysis suggests a small number of oligomers and/or polymers may have formed with some amine and bromide end groups still present. It is unlikely full crosslinking polymerization occurred due to the low yields and presence of diminished peaks in the FTIR spectra. Further analysis such as solid-state NMR may help to reveal the true structures and extent of polymerization of POP-1 and POP-2.

The quantities of catalyst, monomer ratios, reaction temperature and times were all explored (Section 4.1.10). After a variety of reaction conditions were tested it was concluded that the use of melamine as a core was not suitable for this type of reaction. In 2018, Faul et al. reported a successful BH coupling reaction using a triazine core (TAPT), which could be used in place of the melamine core.[117] The synthesis of TAPT was achieved via a trimerization reaction to investigate if this core would be a suitable replacement.

2.2 POP-3 and POP-4

POP-3 and POP-4 were prepared via a two-step synthesis procedure. First, the core TAPT was synthesized by a trimerization reaction (Scheme 5), followed by a BH coupling reaction between TAPT and 1,4-dibromobenzene and, TAPT, 1,4-dibromobenzene and *p*-phenylenediamine to yield POP-3 and POP-4, respectively (Scheme 6).

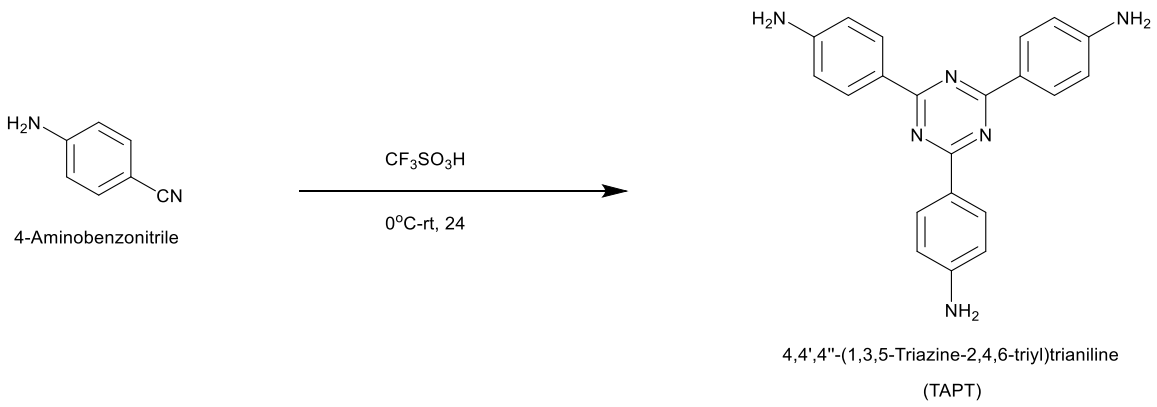

Scheme 5: Synthetic pathway of TAPT.

For the synthesis of TAPT, 4-aminobenzonitrile was mixed with triflic acid following the reaction mechanism outlined in Section 1.3.3 to produce TAPT with a yield of 62%. The successful synthesis of the desired product was confirmed by the absence of the nitrile peak in the FTIR spectrum (Figure 7) typically found at 2212 cm^{-1}.[169] Furthermore, ^{13}C and ^{1}H NMR

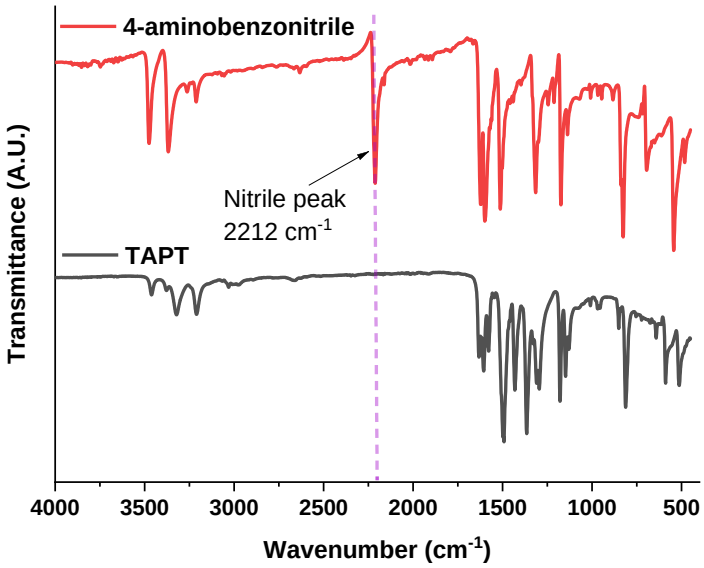

Figure 7: FTIR spectra of 4-aminobenzonitril and TAPT.

confirmed the successful synthesis of TAPT (Section 7.2, Appendix). ^{1}H NMR shows the peaks of the product are shifted downfield compared to those of the starting material, evidence of higher de-shielding by the triazine unit compared to the nitrile unit.

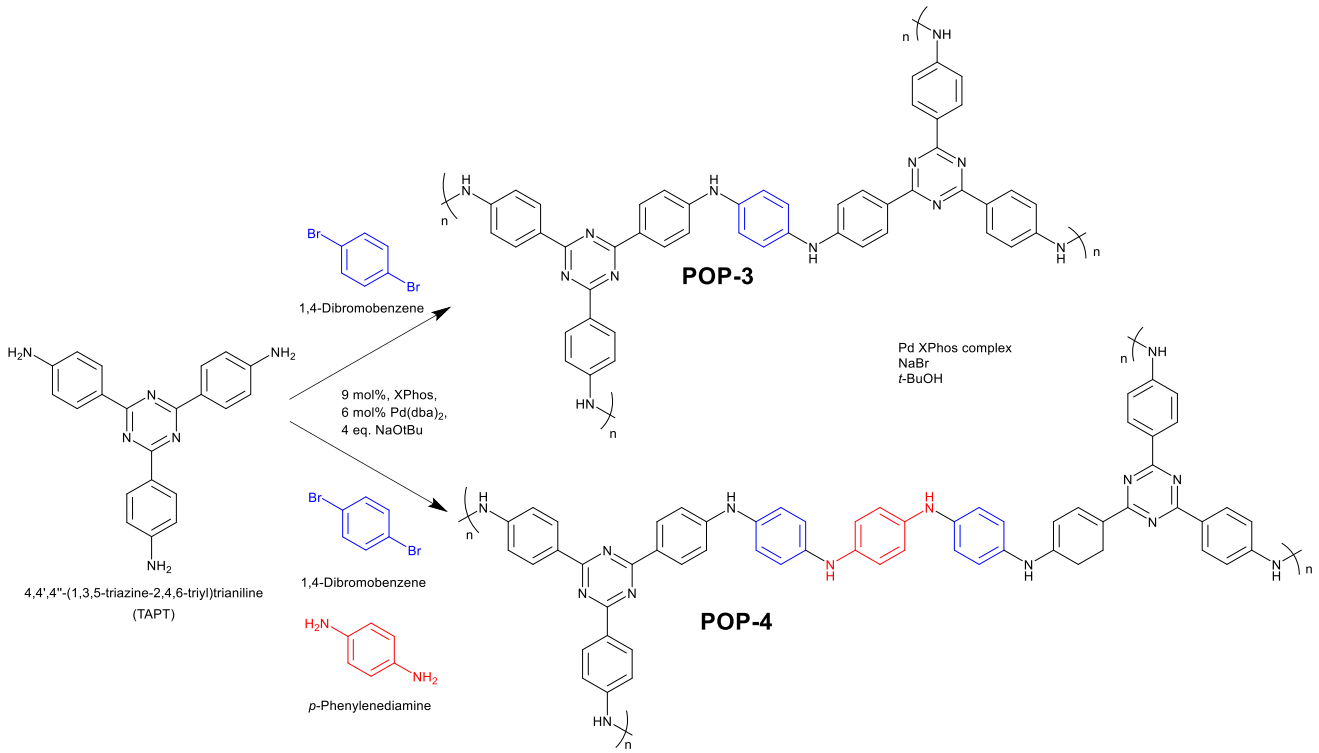

Scheme 6: Synthetic pathway of POP-3 and POP-4.

Following the successful synthesis of the TAPT core, POP-3 was synthesized using TAPT and 1,4-dibromobenzene and POP-4 was synthesized using TAPT, 1,4-dibromobenzene and *p*-phenylenediamine. Initially, the same reaction conditions described for the synthesis of POP-1 and POP-2 (Section 2.1) were used for better comparability between TAPT and the previously used melamine core. A small increase in yield was observed when changing the core alone; a 10% yield of both POP-3 and POP-4 was achieved. Consequently, we can say that increasing the size of the core and thus reducing the steric hindrance around the reactive amine sites had a positive effect on the reaction. However, after changing the solvent to THF, as described by Faul et al. for the synthesis of CMPs using TAPT as a core, [117] we observe a drastic increase in the yields of POP-3 and POP-4. By changing the solvent and using TAPT as a core POP-3 and POP-4 were produced with yields of 98% and 39%, respectively. Owing to the vast difference between DMSO and THF we can confirm DMSO was not a suitable solvent for BH coupling reactions under the conditions used. There may

be a combination of reagents that could be used with DMSO to yield a successful BH coupling reaction, but was not explored in this work.

The successful synthesis of POP-3 and POP-4 was confirmed using FTIR spectroscopy (Sections 7.3 and 7.4, Appendix). The almost complete loss of the primary amine peak at 3460 cm^{-1}, characteristic of N-H stretching vibration, along with the absence of the C-Br peak at 1062 cm^{-1} indicated full polymerization had occurred.[167,170] Amine groups may still be present in the FTIR spectrum due to the presence of amine end groups within the polymer. Figure 8 shows the solid-state UV-Vis spectra, showing the electronic transition from the valence band to the conducting band of POP-3 and POP-4. POP-3 has a broad absorbance peak at 391 nm spanning to the edge of the visible light range, whilst POP-4 has a very broad absorbance peak at 648 nm spanning into the near infrared range. POP-4 can absorb light at a longer wavelength and therefore a smaller amount of energy is needed to excite an electron from the valence band to the conducting band. A more conjugated system has an increasing number of π-orbitals within the molecular structure and therefore smaller energy gap between the highest occupied molecular orbital (HOMO) and the lowest occupied molecular orbital (LUMO). Thus, from the data we can infer POP-4 has a more conjugated structure than POP-3. It was hypothesized that the additional linker used in POP-4 helped to extend the chain length of the polymer thereby increasing the extent of conjugation. By extending the linking chain between the core molecules, steric hinderance around the core is likely to be reduced and further polymerization and therefore

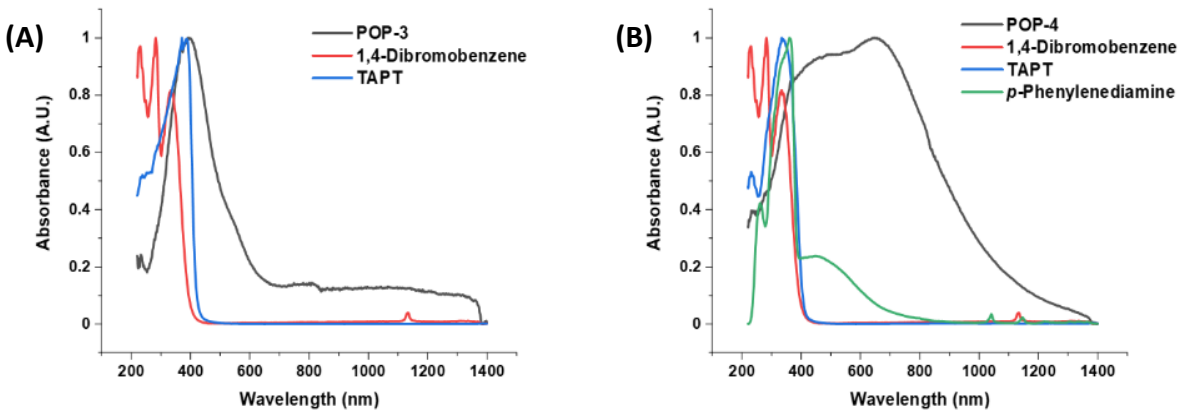

Figure 8: Solid state UV-Vis spectra normalized to 1. (A) POP-3, 1,4-dibromobenzene, TAPT. (B) POP-4, 1,4-dibromobenzene, p-phenylenediamine, TAPT.

conjugation may have been possible. However, with the use of the additional linker in POP-4 the complexity of the reaction was increased, hence the lower yield compared to POP-3. Further optimization of the synthesis of POP-4 would be of interest for electronic applications and is explored in Section 3.2.

XRD analyses confirm amorphous structures for both polymers due to the broad peak at 12.5^{o} and the lack of sharp peaks in other areas of the diffractograms of the polymers (Sections 7.3 and 7.4, Appendix).

BET characterization yielded surface areas of 73 m^2/g and 10 m^2/g for POP-3 and POP-4, respectively, and pores mostly in the mesoporous and macroporous regions (Sections 7.3 and 7.4, Appendix). The N_2 isotherm of POP-3 is indicative of a type VI isotherm, suggesting a layer-by-layer adsorption on a uniform non-porous structure. The isotherm of POP-4 indicates a type V isotherm with a hysteresis loop showing weak interactions between adsorbent and adsorbate, with adsorbent molecules clustered around the most attractive sites. Hysteresis loops are generally connected to capillary condensation in which a gas condenses to a liquid within the pores of the material.[171]

The amorphous nature of POP-3 and POP-4 typical of CMPs can be observed from the scanning electron microscopy (SEM) images shown in Figure 9. Interestingly, and in contrast to the BET surface areas given, POP-4 appears to have a more disordered surface and more interstitial voids comparted to POP-3. The difference in surface morphology may be due to the different polymeric structures of POP-3 and POP-4. It was hypothesized that the polydispersity of POP-4 was increased comparted to POP-3 because of the additional linker used in the synthesis of POP-4. Increasing the feed ratios of monomers may promote chain growth and increase the distance between core molecules, potentially increasing pore sizes. Micropores and mesopores are unlikely to be visible in the SEM images. We can deduce POP-4 has a higher concentration of macropores compared to POP-3 which may have smaller pores that were undetected by the SEM equipment. It can be concluded that porosity cannot be quantified on SEM images alone.

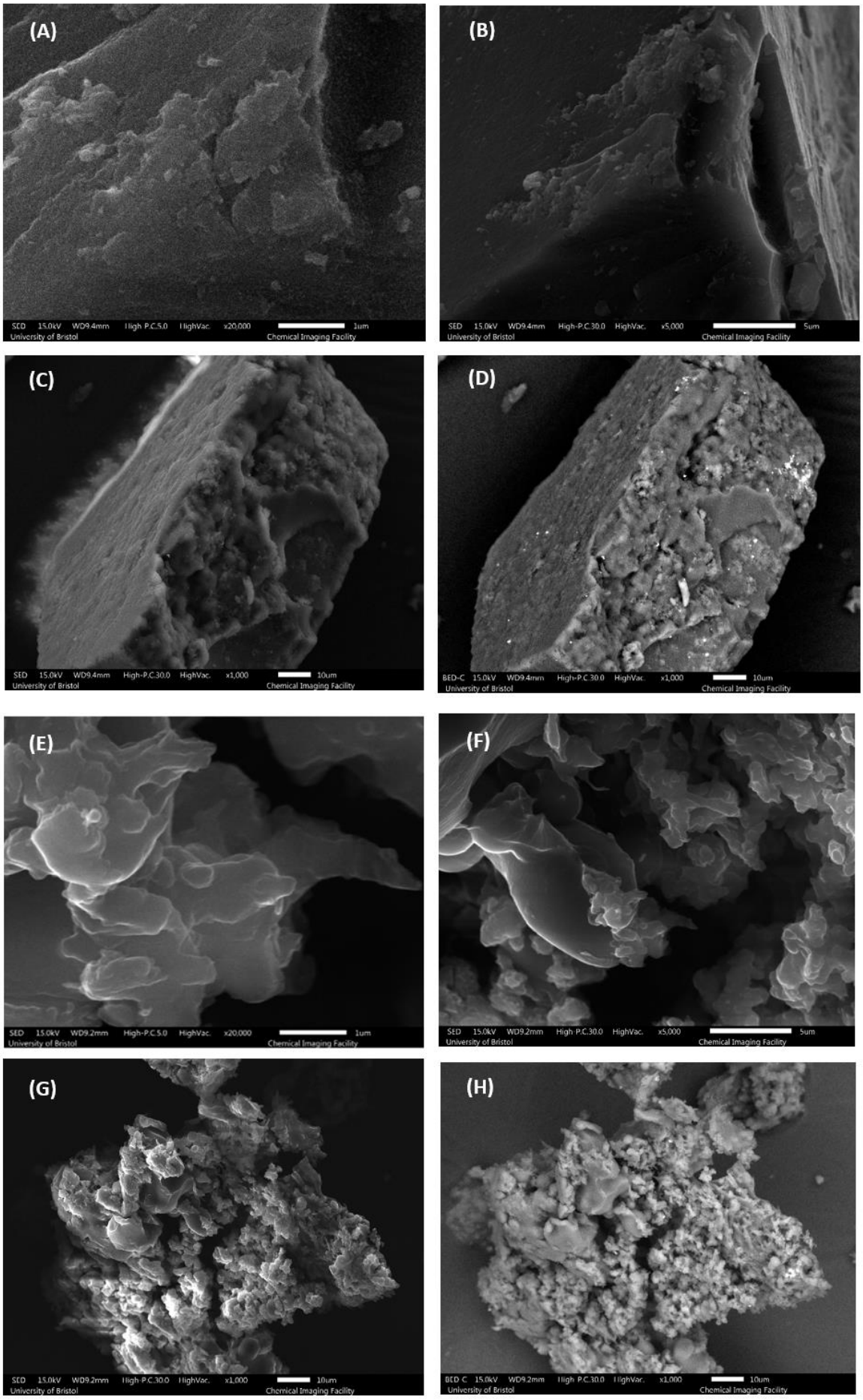

Figure 9: SEM images of POP-3 (A-D) and POP-4 (E-H). Magnification: (A)/(E) x20,000 at 1 um (SED), (B)/(F) x5,000 at 5 um (SED), (C)/(G) x1,000 at 10 um (SED), (D)/(H) x1,000 at 10 um (BED-C).

2.3 POP-5

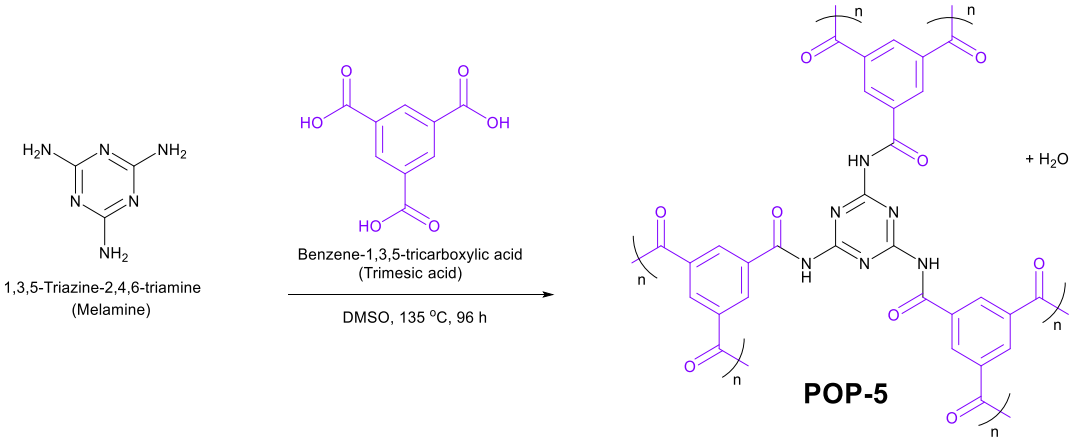

Scheme 7: Synthetic pathway of POP-5.

The synthesis of POP-5 involved the condensation polymerization of melamine and trimesic acid in anhydrous DMSO (Scheme 7). It has been reported that DMSO decomposes when heated to high temperatures and the presence of amides and organic acids increase decomposition of the solvent.[172] Thus, a temperature of 135 °C was used and produced POP-5 with a 62% yield. The successful synthesis of POP-5 was confirmed by FTIR spectroscopy, shown in Figure 10. The broad peak at ~3000 cm^{-1} from the C-OH groups

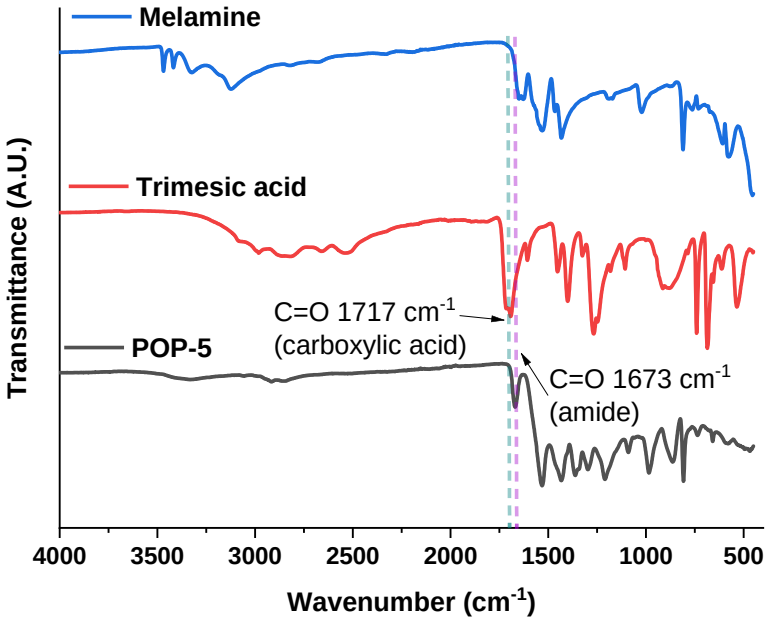

Figure 10: FTIR spectra of POP-5, trimesic acid and melamine.

present in the starting material was extremely diminished in the product suggesting the presence of some terminal alcohol groups. Furthermore, the carbonyl peak bathochromically shifted from 1717 cm^{-1} to 1673 cm^{-1} due to the formation of the amide bond (indicated in Figure 10).[162] The solid-state UV-Vis spectrum (Section 7.5, Appendix) of POP-5 shows the material is only capable of absorbing short wavelengths of light mostly in the ultra violet range. More energy is required to excite an electron from the HOMO to the LUMO of POP-5 compared to POP-3 or POP-4 because POP-5 does not have a fully conjugated backbone. Finally, we observe no sharp peaks in the XRD spectra, confirming an amorphous structure (Section 7.5, Appendix).

Surface characterization of POP-5 (Figure 11) gave a BET surface area of 81 m^2/g and a total pore volume of 1.8 $x10^{-1}$ cc/g. It was observed from the pore size distribution graph that the average pore width was 3.7 nm indicating a predominantly mesoporous structure. The isotherm is characteristic of type IV(a) indicating a mesoporous material with mono-multi layer adsorption. The hysteresis observed can be categorized as type H2(a), indicating pore blockage or cavitation induced evaporation, typical for mesoporous materials.[171]

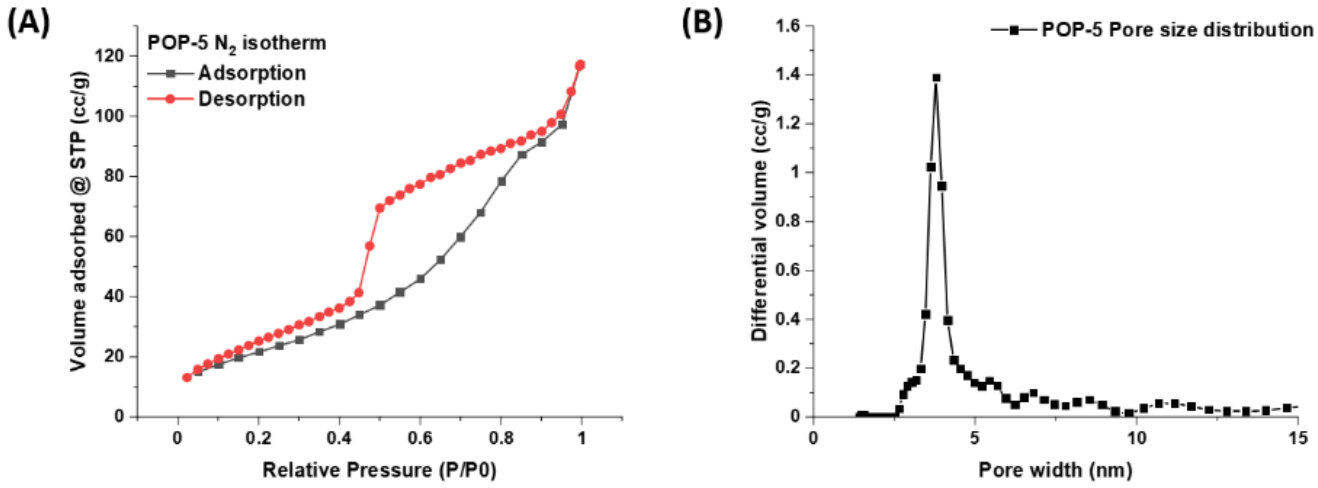

Figure 11: (A) N_2 isotherm of POP-5, (B) pore size distribution of POP-5.

2.4 POP-6

The synesis of POP-6 was achieved by the condensation polymerization of TAPT and trimesic acid (Scheme 8). To the best of the authors knowledge, this reaction has not been reported. TAPT was synthesized by a trimerization reaction of 4-aminobenzonitrile as previously reported in Section 2.2.

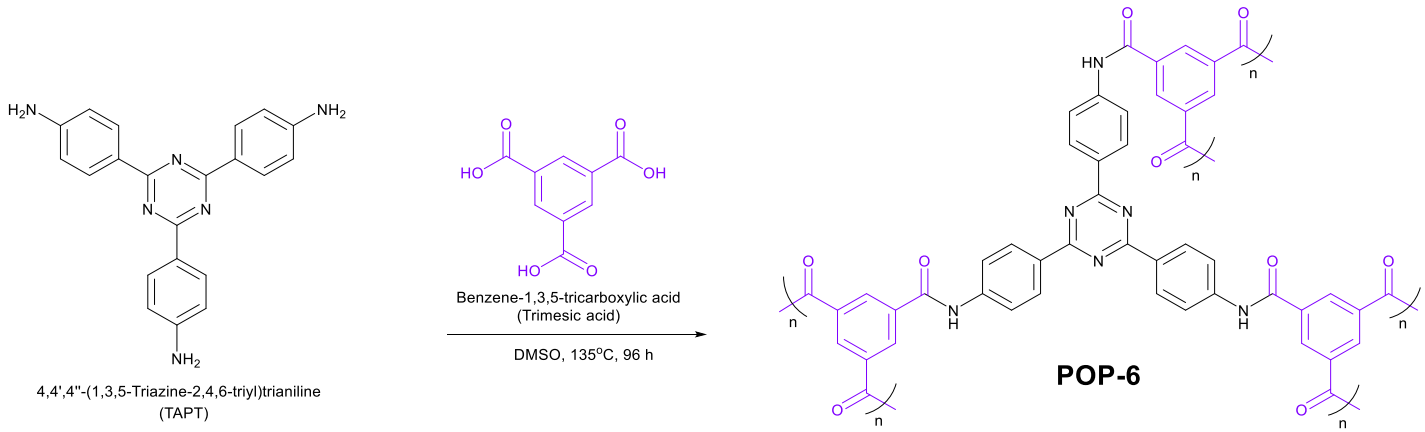

Scheme 8: Synthetic pathway of POP-6.

Due to the novelty of the reaction, synthetic conditions reported for POP-5 were used with slight changes to monomer ratios. Initially a ratio of 1:1 was used and produced POP-6 with a 45% yield. It was found that a slight excess of TAPT (1.15 equivalence) was favorable for the reaction, producing POP-6 with a yield of 87%. The mechanism for the condensation reaction shows the amine groups initiate the reaction by attacking the carbonyl carbon therefore, having an excess of amine groups may increase the number of bonds able to form during the reaction. Thus, longer polymer chain lengths may be encouraged and less side products may be formed, increasing the yield.

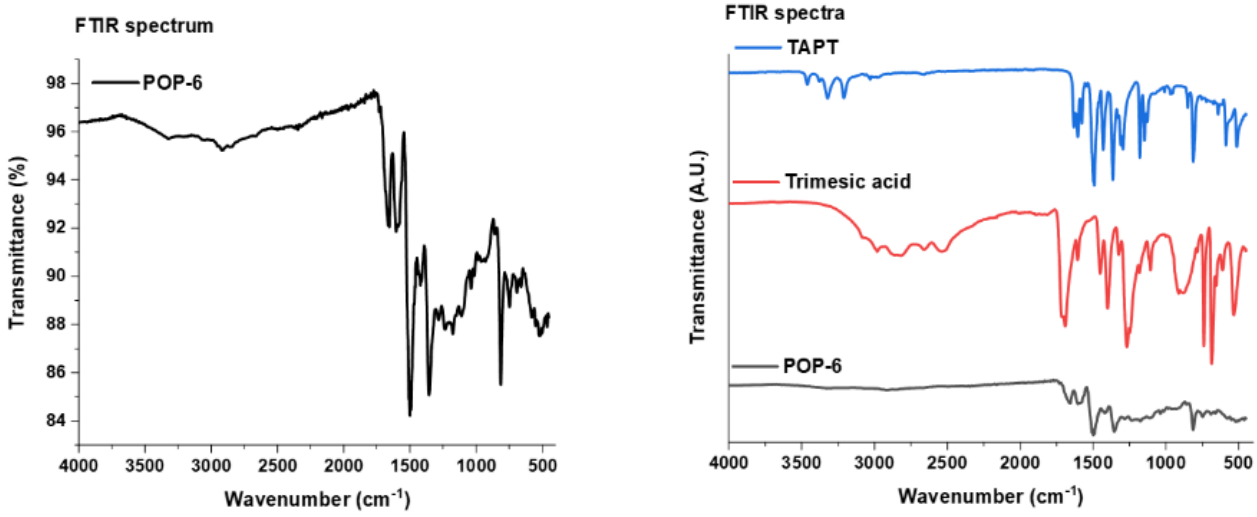

Figure 12: FTIR spectra of POP-6.

The formation of the expected polymer was confirmed using FTIR (Figure 12); the bathochromic shift of the carbonyl peak from the carboxylic acid at 1717 cm^{-1} to the amide peak at 1664 cm^{-1} and the loss of broad C-OH peak at ~3000 cm^{-1} indicative of reaction (Section 7.6, Appendix).[173] Though POP-6 is also not fully conjugated, a slightly broader peak was observed compared to POP-5 in the UV-Vis spectrum (Section 7.6, Appendix). The TAPT core contains more π-bonds compared to the smaller melamine core. Therefore, it can be expected that less energy was required to excite an electron from the HOMO to the LUMO of POP-6 and the material absorbed a longer wavelength of light. Once again, the amorphous nature was confirmed by the singular broad peak observed in the XRD spectra (Figure 13).

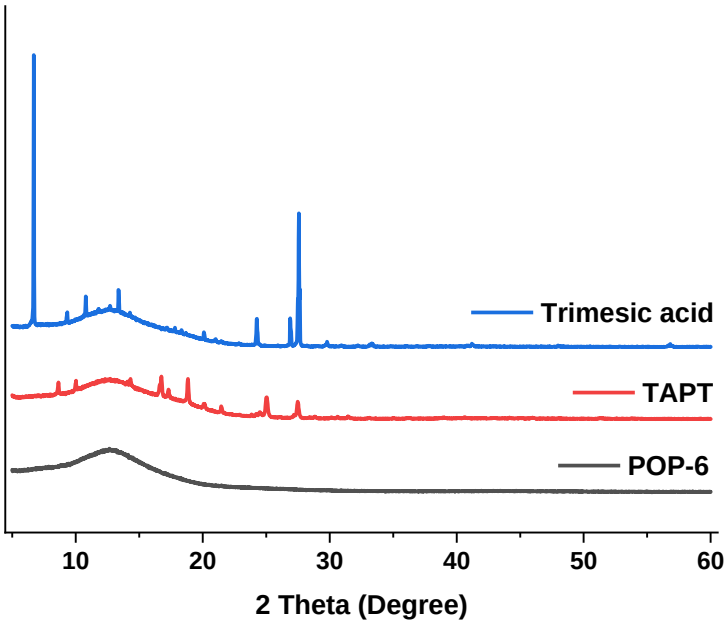

Figure 13: XRD spectra of POP-6, TAPT and trimesic acid.

Analysis of the BET data indicates limited mesoporosity and macroporosity with a surface area of 22 m^2/g (Section 7.6, Appendix). The nitrogen isotherm observed is atypical and difficult to define. The isotherm can be estimated to fit to Type III, indicating the adsorbent is located at the most favorable sites and the interactions are weak. The low total pore volume of 1.3 $x10^{-2}$ cc/g further indicates little porosity. SEM images of POP-6 show a mostly flat surface with some roughness, as seen in Figure 14.

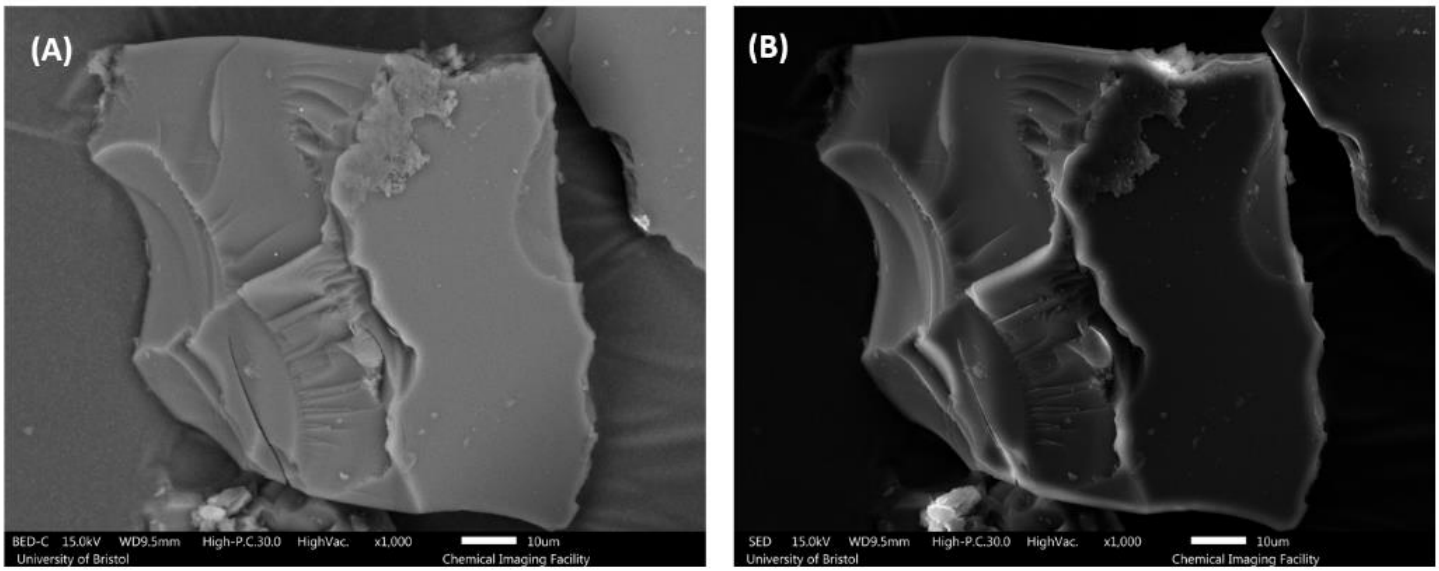

Figure 14: SEM images of POP-6, x1000 magnification at 10 µm. (A) BED image of POP-6. (B) SED image of POP-6.

2.5 POP-7

The synthesis of POP-7 proceeded much in the same way as POP-6 (Section 2.4), using TAPT-N as a core instead of TAPT. TAPT-N was used to further increase the heteroatom content within the polymer with the aim of interacting more effectively with target pollutants. TAPT-N was synthesized with a yield of 44% via a trimerization reaction using 6-amino-nicotinonitrile (Scheme 9) and characterized as described in Section 2.2. To the best of the authors knowledge these reactions have not been published.

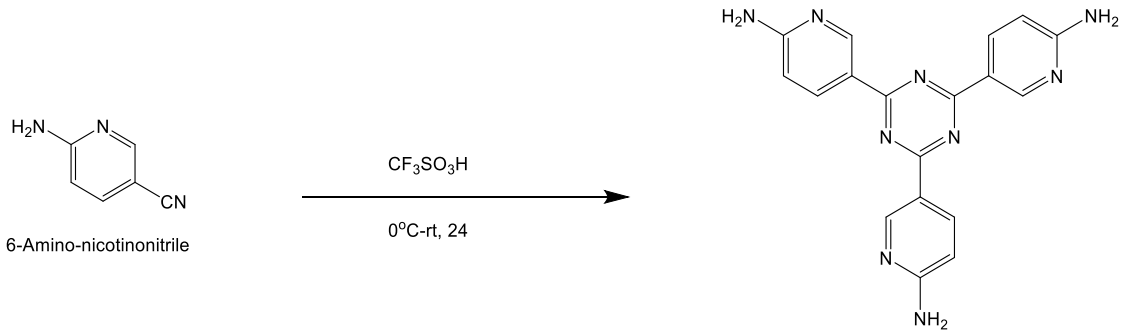

Scheme 9: Synthetic pathway of TAPT-N.

Following the successful synthesis of the TAPT-N core, POP-7 was synthesized via a condensation polymerization reaction between TAPT-N and trimesic acid (Scheme 10), with a yield of 67%.

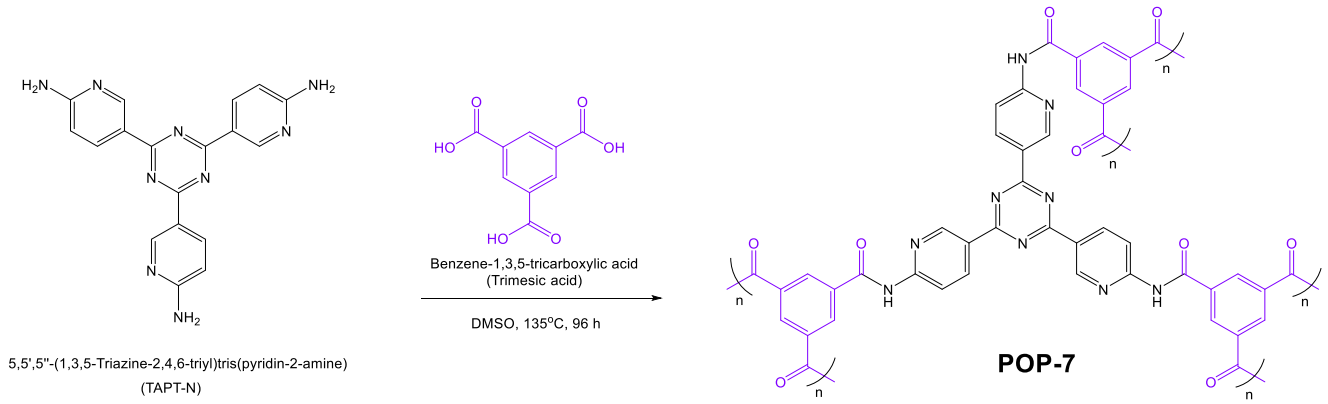

Scheme 10: Synthetic pathway of POP-7.

FTIR spectroscopy confirmed the loss of the broad C-OH peak and the formation of the amide bond from the bathochromic shift of carbonyl peak (Section 7.8, Appendix). The solid-state UV-Vis spectrum of POP-7 (Section 7.8, Appendix) was very similar to that of POP-6, as the TAPT and TAPT-N cores have the same number of π-bonds and the same linker was used for both syntheses. The XRD spectra shows a single broad peak indicating the amorphous nature of the material (Section 7.8, Appendix).

The N_2 isotherm of POP-7 (Section 7.8, Appendix) is characteristic of a Type V isotherm, similar in shape and classification to Type III indicating relatively weak interactions between the polymer and adsorbent gas are observed. A hysteresis loop is also present indicating pore condensation.[171] POP-7 has a BET surface area of 22 m^2/g with a total pore volume of 9.9 $x10^{-2}$ cm^3/g. The pore size distribution indicates the material is primarily macroporous with some mesopores also present.

2.6 Properties

2.6.1 The Brunauer–Emmett–Teller method

The BET surface area is based on the adsorption of nitrogen gas onto the surface of a material and is widely used for the analysis and comparison of the specific surface areas of porous materials.[174]

The BET equation is as follows:[175]

$$\frac{1}{v\left(\left(\frac{P_0}{P}\right)-1\right)} = \frac{1}{v_m C} + \frac{C-1}{v_m C}\left(\frac{P}{P_0}\right)$$

Equation 1: BET equation.[175]

Where: v = weight of gas adsorbed at relative pressure, P/P_0 = relative pressure where P = vapor pressure and P_0 = saturated vapor pressure (mbar), C= BET constant and, v_m = specific monolayer capacity.

Though this method is widely used it has some limitations. The method was developed based on macropores and mesopores thus, the presence of micropores can influence the results and a correction to the calculations is needed. IUPAC have advised extreme caution is to be taken when using BET theory for microporous materials.[176] Furthermore, the interpretation of the isotherms produced by the BET method can vary between researchers. A study conducted in 2022 gave 61 laboratories the same raw isotherms to calculate the surface areas to test the reproducibility of the surface area data. The results showed vastly different values reported by different groups, predominantly because of different sections of the isotherm being used for the surface area calculation.[177] Therefore, though the BET method is successful in providing a standard system for reporting and comparing surface areas, the results can vary significantly depending on the researcher and can make replicating results difficult. However, until a new system is adopted globally the current BET method is the best method to use for compatibility with literature values.

The pore sizes of the materials produced fall within the meso- to macro-porous range, with surface areas calculated using the classical linear BET range of 0.05-0.3 P/P_0. The total pore volume measurements were taken at 0.995 P/P_0. Given that the measurements were all taken in the same way, they can act as a reliable comparison for each material produced

within this investigation. The BET surface areas of the materials produced have generally been low with no material exceeding 100 m^2/g. Table 3 gives a summary of the best surface properties recorded for each material.

Table 3: BET surface areas and total pore volumes of POP 3-7.

Material	**Specific surface area (m^2/g)**	**Total pore volume (cm^3/g)**
POP-3	72	7.3×10^{-2}
POP-4	10	1.7×10^{-2}
POP-5	81	1.8×10^{-1}
POP-6	22	1.3×10^{-2}
POP-7	22	9.9×10^{-2}

The low porosity of the materials can be attributed to the synthetic conditions, the starting materials and ratio of materials used.[178] Further investigation into the synthetic procedure may help to produce materials with higher surface areas. It would be of interest to repeat the condensation polymerization with the equivalent or similar aldehyde (benzene-1,3,5-tricarbaldehyde or terephthalaldehyde) to produce a 2D polymeric structures with imine linkages. Typically, 2D porous materials with high surface areas have a crystalline nature which may be more favorable for metal and dye adsorption. Stacking of polymer layers takes place within the materials making their structure ordered and creating porous voids and thus high surface areas.[179]

Although a useful tool for the comparison of porous materials, the value of the surface area measurements is somewhat limited for the adsorption of water-based contaminants. The low surface areas for the materials are not necessarily a limiting factor, effective adsorbent materials have been reported with low surface areas and applied to wastewater treatment.[167,180] For instance, in 2020 Amin et al. demonstrated excellent adsorption capacities of organic dyes Reactive Black 5 and Congo Red using modified coffee waste with a BET surface area of only 4.9 m^2/g.[181]

2.6.2 Water dispersibility

Contact angle measurements were taken to determine how well the materials interact with water. These measurements can determine the wettability of the materials synthesized. If the contact angle is low then the material is hydrophilic and will easily disperse in aqueous solution.[182] Thus, interactions with water-based pollutants may be increased compared to a more hydrophobic material. [182] Figure 15 shows different contact angle ranges and how they correspond to hydrophobicity and hydrophilicity. Generally, a material is classed as superhydrophobic if the contact angle is above 150°, hydrophobic if the contact angle is between 90°-150°, hydrophilic if it has a contact angle of below 90° and super hydrophilic if the contact angle is less that 5° within 0.5 seconds of measuring.[183,184]

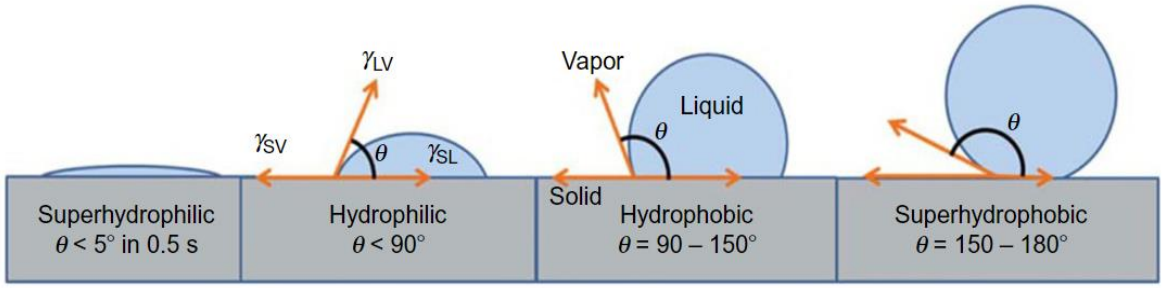

Figure 15: Water contact angle on different surfaces. [184]

POPs 3-7 were pressed into a pellet using a pellet press at 10 tons of pressure for 1-3 hours. Each pellet was analyzed using a 2 µL drop of water and a sessile drop to record the contact angle over a period of 3 minutes. Photos were taken every second to observe how the contact angle changed over time. For materials POP-4 and POP-5 the contact angle showed little change over 3 minutes. But for POP-3, POP-6 and POP-7 the droplet of water was fully absorbed before the 3 minutes were complete. POP-4 indicated the least wettability; the contact angle changed from 76.4° to 64.9° over the 3-minute period. POP-6 demonstrated excellent wettability with the first drop of water being completely absorbed before measurements could be taken and was therefore classed as superhydrophilic.[184] A second drop of water was placed on POP-6 and the contact angle changed from 22.2° to 16.1° over a period of 25 seconds before the droplet was once again absorbed by the material. Figure 16 demonstrates the differences in contact angles of POP-4 and POP-6.

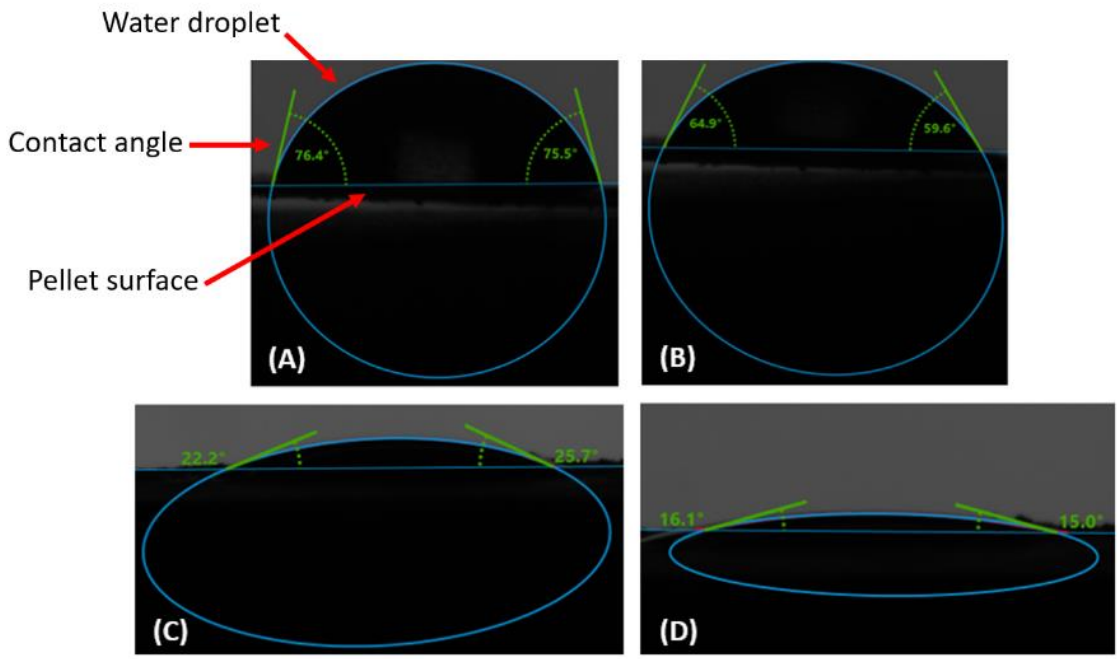

Figure 16: Contact angle measurements. (A) POP-4, 3 sec. (B) POP-4, 300 sec. (C) POP-6, 3 sec. (D) POP-6, 25 sec.

The differences in contact angle can be explained by a number of factors including pore structure, surface roughness and, functional groups within the polymer.[185] The additional functionality of the condensation type polymers could be an explanation for the differences in wettability observed. Though the secondary amines and nitrogen atoms within the structure of POP-4 are capable of hydrogen bonding, the presence of the amide groups in addition to the nitrogen atoms in the triazine core provide more opportunities to form hydrogen bonds between the condensation polymers and water droplet. The less hydrophilic nature of POP-4 can be attributed to the highly conjugated backbone of the material, observed from the UV-Vis spectrum of the material (Figure 8, Section 2.2). Interestingly POP-3 and POP-5 do not follow the expected trend. By the end of the 3-minute measurement period the water droplet on POP-3 had been completely absorbed while the droplet on POP-5 remained present. The difference in water absorption between POP-3 and POP-4 could be attributed to the differences in porosity and degree of conjugation. POP-4 is less porous than POP-3 thus, liquid penetration may be greater in POP-3.[185] Furthermore, POP-3 displayed a less conjugated structure compared to POP-4 (Figure 8, Section 2.2) indicating it may be less hydrophobic. The less hydrophilic nature of POP-5 was intriguing given it had the highest recorded surface area of all the materials produced (Table 3, Section

2.6.1) and contained amide groups capable of hydrogen bonding. Repeating the contact angle experiments would be of interest to further investigate these anomalous results.

Despite some unexpected observations, all the materials tested can be classed as hydrophilic displaying a contact angle of less than 90°, while POP-6 showed superhydrophilic character. The superhydrophilicity of POP-6 indicates the material may have more successful interactions with water-based pollutants.

2.7 Dye adsorption experiments

A range of azobenzene dyes were initially tested with the polymers to give structural diversity and a well-rounded scope of application. A cationic (non-azobenzene) dye was also used as a comparison to see how the materials would interact with differently charged dyes. Figure 17 shows the structures of the dyes used: methyl orange (MO), acid violet 7 (AV7), Congo red (CR) and methylene blue (MB).

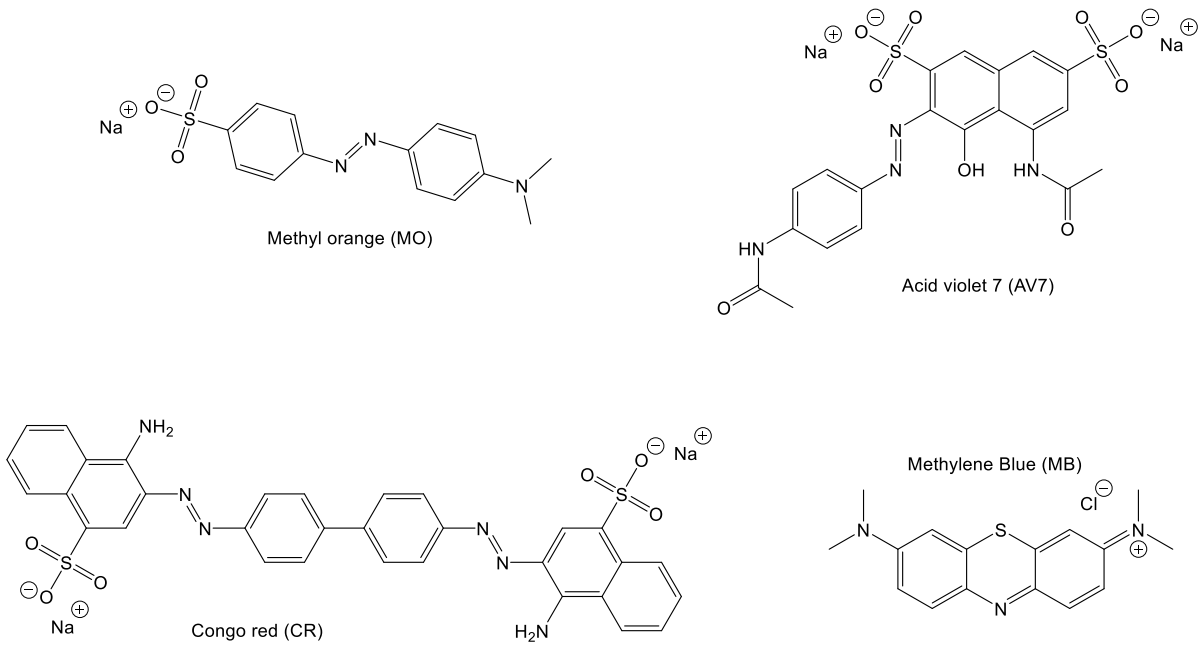

Figure 17: Structures of dyes investigated: methyl orange, acid violet , Congo red, methylene blue.[229–231]

2.7.1 Standard dye adsorption experiments

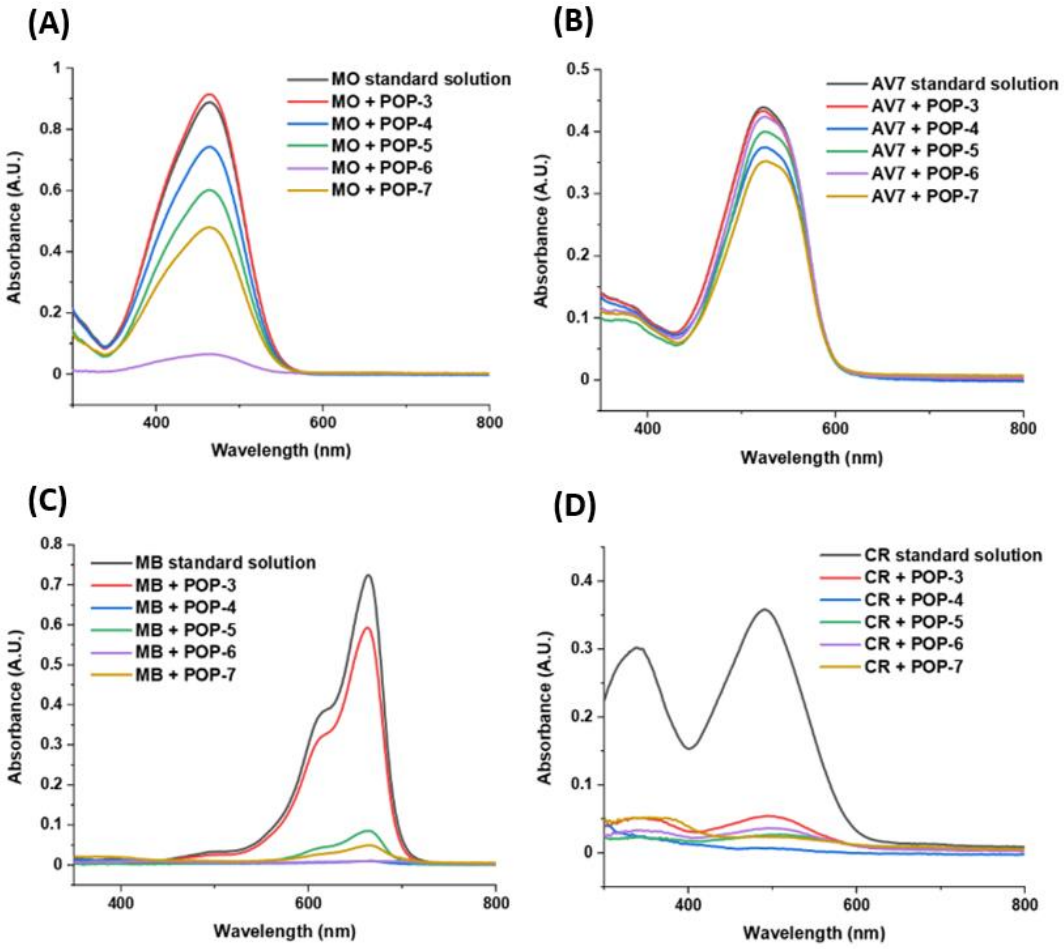

Figure 18: Liquid UV-Vis measurements of adsorption experiments of dyes with POP 3-7. (A) MO, (B)AV7, (C) MB, (D) CR.

Each dye was dissolved and diluted using tap water to prepare a standard stock solution. The use of tap water was the first step towards the aim of simulating wastewater conditions as textile factories generally use tap water in the dying process.[24] The tap water used had a pH of 7.5 and has calcium and magnesium ions present in concentration of roughly 92 mg/L and 6 mg/L, respectively.[186] A standard adsorption experiment was carried out by combining a sample of polymer with a sample of a standard dye solution and shaking overnight. The polymer was separated from the solution and UV-Vis measurements taken to determine any change in concentration (Figure 18). The adsorption experiment was repeated for each dye solution and each POPs 3-7. It was found that the polymers were most successful in adsorbing MO, MB and, CR. However, it was quickly observed that CR precipitated in a tap water solution with no external influence thus, CR was eliminated from further testing.

Superhydrophilic POP-6 was found to be the most successful in adsorbing a range of dyes, particularly MB and MO with adsorption efficiencies of 98% and 93%, respectively. It is noteworthy that POP-6 was able to adsorb both cationic and anionic dyes with over 90% efficiency without the need for changing the pH of solution. Thus, POP-6 was used in all future adsorption experiments with MB and MO. Figure 19 shows the drastic change in colour of the MB dye solution (1.27 x10-5 M) after 18 h contact with 10 mg of POP-6.

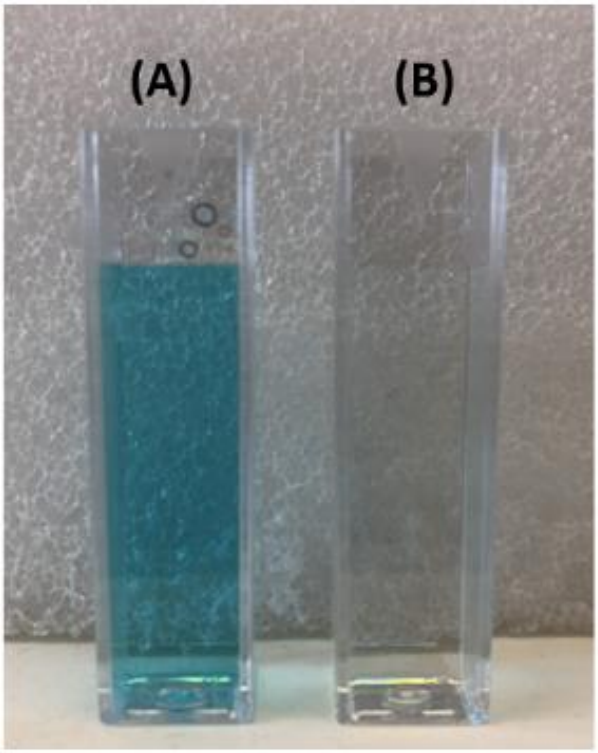

Figure 19: (A) MB stock solution. (B) MB solution after mixing with POP-6 for 18 h (post filtration).

Adsorption efficiency was determined by the following equation:[187]

$$E = (\frac{C_i - C_f}{C_i}) \times 100$$

Equation 2: Adsorption efficiency.[187]

Where: E (%) = adsorption efficiency, C_i & C_f (mg/L) = initial and final concentration of dye.

Generally, the condensation polymers (POPs 5-7) behaved favorably towards the adsorption of the dyes compared to the BH coupling products (POPs 3 and 4). The additional functionality and heteroatom content of the condensation polymers may have allowed for more interactions with the target pollutants. Figure 20 demonstrates some of the possible

interactions between MO and MB with POP-6. Perhaps the most important interactions are the electrostatic interactions (1) between the charged sites of the dye and the areas of high and low electronegativity within the polymers structure.[188] In Section 2.7.2 it was concluded that chemisorption was key in the adsorption process and these electrostatic interactions were vital to the successful adsorption of the dyes. As indicated in Figure 20, there are more possible sites of electrostatic interactions between MB and POP-6 compared to MO suggesting there may be stronger forces of attraction between the cationic dye and the polymer. Furthermore, the charge on MB is delocalized throughout the structure giving multiple points of attraction on the dye itself as opposed to the charge on MO which is localized. The variety of functional groups present in the dyes are also likely to interact with those on the surface of the adsorbate. These interactions can be through hydrogen bonding (2), π-π and π-NH (3) interactions as described by Lui et al.[189] From the results of the pH experiments in Section 2.7.3 we can deduce hydrogen bonding plays a role in the adsorption of both dyes onto the surface of POP-6. At low pH the adsorption of both dyes reduced indicating competitive hydrogen bonding interactions. Additionally, the rate experiments in Section 2.7.2 showed the adsorption process was characteristic of chemisorption and physisorption at pH 3 and pH 11 indicating other physical interactions, such as π-π interactions, were likely to also be taking place. Though all three condensation polymers were capable of having these interactions with the aqueous dyes, POP-6 demonstrated the best interactions with water itself (Section 2.6.2) proving to be favorable for the adsorption of water-based pollutants.

Following the initial adsorption experiments, a number of experiments were undertaken to further understand the interactions between the adsorbate and adsorbent including the calculation of rate and adsorption models of MB and MO with POP-6. Additionally, the effect of simulated wastewater conditions on uptake capacity and the recyclability of POP-6 were explored. A full list of methods can be found in Section 4.2.

A range of control experiments were undertaken to evaluate the impact of external factors. For the standard adsorption experiments, the influence of the method of separation was investigated (Section 7.9, Appendix). It was found that filtration and centrifugation made negligible difference to the concentrations of the dye solutions. Centrifugation was used for all future separations due to the ease of polymer recovery.

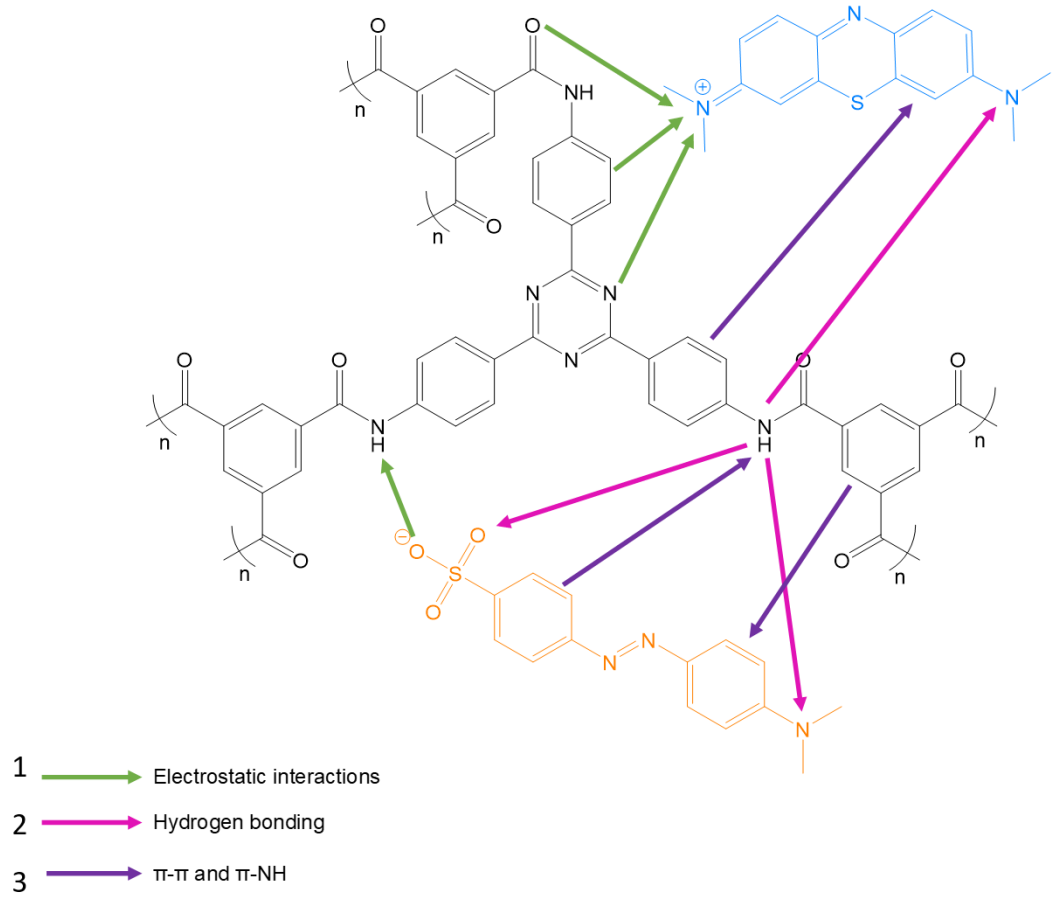

Figure 20: Possible interactions of MB and MO with POP-6.[188, 189]

2.7.2 Rate

Looking at kinetics provides insight into the adsorption pathway and is therefore valuable knowledge for wastewater treatment, especially when considering the design and operation of treatment plants.[190] We can assume the adsorption process is controlled by the interactions at the liquid/solid interface of the adsorbent.[191] To determine the kinetics of the adsorption of MB and MO, Lagergren pseudo first-order and second-order plots were investigated. A number of rate experiments were conducted to achieve this aim. It has been reported that pseudo first-order kinetics for many adsorption processes are only suitable for the initial 20 to 30 minutes, whereas pseudo second-order kinetics require a 24 h period to give an accurate determination.[192] Each dye was prepared and mixed with POP-6 as described in Section 2.7.1. Initially, UV-Vis measurements were taken every 5 minutes for the first half an hour. UV-Vis measurements were then taken every hour for 8 hours and again after 24 hours. The percentage of dye adsorbed over the 24 h period is shown in Figure 21.

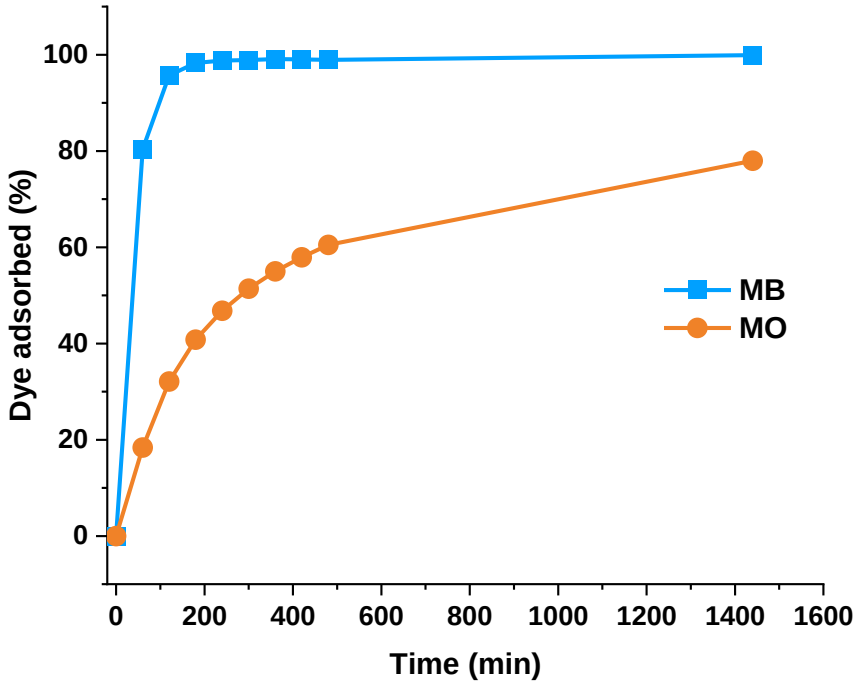

Figure 21: Percentage of dye (MO, MB) adsorbed by POP-6 over 24 h.

The mass of dye adsorbed onto POP-6 at any given time was calculated using the following equation:[193]

$$q_t = \frac{(C_o - C_t) \times V}{M}$$

Equation 3: Mass of dye adsorbed per unit mass of adsorbent.[193]

Where: q_t (mg/g) = mass adsorbed per unit mass of adsorbent at t = time, C_o (mg/L) = initial concentration, C_t (mg/L) = concentration at time t, V (mL) = volume of solution, M (mg) = mass of adsorbent.

To determine the rate of reaction the linearized form of the pseudo first-order and second-order equations were used.

Lagergren pseudo first-order linear equation:[194]

$$\ln(q_e - q_t) = \ln q_e - K_1 t$$

Equation 4: Lagergren pseudo first-order linear equation.[184]

Where: K_1 (min) = pseudo 1st order rate constant, q_e and q_t (mg/g) = mass adsorbed per unit mass of adsorbent at t = time and e = equilibrium, t (min) = time.

Lagergren pseudo second-order linear equation:[194]

$$\frac{t}{q_t} = \frac{1}{K_2 q_e^2} + \frac{1}{q_e} \times t$$

Equation 5: Lagergren pseudo second-order linear equation.[194]

Where: K_2 (mg/min) = pseudo 2nd order rate constant, q_e and q_t (mg/g) = mass adsorbed per unit mass of adsorbent at t = time and e = equilibrium, t (min) = time.

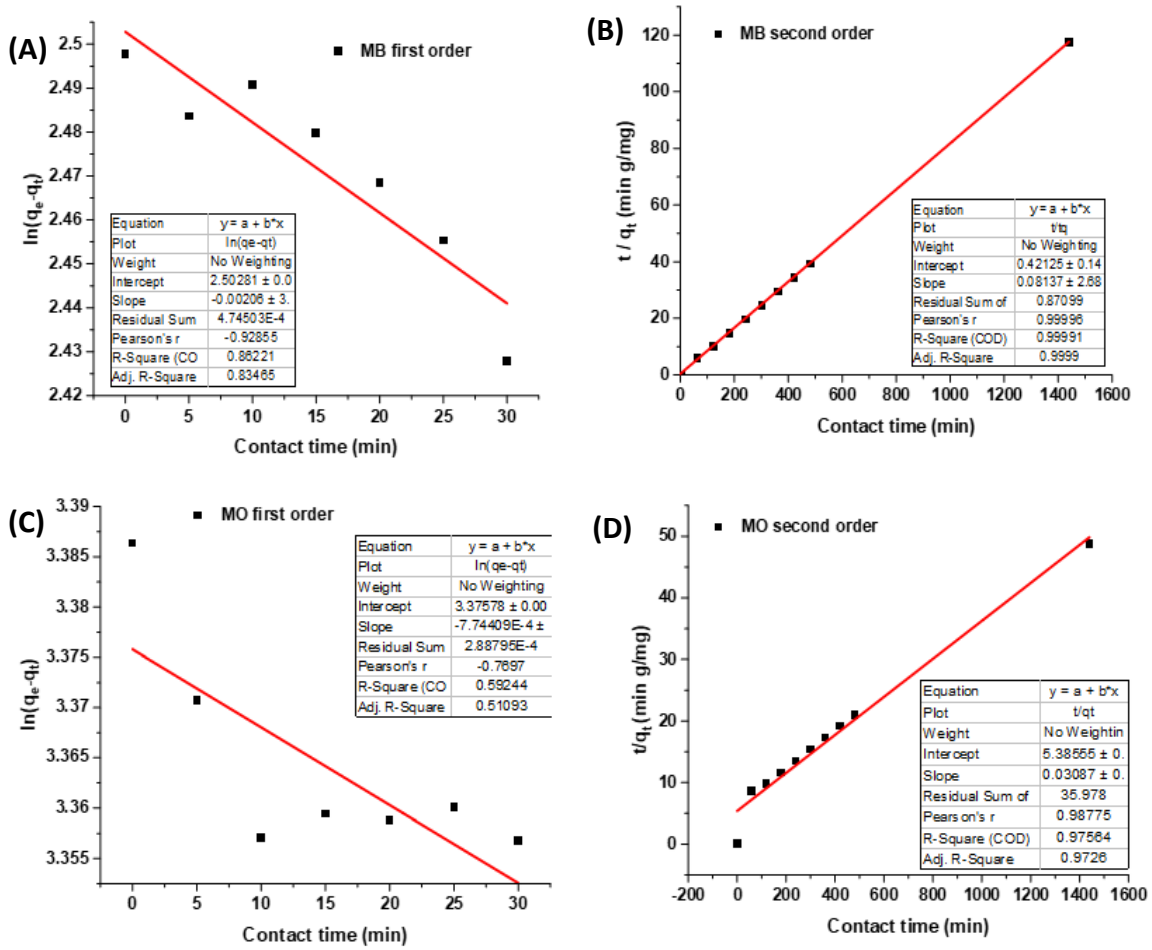

Figure 22: Lagergren pseudo 1st and 2nd order rate plots with regards to POP-6. (A) MB 1st order. (B) MB 2nd order. (C) MO 1st order. (D) MO 2nd order.

A straight-line graph was plotted for each data using Equations 3 and 4, and degree of fit determined to give an R^2 value. The graph with the value closest to 1 indicated the correct kinetic profile for the adsorption of the dye from solution. Figure 22 shows the Lagergren pseudo first-order and second-order plots for MO and MB with regards to POP-6 under standard conditions. The linear pseudo first-order plots gave R^2 values of 0.834 and 0.510 for MB and MO, respectively, whereas the linear pseudo second-order plots gave R^2 values of 0.999 and 0.972, respectively. It was concluded that the adsorption of MB and MO by POP-6 was therefore pseudo second-order. In 2021 Wang et al. found the adsorption of MB onto cellulose fibers was pseudo second-order and concluded chemisorption was taking place.[70] In 2022 He et al. determined the adsorption of MB and MO onto a hyper-crosslinker polymer to be pseudo second-order, deeming the rate of adsorption to depend on the availability of active sites.[195] Thus, it was determined the rate determining step of the

adsorption of MB and MO involved chemisorption and was dependent on the availability of active sites on the surface of the polymer.

In 2019 Huang et al. synthesized porous materials containing triazine rings and amide bonds for the adsorption of Hg^{2+} ions from water. The rate of adsorption was found to be pseudo second-order and the adsorption process was deemed to be chemisorption. It was concluded that chelating interactions between the adsorbent and adsorbate (Figure 23) were responsible for the successful adsorption of Hg^{2+} ions. [162]

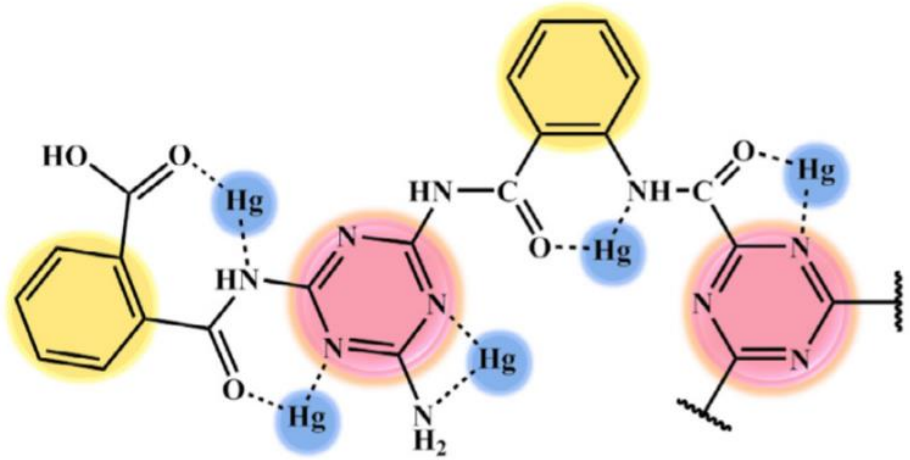

Figure 23: Possible chelating interactions between Hg^{2+} and polymer.[162]

It is hypothesized that similar interactions may therefore be taking place between the charged sites of the dyes and the amide groups and triazine rings within the polymeric structure. The lone pair of electrons on the nitrogen atom within the amide groups are partially delocalized through resonance and the electron density is shifted towards the oxygen atom. The localization of electron density around the oxygen may allow the oxygen to donate electrons to the positively charged site of MB. Conversely, the electron withdrawing effect of the oxygen within the amide bond may allow the carbon and nitrogen atoms to accept electrons from the negatively charged sulfonate group of MO. Due to the polarity of the C=N bonds within the triazine rings more π-electrons may be partially located on the nitrogen atoms, as described by Bartholomew.[196] Thus, the nitrogen atoms within the triazine ring may be open to electrophilic attack from MB, while the carbon atoms within the ring may be reactive towards nucleophile MO.[196,197] It was theorized that for

these reasons POP-6 was able to adsorb MO and MB though chemisorption without the need to change the pH of solution.

The pseudo rate constant (K_2) was calculated from the straight-line graphs giving values of 0.01572 mg/min and 0.00018 mg/min for MB and MO, respectively. The faster rate of MB over MO can also be observed from the percent of dye removed over time (Figure 21). K_2 depends on pH, concentration, time, temperature and agitation.[192] Thus, to further investigate the kinetics of the adsorption, rate experiments at different concentrations, pH levels and temperature were investigated. Table 4 and 5 gives the pseudo rate constants and R^2 values of each pseudo second-order and pseudo first-order rate experiment, respectively, under different experimental conditions.

Table 4: Pseudo second-order experimental data for MB and MO with regards to POP-6 under standard conditions, 40 ℃, pH 11 and pH 3.

Dye	**Intercept**	**Slope**	**q_e (mg/g) (calculated from graph)**	**q_e^2**	**K_2 (mg/min)**	**R^2**	**q_t (mg/g) (experimental data, t = 24 h)**
Standard conditions							
MB	0.4212	0.0813	12.28	151.03	0.0157	0.999	12.242
MO	5.3855	0.0308	32.39	1049.36	0.0001	0.972	29.558
40 ℃							
MB	2.4896	0.0855	11.68	136.63	0.0029	0.994	11.382
MO	0.0374	0.0374	26.70	713.01	0.0374	0.891	23.527
pH 11							
MB	6.7956	0.0911	10.96	120.25	0.0012	0.993	10.490
MO	29.412	0.0880	11.35	128.92	0.0002	0.848	9.817
pH 3							
MB	35.5256	0.6033	1.65	2.74	0.0102	0.992	1.588
MO	20.9398	0.0767	13.02	169.67	0.0002	0.904	11.475

The highest mass adsorbed per unit mass of adsorbent was seen under standard conditions for MB and MO. Interestingly, the mass of MO adsorbed per unit mass of POP-6 was higher than that of MB. The value of q_e can be explained by the difference in concentrations of the stock solutions. The initial weight of MO in each 30 mL sample was 0.37 mg compared to 0.12 mg of MB (to achieve absorbance values of 0.5-1 in UV-Vis measurements). The weight

of POP-6 added to each dye solution was the same at 10 mg. Thus, POP-6 has to remove roughly 3 times the amount of dye from the MO solution compared to the MB solution. Due to the difference in initial dye concentration, the comparison between the rate of adsorption of these dyes is somewhat limited. Nevertheless, we can fundamentally conclude that under standard conditions both dyes were undergoing chemisorption in the rate-determining step.

Table 5: Pseudo first-order experimental data for MB and MO with regards to POP-6 under standard conditions, 40 ℃, pH 11 and pH 3.

Dye	**Intercept**	**Slope**	**q_e (mg/g)**	**K_1 (min)**	**R^2**
Standard conditions					
MB	2.5021	-0.0020	12.20	-6.8666×10^{-5}	0.834
MO	3.3757	-7.7440	29.24	-0.2581	0.510
40℃					
MB	2.4014	-0.0064	11.03	-0.0002	0.922
MO	3.0519	-0.0045	21.15	-0.0001	0.286
pH 11					
MB	2.3364	-0.0108	10.34	-0.0003	0.986
MO	2.2776	-0.0062	9.75	-0.0002	0.858
pH 3					
MB	0.4606	-0.00417	0.995839	-0.00014	0.980
MO	2.4369	-0.0046	11.43	-0.0001	0.971

When considering the rates of reaction under different conditions, it was generally observed the adsorption process was better suited to the pseudo second-order model compared to the pseudo first-order model with a few exceptions. For the adsorption of MO and MB under acidic conditions, both the pseudo first-order and second-order plots fitted the data well. Furthermore, under alkaline conditions fit of the pseudo first-order and second-order plots for MB and MO are almost the same. Finally, the adsorption of MB at 40 ℃ fits both pseudo first-order and second-order models. Consequently, we can conclude that it was not only chemisorption taking place within the adsorption mechanism. In 2021, Sharma et al. found the adsorption of MB using a hydroxyapatite/gold nanocomposite was pseudo first-order and determined that physisorption was involved in the rate determining step. [198] We can infer from the close-fitting pseudo first-order data that physisorption was also taking place in the adsorption process under certain conditions. Thus, it is very likely that physical interaction such as dipole-dipole interactions, hydrogen bonding and π-π interactions were

also taking place. The effect of the changing conditions on the adsorption mechanism is further investigated in Sections 2.7.3 and 2.7.6.

2.7.3 pH

The pH of the dye solution is an important factor in the adsorption process as the charged sites within the structure of the dyes and polymer will interact differently if they are protonated or deprotonated. To investigate this effect, adsorption experiments were undertaken at pH 3 and pH 11. As described in Section 2.7.1, a standard test was carried out with the addition of either HCl or NaCl and Na_2CO_3 to adjust the pH of the dye solutions to pH 3 and pH 11, respectively, and UV-Vis measurements were taken to determine any changes in concentration (Figure 24). To assess the impact of changing the pH on the dye itself, the experiment was replicated without the addition of POP-6 (Section 7.10, Appendix).

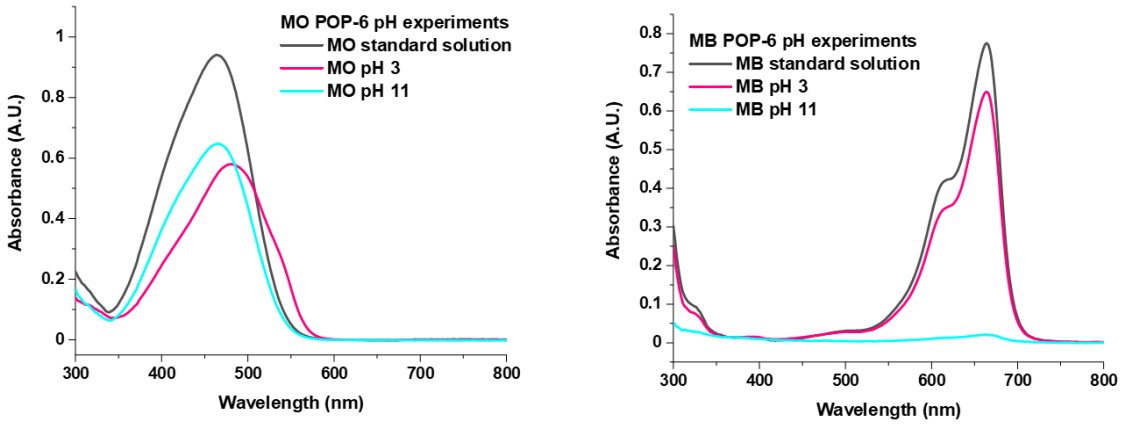

Figure 24: UV-Vis spectra from adsorption experiments of POP-6 with MO (left) and MB (right) at pH 3 and 11.

When investigating the influence of pH on the adsorption process it is important to consider the acid dissociation constants (pKa) of the functional groups within the adsorbent as well as the adsorbate. Firstly the secondary amides within the structure of POP-6 should be considered. The proton of the amide bond does not readily dissociate in water and the amide forms resonance structures (Figure 25). The conjugate acid has a pKa value of -0.5, while the conjugate base has a pKa value of 17. Thus, extreme conditions, outside of the pH range used, are required to protonate or deprotonate the amide group and it can be assumed that the amide takes its usual form during the experiments. Though the amide bond itself may not change due to the pH conditions used, phenyl rings adjacent to the C=O

bond within the amide groups may become electropositive due to the electron withdrawing effect of the amides.[197] This electron withdrawing effect may help to explain some of the adsorption processes observed.

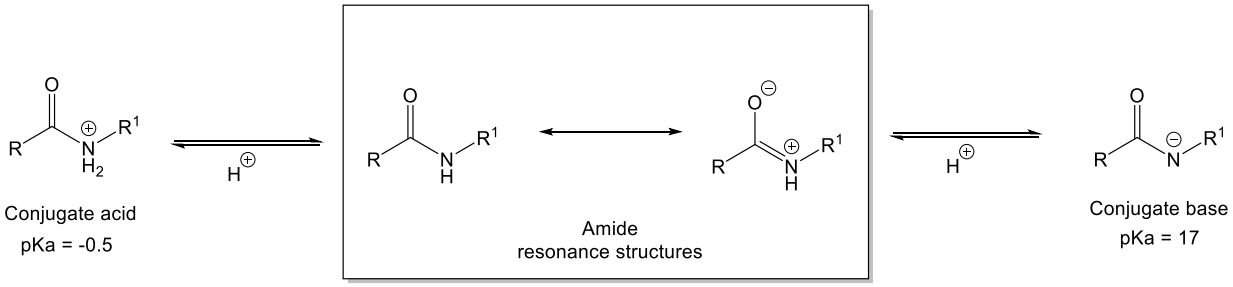

Figure 25: Resonance structures and pKa values of an amide. [232]

Jang et al. reported that melamine has a pKa of 5 and the nitrogen atoms within the triazine ring are protonated first.[199] Thus, we can hypothesize that the triazine ring within POP-6 are protonated at pH 3 and deprotonated at pH 11. Looking at the FTIR data for POP-6 (Section 2.4) we observe a small peak at 3335 cm^{-1} indicative of the primary amine N-H stretching vibration; thus, there is likely also to be a small number of aryl amine end groups within the polymeric structure of POP-6, with pKa values of ~4.[200,201]

Methylene blue is a rather more complex molecule to determine the pKa of. Figure 26 demonstates the different structures of MB over a range of pH values as determined by Bensedira et al. [202] The nitrogen atom within the central ring has a pKa value of 2.6 while the tertiary amines have a pKa value of 11.2. It was reported that between pH 2.6 and the calculated isoelectric point (IEP) of 8.33, MB exists in mono protonated (MBH) and di-protonated (MBH_2^+) forms. At pH values lower than 2.6, all nitrogen atoms within the structure are protonated (MBH_3^{2+}), while at pH values above 8.3, the aromatic nitrogen atom of MB is deprotonated (MB^-).

When considering MB under acidic conditions we can deduce it takes the form of MBH_3^{2+} or MBH_2^+, giving the dye molecule an overall positive charge. Theretically, the positively charged MB molecule would interact favourably with the electron rich oxygen atoms within the amide donds present in the structure of the polymer. However, it was found that the acidic conditions greatly hindered the adsorption of MB. The unfavorable interaction may be due to the presence of positively charged triazine units, protonated amine end groups

and the electropositive phenyl rings within the polymer creating repulsive interactions between MB and POP-6.

In contrast, the presence of the OH^- ions did not hinder the adsorption of MB. We can assume MB is in the MB^- form when under pH 11 (see Figure 26). The negatively charged MB may have favorable electrostatic interactions with the δ^+ carbonyl carbon within the amide groups. Furthermore, the negative charge associated with MB is delocalized due to resonance and may be capable of interacting with the electropositive phenyl rings within the polymer structure. Surprisingly, the repulsion from the negatively charged dye and the polymer end groups does not seem to hinder the adsorption process, perhaps due to the low concentration of the polymer end groups. It has been reported that sodium salts decrease the solubility of MB, causing the dye to aggregate and adsorption to increase.[203,204] It should be noted that keeping an MB solution in alkaline conditions for a week the concentration was severely diminished, indicating these conditions cause the dye to precipitate. However, over an 18 h period these effects were minimal as observed in the control experiments shown in Section 7.10 of the Appendix.

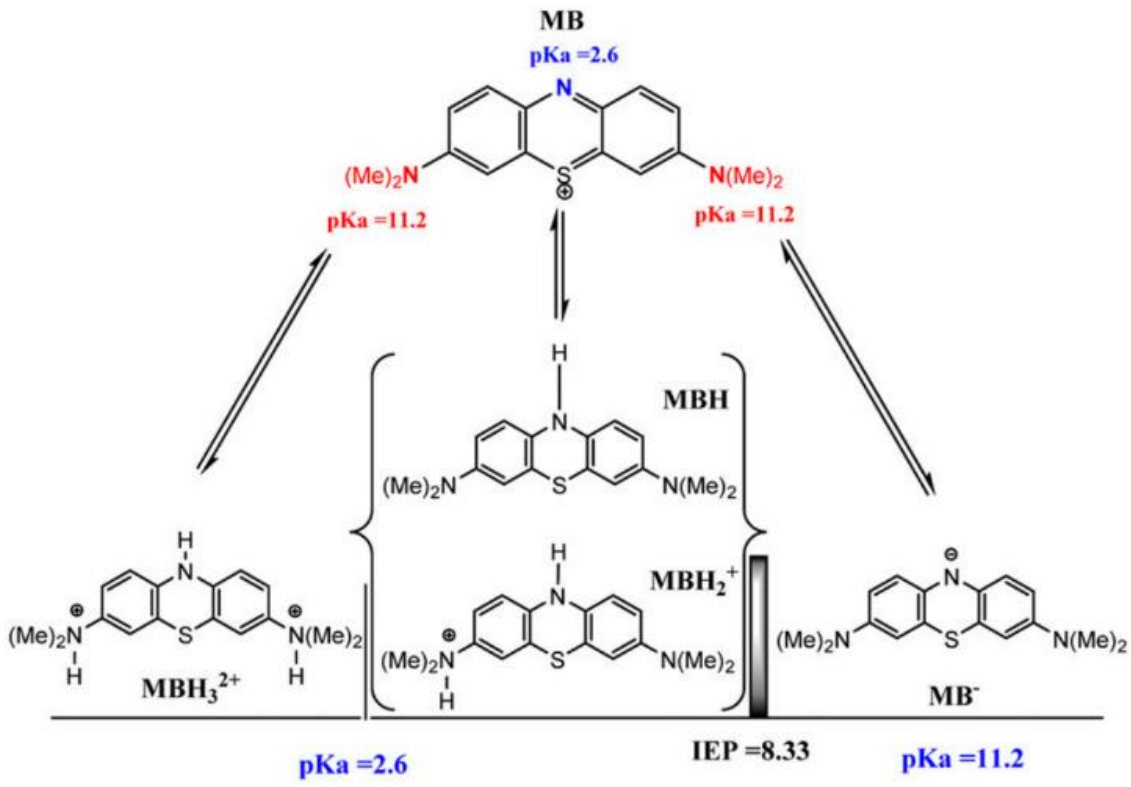

Figure 26: pKa values and structures of MB over a broad pH range.[202]

MO has a pKa value of 3.5,[205] and under acidic conditions the azo group of dye is protonated, giving the dye a positive charge and simultaneously creating a zwitter ion (Figure 27). The sulfonate is unlikely to become protonated as it has a pKa value of around -2. The adsorption of MO was hindered by both acidic and alkaline conditions. At pH 3 the molecule is in its conjugated acid form meaning the azo group is protonated. The protonated form of MO may have repulsive and attractive forces towards the adsorbent and overall the adsorption process was hindered but not completely prevented.

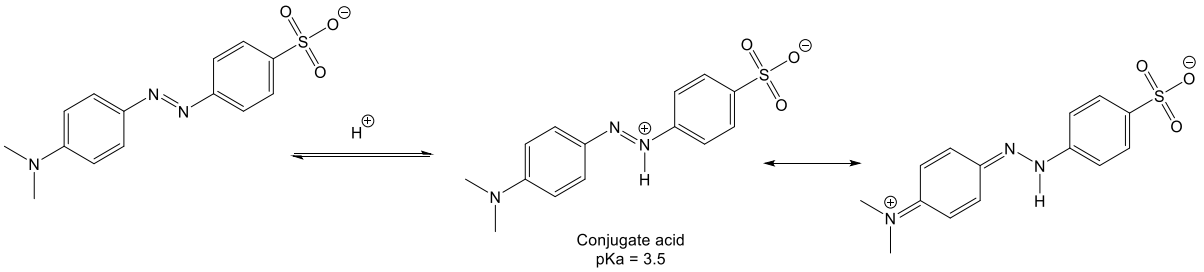

Figure 27: pKa and resonance structures of methyl orange.[205]

At pH 11 MO is not protonated and is negatively charged. Increasing the pH of the solution does not change the chemical structure of the dye. We can assume the end groups within the polymer are also negatively charged and will repel the dye. Some adsorption is still observed however, and can be explained by the potential interactions between the sulfonate group and the electropositive carbons within the amide groups and phenyl rings of the polymer.

2.7.4 Adsorption isotherms

Langmuir and Freundlich isotherm models are widely used to investigate the adsorption mechanism of removing pollutants from water. Traditionally these models were used to determine the adsorption of gasses however, in more recent years the equations have been adapted to better suit the adsorption from liquids giving an insight into their adsorption mechanisms.[206]

To determine which model best fits the adsorption process, a standard test of 5 different concentrations of each dye was conducted. Samples of MO and MB standard solutions were taken and diluted with water before mixing with POP-6. UV-Vis measurements were taken to determine the changes in concentration and the recorded results were plotted to fit a straight-line graph of each adsorption model. The R^2 value of each graph was used to indicate the correct isotherm for each dye.

Langmuir linear equation:[207]

$$\frac{C_e}{q_e} = \frac{1}{Q_o h} + \frac{C_e}{Q_o}$$

Equation 6: Langmuir linear equation.[207]

Where: C_e (mg/L) = concentration at equilibrium, q_e (mg/g) = mass adsorbed per unit mass of adsorbent at equilibrium, Q_o (mg/g) = maximum adsorbent capacity, *h* (L/mg) = Langmuir equilibrium constant related to energy of adsorption.

Freundlich linear equation:[207]

$$\ln(q_e) = \ln\left(K_f\right) + \frac{1}{n} \ln\left(C_e\right)$$

Equation 7: Freundlich linear equation.[207]

Where: C_e (mg/L) = concentration at equilibrium, q_e (mg/g) = mass adsorbed per unit mass of adsorbent at equilibrium, K_f (mg/g)(mg/L) = Freundlich constant, n = adsorption intensity of Freundlich constant.

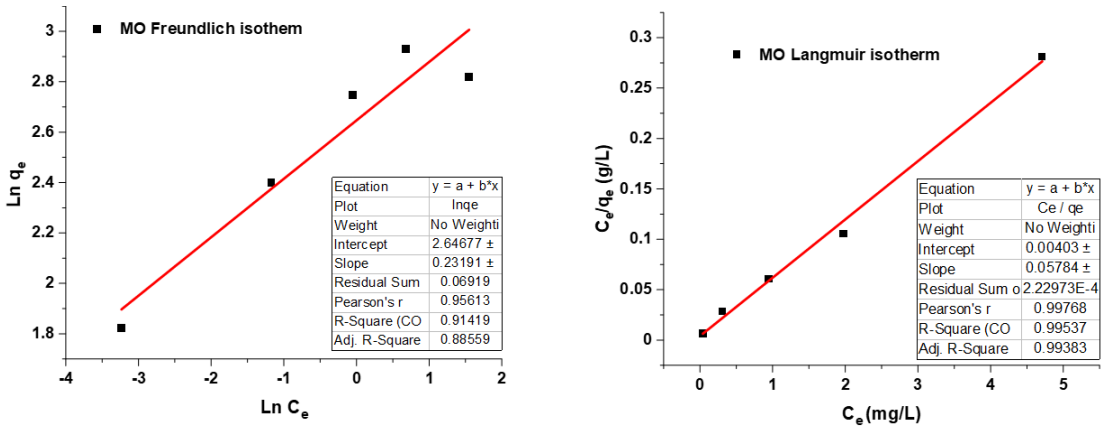

Figure 28: Langmuir (left) and Freundlich (right) adsorption isotherms for MO with POP-6.

From the isotherms shown in Figure 28, MO best fits the Langmuir isotherm with a maximum adsorption capacity of 17 mg/g calculated. The isotherms suggest MO is adsorbed onto a homogeneous surface via chemisorption and a monolayer is formed, as described by Irfan et al.[208] By comparing the data collected from the rate experiments (Section 2.7.2), we observe both the rate and the adsorption isotherm give evidence that shows chemisorption was the primary adsorption mechanism with regards to MO and POP-6. However, the adsorption model of MO can also be seen to fit the Freundlich model, indicating some physical interactions may be present during the adsorption process.

The adsorption studies for MB proved more difficult to obtain due to the excellent adsorption properties demonstrated by POP-6. Figure 29 demonstrates the different isotherm plots obtained for MB. Initially, the same process was conducted for the adsorption experiments of MO however, the result gave a scattered and inaccurate adsorption isotherm plot for both models (Figure 29, A and B). The dye was almost completely removed from the samples and it was found that the adsorption models did not give accurate plots at these low concentrations. A second attempt using higher starting concentrations gave a little more success; three solutions gave incomplete adsorption enabling the data to be plotted for both isotherm models (Figure 29, C and D). From the data it was deduced that the adsorption of MB was slightly better suited to the Freundlich model indicating MB was adsorbed onto a heterogeneous surface via physisorption, with the possibility of multilayers forming. [209,210] However, the data also fits the Langmuir model well and we can conclude more than one mechanism may be responsible for the adsorption of MB. It was theorized that elements of both adsorption mechanisms were taking place,

potentially with MB undergoing chemisorption to the surface of the adsorbate followed by the aggregation of dye molecules forming multiple layers.[211]

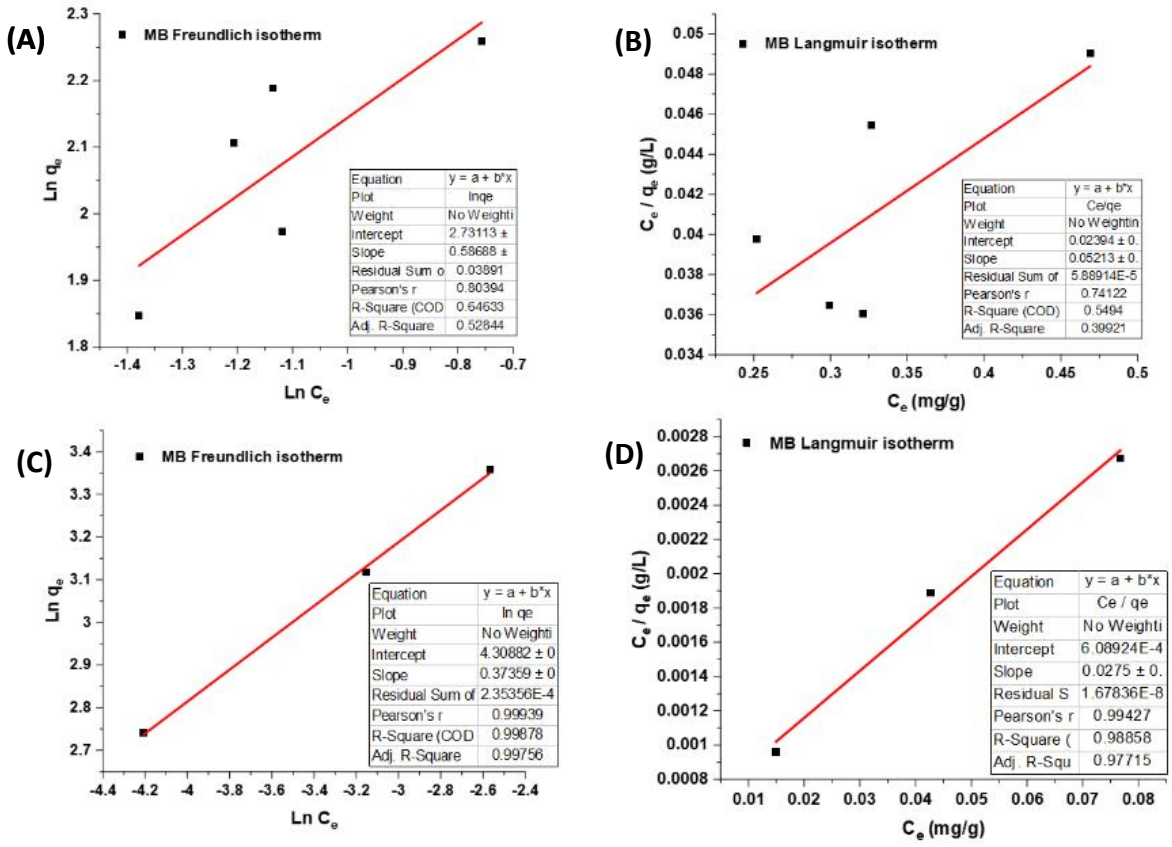

Figure 29: Langmuir (left) and Freundlich (right) adsorption isotherms for MB with POP-6.

2.7.5 Recycling and re-using POP-6

The re-usability of new materials is an important factor in creating porous materials. The more a material can be reused, the less waste is produced from the adsorption process, making it a more sustainable method of removing pollutants. Furthermore, the ease of regeneration also plays a role in the environmental impact of an adsorbent. If harsh chemicals and conditions are needed to re-generate the material, the use of said materials may be outweighed by the costs and waste produced from the process.

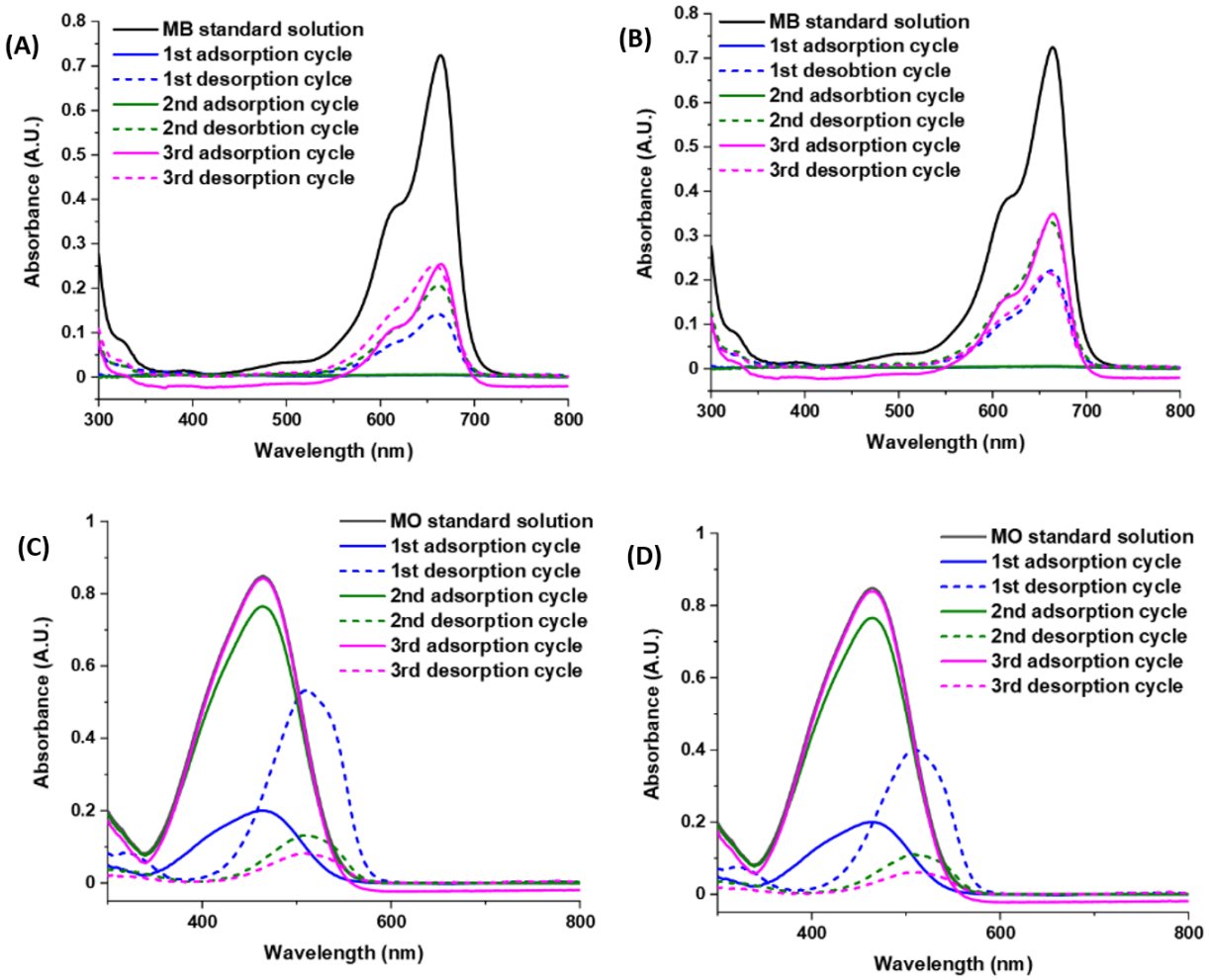

Figure 30: UV-Vis measurements displaying adsorption/desorption tests of POP-6 with MB (A/B) and MO (C/D).

The procedure for the regeneration of the polymer was used as described by Hui et al. in 2021.[212] After a standard adsorption experiment (Section 2.7.1), POP-6 was separated from the dye solution by centrifugation. The polymer was then stirred overnight with methanol and HCl (0.1 mol/L) overnight to desorb the dye from the surface of the polymer. Following

the desorption process, the polymer was washed with sodium carbonate solution (0.1 mol/L), water and, methanol to neutralize and re-generate the material. The polymer was then re-used for a standard adsorption experiment and the process was repeated until the adsorption capacity of the polymer had diminished. The recycling experiments were carried out in duplicate to evaluate the reproducibility of the results. UV-Vis measurements were taken to determine the success of the adsorption and desorption processes, seen in Figure 30. The adsorption efficiency was calculated for each adsorption cycle to evaluate the effectiveness of the recycled polymer (Figure 31).

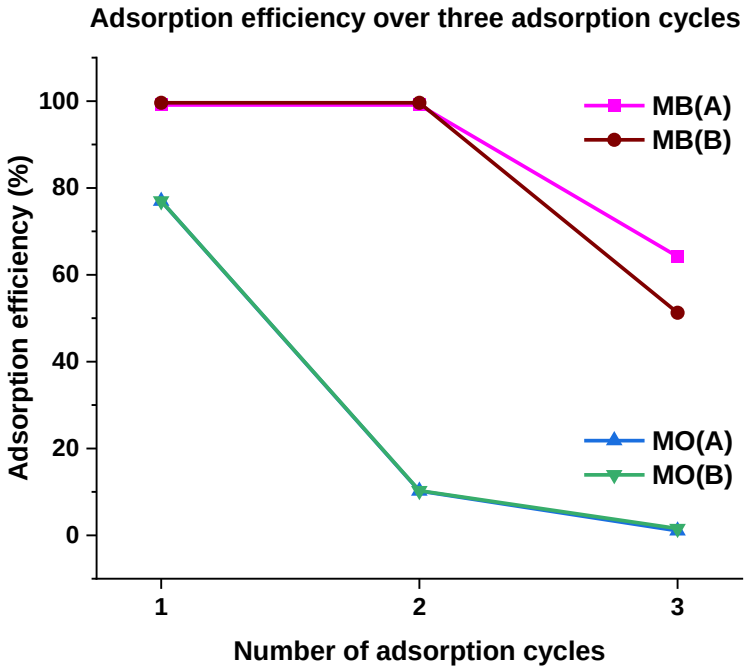

Figure 31: Adsorption efficiency of POP-6 over three adsorption cycles.

With regards to MB, POP-6 was effective in adsorbing the dye for two cycles before the adsorption capacity of the polymer diminished (Figure 29). Going from almost 98% adsorption efficiency in the first and second adsorption cycles to 65% and 52% in the third adsorption cycles for (A) and (B), respectively. In Section 2.7.4, it was found that the adsorption of MB was due to physical interactions as well as chemisorption between the adsorbent and adsorbate. The physiosorbed dye molecules may be more easily desorbed to allow for the adsorption of more dye molecules in future adsorption cycles.

In contrast, the adsorption efficiency of MO greatly diminished after just 1 cycle; going from 77% adsorption efficiency to just 10% for both (C) and (D) (Figure 31). From the adsorption

and rate experiments conducted (Sections 2.7.4 and 2.7.2, respectively) it was concluded that the driving force behind the adsorption of MO was chemisorption. Thus, it can be expected that the desorption of MO from the surface of POP-6 may be more difficult than the desorption of MB. It is likely that most of the active sites on the surface of the polymer would already be bonded to MO molecules making it difficult to adsorb more dye onto the surface of the material in the second cycle.

It was concluded that POP-6 was capable of being reused for the adsorption of MB and perhaps other cationic dyes whereby physisorption played a key role in the adsorption process. The argument can therefore also be put forward that POP-6 is a sustainable material in terms of re-useability when applied to the adsorption of MB and related dyes.

2.7.6 Simulated wastewater conditions

When investigating textile wastewater conditions, it was found effluent conditions varied considerably depending on the dying process and the company responsible for the effluents. It was generally concluded that temperatures of between 35-45 ℃ and pH conditions of 6-11 were often used.[40] Dye adsorption tests were repeated with the addition of sodium salts often used industry, Na_2CO_3 and NaCl (500 mg each) at 40℃ as suggested by Macedo et al.[213] Figure 32 demonstrates the effects of these simulated conditions on the adsorption of MO and MB.

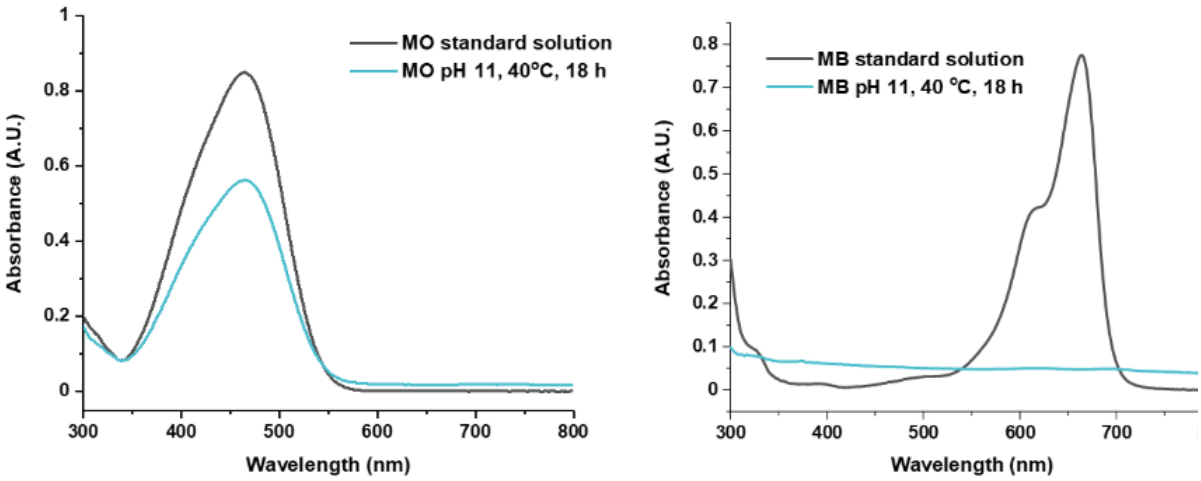

Figure 32: Adsorption of MO (left) and MB (right) with POP-6 under simulated wastewater conditions of pH 11 and 40 ℃.

As previously observed in Section 2.7.3, the addition of sodium salts aided the adsorption of MB and hindered the adsorption of MO. Thus, it was unsurprising to find less successful adsorption for MO than MB under these conditions.

From the control experiments (Section 7.14, Appendix) over a 18 hour period it was observed that the combination of high pH and temperature had a significant effect on MB, showing the concentration severely diminished. It was reported by Samiey that MB will aggregate in the presence of sodium salts due to the salting out effect and an increase in temperature enhanced this effect.[203] We can deduce that this salting out effect may be taking place in the simulated wastewater experiments conducted in this work. Despite the observed precipitation in the control experiments, some adsorption was likely to also be

taking place. In the control experiment the concentration of MB reduced from $1.27x10^{-5}$ M to $5.2x10^{-6}$ M, whereas in the adsorption experiment the concentration reduced from $1.27x10^{-5}$ M to $1.3x10^{-6}$ M. Thus, we can conclude that some adsorption was taking place.

By comparing the adsorption of MO under conditions of pH 11 and 40 °C (Figure 32) to the adsorption under conditions of pH 11 at room temperature (Figure 24) we observe little difference in the adsorption capacity of POP-6. It was found that the simulated conditions had little effect on the dye itself; only a small change was observed in the concentration of MO in the control experiments.

As discussed in Section 2.7.3, when considering the two dyes at pH 11 we can assume they will both be negatively charged. We can also assume any unreacted end groups of the polymer will be negatively charged. It was deduced that some adsorption was possible through interactions with electropositive phenyl rings and the carbonyl carbons present in the structure of POP-6.

Overall, we can conclude that the adsorption of MB and MO under the simulated wastewater conditions was limited. If these conditions were found in textile effluents it is unlikely that POP-6 would be effective in adsorbing the dyes. However, these conditions are extreme and the contents of effluents released by different textile factories can vary significantly. Thus, there is still a possibility that POP-6 could be effective in removing dye pollutants discharged by the textile industry and is further discussed in Section 3.2, Future work.

2.8 Metal adsorption

Following the successful adsorption of MO and MB, the adsorption of heavy metals was investigated. Copper, cobalt and chromium were chosen to be studied as these metals are used in the textile industry and can have harmful effects on the environment.[214]

Table 6: Metal and ligand classification.[233]

	Metals (acids)	**Ligands (bases)**
Hard	Cr(VI), Cr(III), Co(III), Ti(IV), Fe(III), Mg(II), Sn(II), Al(III)	NH_3, OH^-, F^-, Cl^-, CH_3COO^-, RNH_2, SO_4^{2-}, H_2O, ROH, R_2O
Soft	Hg(II), Pt(II), Pd(II), Cd(II), Au(I), Cu(I), Ti(I), Ag(I)	S, I^-, PR_3, RSH, CN^-, CO, C_6H_6, R^-, H^-, RNC, C_2H_4
Borderline	Co(II), Ni(II), Cu(II), Fe(II), Zn(II), Pb(II), Sn(II)	N_2, Br^-, NO_2^-, SO_3^{2-}, N_3^-

The ionic theory of metal-to-ligand interactions says that like will react with like. We can think of metal ions as Lewis acids and their ligands as Lewis bases. 'Hard' acids are those with a small ionic radius with high positive charges whereas, 'soft' acids generally have a larger ionic radius with a less positive charge. Similarly, 'hard' bases have a smaller ionic radius and a larger negative charge in contrast to 'soft' bases that are larger in size and have a smaller negative charge. There is also a third category made up of ions that have both 'hard' and 'soft' characteristics; these are referred to as borderline. Table 6 gives examples of what categories different acids and bases fall into.

It has been reported that heavy metal ions can have chelating interactions with hetero-atoms within the structure of a POP and bind to its surface.[215–218] For instance, Liu et al. demonstrated effective copper adsorption by functionalizing adsorbent materials with polyamides.[219]

2.8.1 Metal adsorption experiments

Stock solutions of $CuCl_2$, $CoCl_2$ and, $CrCl_3$ were prepared and the adsorption tested (as described in Section 2.7.1) with POPs 3-7 (Figure 33).

No visible reduction in concentration from the standard solutions was observed after exposure to the various POP materials. We can therefore assume that no adsorption had taken place. Potentially the use of a more specific analytic technique such as atomic adsorption spectroscopy could have shown if there were any minor changes in concentration. However, given that there was no visible indication of adsorption from the UV-Vis spectrum it was not deemed necessary to further analyse the samples.

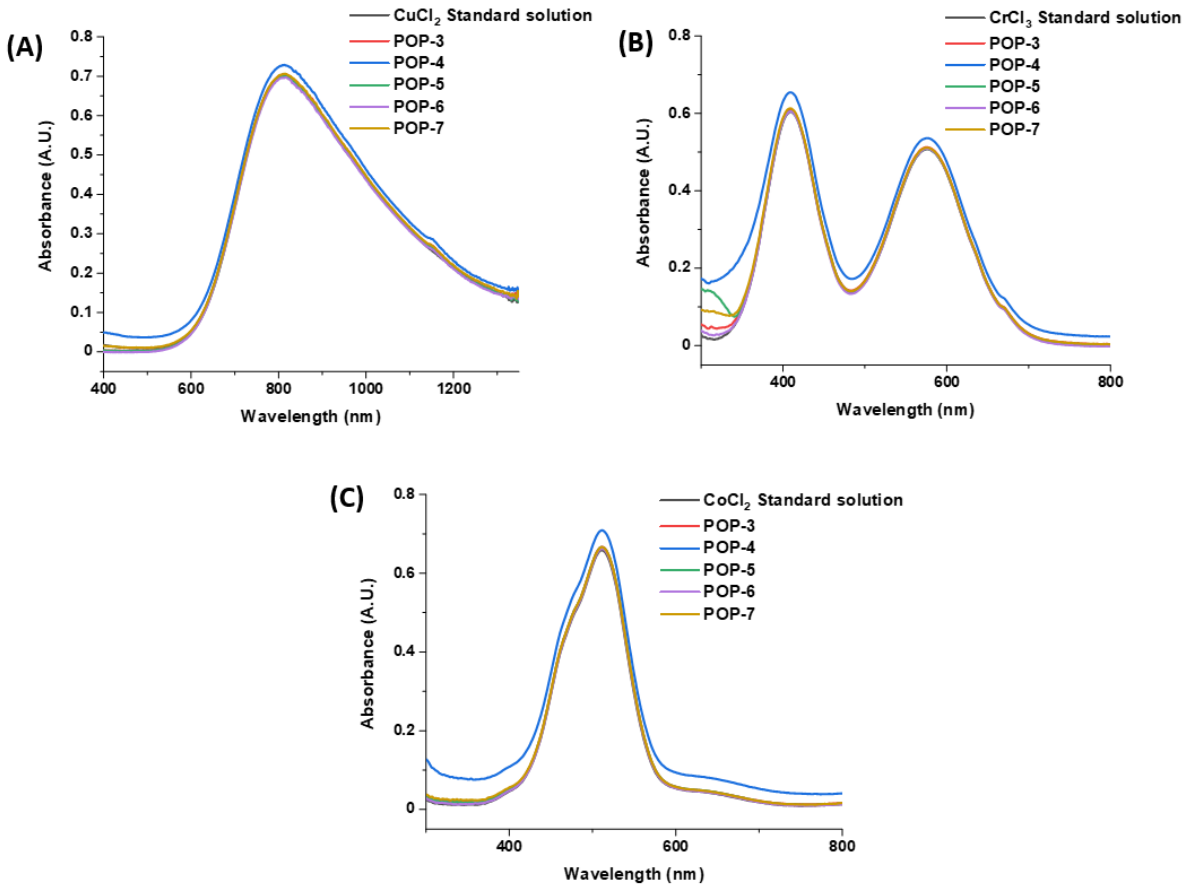

Figure 33: Metal adsorption studies of Cu(II), Cr(III), and Co(II) with POP-6 (left-right).

Theoretically, the metal ions used should be attracted to the heteroatoms within the structure of the polymers. In particular, Zhao et al. found that metal ions Co(II), Cu(II) and Cr(III) have strong interactions with porous polymers containing hooped amino-group

chains.[218] Additionally, Anfar et al. synthesized amino functionalized porous carbon that demonstrated strong chelating interactions with Cu(II) and Pb(II) ions in solution.[220] However, there are other factors that influence the adsorption of metal ions including pH, temperature, contact time, concentration, adsorbent dosage and adsorbent surface properties.[221] Typically porous materials that have been successful in adsorbing metal ions have had large surface areas and are microporous in nature as well as having hetero-atoms or negatively charged atoms within their structures.[222] The materials produced in this research have little porosity and available pores are mostly in the mesoporous region. Therefore, there are less accessible binding sites for metal ions to interact with and those that are available are not the ideal size to trap the small metal ions. To achieve metal adsorption a more in-depth study into the properties and therefore synthesis of the materials is required and is discussed in Sections 3.1 and 3.2. Due to the lack of success with the initial adsorption experiments, other reaction conditions (pH, temperature, concentration) were not investigated.

3 Conclusion

3.1 Project reflection and conclusions

The main aim of this project was to synthesize porous materials capable of adsorbing water-based pollutants produced by the textile industry. To this end, five porous organic polymers (POPs 3-7) were successfully synthesised using BH coupling and condensation polymerization. Of these five materials it is believed that four (POP-3, POP-4, POP-6 and POP-7) have not been reported in literature and are therefore novel. The materials contain an abundance of heteroatoms along with a range of functional groups, which makes them materials of interest for the intended application – water purification. To this end we can consider the first objective of the project (synthesis of porous materials containing a high concentration of heteroatoms) to have been achieved.

Three triazine monomers (melamine, TAPT, TAPT-N) were used as core molecules in the polymerization reactions explored in this work. It was found that the BH coupling reaction of the TAPT core of POP-3 and POP-4 was superior for reasons related to solubility and steric hinderance, with significantly better yields than materials synthesized using melamine. However, for the condensation polymerization all three cores were suitable for synthesis and produced POPs 5-7 in good yields. By comparing the adsorption studies of POP-3 and POP-4 it is evident POP-4 has a higher adsorption capacity towards organic dyes, explained by the extended polymeric structure of POP-4 compared to POP-3. When comparing the adsorption capacity of POPs 5-7 we observe all were effective in adsorbing at least one organic dye. However, POP-6 was identified as superior; having the best range of dye adsorption compared to the other materials produced. The surface areas of the materials produced were generally low and the pore sizes fell mostly within the mesoporous range. POP-3 and POP-5 had the largest surface areas of 72 m^2/g and 81 m^2/g, respectively, while POP-6 had a surface area of just 22 m^2/g. Further tuning of the synthesis to increase the surface area of POP-6 may increase the availability of active sites, potentially increasing the adsorption capacity of the material.

Though POP-6 possessed low porosity, it was capable of effectively interacting with aqueous dyes. Rate experiments reviled the adsorption of dyes MO and MB with regards to POP-6 were pseudo second-order, meaning the rate-determining step was governed by

chemisorption. The adsorption isotherms of MB and MO were studied and the conclusions drawn were in agreement with those drawn from the rate experiments. The adsorption of MO was characteristic of the Langmuir model, indicative of monolayer chemisorption. The adsorption of MB was characteristic of the Freundlich model, indicative of multilayer physisorption. However, both adsorption models fitted the data well and it was therefore concluded that both chemical and physical processes were important in the adsorption of MB and MO onto POP-6. It was advantageous that POP-6 was capable of interacting with pollutants through physical and chemical processes as the possible interactions between the adsorbent and adsorbate were maximized. Furthermore, POP-6 interacted with both anionic and cationic dyes without changing the pH of solution. We can attribute this desirable property to the range of heteroatoms and functional groups within the structure of the polymer creating ample opportunity to interact with the target dye molecules. Furthermore, when considering applications such as water filtration, it is favorable to be able to adsorb pollutants without the need to change the environment they are adsorbed in.

POPs are well known for their chemical and thermal stability and should therefore be re-used to reduce waste, make them more sustainable and cost-effective. The re-usability of POP-6 was evaluated by conducting adsorption and desorption cycles with dyes MO and MB. It was found that POP-6 was more effective at desorbing and re-sorbing MB over MO. The adsorption of MB was deemed to be due to chemisorption and physisorption whereas, the adsorption of MO was mainly attributed to chemisorption. Thus, desorbing the physisorbed MB molecules from the surface of POP-6 was easier than desorbing the chemisorbed MO molecules meaning POP-6 was more effective at removing MB from water for multiple cycles compared to MO. It can be said POP-6 was effective for re-use with regards to MB and potentially other positively charged dyes. The second objective of the project was therefore successfully addressed and achieved.

Following the successful adsorption of dyes MO and MB, simulated wastewater conditions were investigated. To this end, heat and high concentrations of sodium salts were used to simulate some of the conditions that may be found in industry. The adsorption of MB appeared to be effective under these simulated conditions. However, it was found that the conditions themselves caused the dye to precipitate, though some adsorption was still observed. The adsorption of MO was hindered by the simulated conditions due to

electrostatic repulsions between the negatively charged dye and the polymer. We can conclude POP-6 would not be very effective at adsorbing dyes MO and MB from wastewater under high pH and temperature conditions. However, the conditions tested were extreme and further exploration into less harsh conditions would be of interest. We can consider the third objective of the project addressed.

Unfortunately, the materials synthesised were incapable of adsorbing heavy metal ions from water. It has been reported in literature that a high surface area and microporosity is needed along with the presence of heteroatoms or charged sited within the material to successfully adsorb heavy metal ions from water. With more time the synthesis of these materials could have been further optimized and a successful metal adsorption may have been achieved.

Overall, the main aim of the project was achieved. A number of porous materials capable of adsorbing toxic dyes typically produced by the textile industry were synthesized. POPs with different triazine cores produced materials with considerably different surface areas, adsorption abilities and hydrophilicity. Despite the low surface area observed, POP-6 was identified as the best adsorbent due to its superior ability to adsorb a number of toxic dyes. It was concluded that materials with high surface areas do not directly correspond to materials with superior adsorption towards water-based pollutants. Other factors such as hydrophilicity and heteroatom content play an important role in the adsorption of dyes from water.

3.2 Future work

Future work should focus on improving the synthetic yields and BET surface areas of the POPs. To the authors knowledge, the synthesis of POPs 3, 4, 6 and, 7 have not been published. Thus, further investigation into their syntheses could result in higher yields and porosity. A full investigation of the Hansen solubility parameters of each reaction and trialing a range of monomer ratios could provide insight into the best reaction conditions and therefore yields. To see an improvement in the BET surface area of the materials, further exploration of the Bristol-BXJ method may be undertaken. The addition of inorganic salts with the aim of tuning HSPs, and thus porosity, within the materials has been investigated for BH coupling reactions and has been touched upon in this work. However, the addition of salts was not investigated for the condensation reactions. Therefore, a full and rounded investigation into these methods could help improve both the synthetic yields and porosity of the polymers.

The aim of adsorbing heavy metal ions from solution is still of great interest. Higher porosity and smaller pore sizes may be more attractive for metal binding. Additionally, post synthetic modification of polymers has shown to improve the adsorption capacity of a variety of materials as well as heavy metals and would therefore be of interest to explore in the future.

The aim of testing the adsorption capacity of the materials under simulated wastewater conditions was addressed however, the results were less than desirable. Many textile effluents are not only of high pH and temperature; they may contain multiple types of dyes, suspended solids, species of COD and BOD, heavy metals and, have varying pH and temperatures. It would be of interest to further explore different waste effluent conditions to fully evaluate how these materials may perform under real-world conditions.

It is of interest to expand the scope of this work and produce materials that are multifunctional. This work was focused on the adsorption of pollutants from water. However, POPs and more specifically CMPs are important in electronic applications. POP-4 showed evidence of a highly conjugated system and therefore has potential to be useful in energy storage applications such as electrode materials for batteries or supercapacitators.

Finally, to improve the reliability of this work, each experiment should be repeated in triplet to account for errors and anomalies observed. Repetition of experiments in combination with fully exploring the synthetic procedures would give further confidence in the conclusions reached for this investigation. Furthermore, to fully characterize the materials produced a few additional analytical techniques should be explored. Thermal gravimetric analysis should be undertaken to assess the degree of thermal stability. Energy dispersive X-ray analysis would help to define the amount of hetero atoms and the overall composition of the materials. Finally, BET analysis of the materials after adsorption and desorption of dyes should be undertaken to understand the pore-filling behavior of these processes.

4 Experimental

4.1 Synthesis

4.1.1 POP-1

A dry Schlenk tube was charged with melamine (126 mg, 1 mmol), 1,4-dibromobenzene (353.7 mg, 1.5 mmol), $Pd(dba)_2$ (dba = dibenzylideneacetone, 17.3 mg, 0.03 mmol), 2-dicyclohexylphosphino-2',4',6'-triisopropylbiphenyl (XPhos, 21.5 mg, 0.045 mmol), and sodium *tert*-butoxide (NaO*t*Bu, 192.2 mg, 2 mmol) and placed under a nitrogen atmosphere. Dry DMSO (40 mL) was added, the reaction mixture was heated under stirring to 180°C and left for 120 h. 2 M HCl was added to the reaction mixture and the resultant precipitate was centrifuged and washed with hot MQ water, chloroform and methanol (200 mL each) and dried under vacuum for 48 h.

4.1.2 POP-2

A dry Schlenk tube was charged with melamine (63 mg, 0.5 mmol), 1,4-dibromobenzene (353.7 mg, 1.5 mmol), *p*-phenylenediamine (54 mg, 0.5 mmol), $Pd(dba)_2$ (dba = dibenzylideneacetone, 17.3 mg, 0.03 mmol), 2-dicyclohexylphosphino-2',4',6'-triisopropylbiphenyl (XPhos, 21.5 mg, 0.045 mmol), and sodium *tert*-butoxide (NaO*t*Bu, 192.2 mg, 2 mmol) and placed under a nitrogen atmosphere. Dry DMSO (40 mL) was added, the reaction mixture was heated under stirring to 180°C and left for 120 h. 2 M HCl was added to the reaction mixture and the resultant precipitate was centrifuged and washed with hot MQ water, chloroform and methanol (200 mL each) and dried under vacuum for 48 h.

4.1.3 TAPT

A dry 100 mL two neck round bottom flask was charged with 4-aminobenzonitrile (767 mg, 6.5 mmol) under inert conditions and immersed into an ice and water bath. Trifluoromethanesulfonic acid (2 mL) was added dropwise for 20 minutes maintaining a temperature of 0°C. The temperature was allowed to rise to room temperature and the resultant mixture was stirred for 24 h under nitrogen atmosphere. After completion, 20 mL distilled water was added to the mixture and neutralized by adding 2 M NaOH solution until the pH reached 7. The resultant product was filtered and washed several times with distilled water and ethanol. The product was dried under vacuum for 24 h.[223]

4-Aminobenzonitrile:

^{1}H NMR (400 MHz, $CDCl_3$) δ 7.44 – 7.40 (m, 2H), 6.67 – 6.62 (m, 2H), 4.12 (s, 2H).
^{13}C NMR (101 MHz, $CDCl_3$) δ 163.64, 150.26, 133.82, 114.44, 100.44.

TAPT:

^{1}H NMR (400 MHz, DMSO-d_6) δ: δ 8.34 (d, *J* = 8.7 Hz, 6H), 6.68 (d, *J* = 8.7 Hz, 6H), 5.88 (s, 6H).
^{13}C NMR (101 MHz, DMSO) δ 169.54, 152.95, 130.11, 122.90, 113.08.

4.1.4 POP-3

A dry Schlenk tube was charged with TAPT (88.5 mg, 0.25 mmol), 1,4-dibromobenzene (176.85 mg, 0.75 mmol), $Pd(dba)_2$ (dba = dibenzylideneacetone, 17.3 mg, 0.03 mmol), 2-dicyclohexylphosphino-2',4',6'-triisopropylbiphenyl (XPhos, 21.5 mg, 0.045 mmol), and sodium *tert*-butoxide (NaO*t*Bu, 192.2 mg, 2 mmol) and placed under a nitrogen atmosphere. Dry THF (30 mL) was added and the reaction mixture was heated under stirring to 65℃ for 48 h. The reaction was cooled to room temperature and 30 mL methanol was added and stirred for 1 h. The resultant precipitate was washed with hot MQ water, chloroform and methanol (200 mL each) and dried under vacuum for 48 h.[117]

4.1.5 POP-4

A dry Schlenk tube was charged with TAPT (88.5 mg, 0.25 mmol), 1,4-dibromobenzene (353.7 mg, 1.5 mmol), *p*-phenylenediamine (81mg, 0.375 mmol), $Pd(dba)_2$ (dba = dibenzylideneacetone, 17.3 mg, 0.03 mmol), 2-dicyclohexylphosphino-2',4',6'-triisopropylbiphenyl (XPhos, 21.5 mg, 0.045 mmol), and sodium *tert*-butoxide (NaO*t*Bu, 192.2 mg, 2 mmol) and placed under a nitrogen atmosphere. Dry THF (30 mL) was added and the reaction mixture was heated under stirring to 65℃ for 48 h. The reaction was cooled to room temperature and 30 mL methanol was added and stirred for 1 h. The resultant precipitate was washed with hot MQ water, chloroform and methanol (200 mL each) and dried under vacuum for 48 h.

4.1.6 POP-5

A dry two neck round bottom flask, equipped with a condenser and a Dean Stark tap and charged with melamine (189 mg, 1.5 mmol) and trimesic acid (105 mg, 0.5 mmol). Dry DMSO (25 mL) was added and the reactants were heated under stirring to 135℃ for 96 h. The resultant precipitate was filtered and washed with hot MQ water, methanol and THF (200 mL each). The product was further purified by Soxhlet extraction with acetone for 24h and dried under vacuum for 48 h.[162,163]

4.1.7 POP-6

A dry two neck round bottom flask was equipped with a condenser and dean stark tap and charged with trimesic acid (83 mg, 0.5 mmol) and TAPT (177 mg, 0.5 mmol). Dry DMSO (25 mL) was added and the reactants were heated under stirring to 135℃ for 96 h. The resultant precipitate was filtered and washed with hot MQ water, methanol and, THF. The product was further purified by Soxhlet extraction with acetone for 24h and dried under vacuum for 48 h.

4.1.8 TAPT-N

A dry two neck round bottom flask was charged with 6-aminonicotinonitrile (773.5 mg, 6.5 mmol) under inert conditions and immersed into an ice and water bath. Trifluoromethanesulfonic acid (2 mL) was added dropwise for 20 minutes maintaining a temperature of 0℃. The temperature was allowed to rise to room temperature and the resultant mixture was stirred for 24 h under nitrogen atmosphere. After completion, distilled water (20 mL) was added to the mixture and neutralized by adding 2 M NaOH solution until the pH reached 7. The resultant product was filtered and washed several times with distilled water and ethanol and dried under vacuum for 24 h.

6-aminonicotinonitrile:

^{1}H NMR (400 MHz, DMSO-d_6) δ: 8.31 (dd, *J* = 2.3, 0.8 Hz, 1H), 7.67 (dd, *J* = 8.8, 2.4 Hz, 1H), 7.00 (s, 2H), 6.48 (dd, *J* = 8.8, 0.8 Hz, 1H).

^{13}C NMR (101 MHz, DMSO) δ 161.56, 153.22, 139.33, 118.99, 107.74, 94.56.

TAPT-N:

^{1}H NMR (400 MHz, DMSO-d_6) δ: 9.20 (dd, *J* = 2.3, 0.7 Hz, 1H), 8.50 (dd, *J* = 8.8, 2.4 Hz, 1H), 6.79 (s, 2H), 6.58 (dd, *J* = 8.8, 0.8 Hz, 1H).

^{13}C NMR (101 MHz, DMSO) δ 169.02, 162.44, 150.50, 136.91, 119.38, 107.41.

4.1.9 POP-7

A dry 100 mL two neck round bottom flask was equipped with a condenser and a Dean Stark tap, then charged with TAPT-N (250 mg, 0.7 mmol) and trimesic acid (127 mg, 0.6 mmol). Dry DMSO (25 mL) was added and the reactants were heated under stirring to 135^{o}C for 92 h. The resultant precipitate was filtered and washed with hot MQ water, methanol and THF (200 mL each). The product was further purified by Soxhlet extraction with acetone for 24h and dried under vacuum for 48 h.

4.1.10 Summary table of synthesis (POP-1 to POP-7)

Reaction (starting materials)	**Molar ratios**	**Solvent (anhydrous)**	**Temperature (℃)**	**Time (h)**	**Additional reagent**	**Maximum yield achieved (%)**
POP-1 *(melamine, 1,4-dibromobenzene)*	1:1.5, 1:2, 1:3, 2:1, 3:1	DMSO	180	48-168	N/A	6
POP-2 *(melamine, 1,4-dibromobenzene, p-Phenylenediamine)*	1:6:3, 1:3:1	DMSO	180	48-168	N/A	1
POP-3 *(TAPT, 1,4-dibromobenzene)*	1:3	DMSO	180	48-168	N/A	10
POP-3 *(TAPT, 1,4-dibromobenzene)*	1:3	THF	65	72	N/A	98
POP-3 *(TAPT, 1,4-dibromobenzene)*	1:3	THF	65	72	$NaNO_3$	91
POP-4 *(TAPT, 1,4-dibromobenzene, p-Phenylenediamine)*	1:6:3	DMSO	180	48-168	N/A	10
POP-4 *(TAPT, 1,4-dibromobenzene, p-Phenylenediamine)*	1:6:3	THF	65	72	N/A	39
POP-4 *(TAPT, 1,4-dibromobenzene, p-Phenylenediamine)*	1:6:3	THF	65	72	$NaNO_3$	7
POP-4 *(TAPT, 1,4-dibromobenzene, p-Phenylenediamine)*	1:9:3	THF	65	72	N/A	11
POP-5 *(melamine, trimesic acid)*	3:1	DMSO	135	72	N/A	62
POP-6 *(TAPT, Trimesic acid)*	1:1	DMSO	135	72	N/A	45
POP-6 *(TAPT, Trimesic acid)*	1.15:1	DMSO	135	72	N/A	87
POP-7 *(TAPT-N, Trimesic acid)*	1.15:1	DMSO	135	72	N/A	67

Table 7: Summary of rection conditions investigated for POP-1 to POP-7.

4.2 Dye adsorption

4.2.1 Dye stock solutions

A standard solution of each dye was made up using tap water to give a reliable UV-vis absorbance spectrum (absorbance below 1 in accordance with the Beer-Lambert law) with concentrations of 1.27 $x10^{-5}$ M, 3.85 $x10^{-5}$ M, 3.45 $x10^{-5}$ M, 1.93 $x10^{-5}$ M for MB, MO, AV7 and, CR, respectively.

4.2.2 Standard tests

A centrifuge tube was charged with polymer (POP 3-7, 10 mg) and dye solution (30 mL). The centrifuge tube was sealed and placed on an orbital shaker at room temperature for 18 h. The polymer-dye mixture was then separated by centrifugation and UV-Vis measurements were taken to determine any change in concentration. The procedure was repeated for each polymer and dye solution.

4.2.3 pH tests

A centrifuge tube was charged with POP-6 (10 mg) and dye solution (MB or MO, 30 mL). NaCl and Na_2CO_3 (500 mg each) were added to the tube to reach pH 11. The centrifuge tube was sealed and placed on an orbital shaker at room temperature for 18 h. The polymer-dye mixture was then separated by centrifugation and UV-Vis measurements were taken to determine a change in concentration. The procedure was repeated for each dye solution.

A centrifuge tube was charged with POP-6 (10 mg) and dye solution (MB or MO, 30 mL). HCl (0.1 M, 1 mL) was added to the tube to reach pH 3. The centrifuge tube was sealed and placed on an orbital shaker at room temperature for 18 h. The polymer-dye mixture was then separated by centrifugation and UV-Vis measurements were taken to determine a change in concentration. This procedure was repeated for each dye solution.

4.2.4 Dye standard rate test

A centrifuge tube was charged with POP-6 (10 mg) and dye solution (MB or MO, 30 mL). The centrifuge tube was sealed and placed on an orbital shaker at room temperature. For the first half an hour UV-Vis measurements were taken every 5 minutes. After half an hour, UV-Vis measurements were taken every hour for 7 h and again after 24 h.

4.2.5 Dye adsorption studies

Five different centrifuge tubes were charged with POP-6 (10 mg) and dye solution (MB or MO, 30 mL) with concentrations differing by 6 $x10^{-5}$ M. The centrifuge tubes were sealed and placed on an orbital shaker at room temperature for 18 h. The polymer-dye mixture was separated by centrifugation and UV-Vis measurements were taken to determine a change in concentration. This procedure was repeated for each dye solution.

4.2.6 Recycling tests

A standard adsorption test for MO and MB with POP-6 was conducted as described in Section 4.2.1. The remaining dye solution was removed by centrifuge leaving POP-6. To the tube methanol (8 mL) and HCl (0.1 M, 12 mL) was added and placed on an orbital shaker at room temperature for 18 h. The mixture was separated by centrifugation and UV-Vis measurements were taken to determine the concentration of dye desorbed from the polymer. The polymer was then washed with Na_2CO_3 solution (0.1 M), water and, methanol (20 mL each) and dried under vacuum for 24 h. The procedure was repeated using the dried polymer for the next adsorption experiment.[212]

4.2.7 Simulating wastewater

4.2.7.1 Change in temperature

Two round bottom flasks were charged with stirrer bars and dye (MB or MO, 30 mL) and placed in an oil bath. The oil bath was allowed to reach 40℃ before POP-6 (10 mg) was added to each flask. After 18 h the polymer was separated from the solution by filtration and UV-Vis measurements of the solutions were taken. This procedure was repeated for each dye solution.

4.2.7.2 Change in pH and temperature

Two round bottom flasks were charged with stirrer bars and dye (MB or MO, 30 mL) and placed in an oil bath. NaCl and Na_2CO_3 (500 mg each) were added to each flask to reach pH 11. The oil bath was allowed to reach 40℃ before POP-6 (10 mg) was added to each flask. After 18 h the polymer was separated from the solution by filtration and UV-Vis measurements of the solutions were taken.

4.3 Metal adsorption

4.3.1 Standard tests

A centrifuge tube was charged with polymer (POP 3-7, 10 mg) and metal solution (0.059 M $CrCl_3$, 0.145 M $CoCl_2$, 0.055 M $CuCl_2$, 30 mL). The centrifuge tube was sealed and placed on an orbital shaker at room temperature for 18 h. The polymer-metal mixture was separated by centrifugation and UV-Vis measurements taken to determine a change in concentration. The procedure was repeated for each polymer and metal solution.

4.3.2 Control experiments

Each adsorption experiment was repeated without the use of polymer as a comparison and to fully evaluate the effects of changing the reaction conditions on the adsorption of each pollutant. Additionally, each separation method (centrifuge and syringe filter) was investigated to determine if any effect was had on the concentrations of the dyes.

5 Materials and instruments

5.1 Chemicals

All chemicals and solvents were purchased from Merk or Sigma-Aldrich and used without modification unless otherwise stated. All solvents used in the synthesis of porous materials were anhydrous unless otherwise stated.

5.2 Instruments

Surface area measurements were performed using a Quantachrome Quadrasorb SI-MP instrument with the QuandraWin 5.05 software package. The relative pressure (P/P_0) range of the instrument was from 10^{-8} to 0.999 and the instrument was capable of recording a minimum surface area of 0.01 m^2/g. Each sample was degassed in three stages: 1) heated to 50 ℃ at 1 ℃/min, held for 10 minutes. 2) heated to 100 ℃ at 2 ℃/min, held for 30 minutes. 3) heated to 150 ℃ at 2 ℃/min, held for 200 minutes. The adsorption isotherms were recorded using N_2 at 77.2 K and maintained using a liquid nitrogen bath. 20 adsorption data points were recorded and 40 desorption points. The QuandraWin 5.05 software package was used to perform BET (Brunaur-Emmett-Teller) and QSDFT (Quenched Solid Density Functional Theory) measurements.

Fourier Transform Infrared (FTIR) spectroscopy was performed using a PerkinElmer Spectrum One FTIR Spectrometer in conjunction with PerkinElmer Universal ATR Sampling Accessory.

Solid and liquid state Ultra-violet Visible (UV-Vis) spectroscopy measurements were performed using a Shimadzu UV-2600 UV-Vis spectrophotometer using the software UV-2600 UVProbe 2.43. Baselines measurements were taken using barium sulphate (solid-state) or water (liquid-state) and were subtracted from the data using UVWin5 software.

X-ray diffraction (XRD) was performed using a Bruker-AXS D8 Advance power diffractometer (40 kV, 30 Ma) with Cu sealed tube x-ray source. Measurements were taken using a 2-theta range of 5-60, a step size of 0.02/step at 1 second per step.

Scanning Electron Microscopy (SEM) images were taken using Jeol IT300 SEM instrument. The samples were attached to aluminium sample holders and coated with a conductive coating of graphene before analysis.

Contact angle measurements were performed using a Drop Shape Analyzer, DSA100 (KRUSS), with 10 µL of Milli-Q water droplets. Images of the droplet was recoded for 300 seconds in 1 second intervals. The materials were prepared by pressing 30 mg of material at 10 tons of pressure.

^{1}H and ^{13}C NMR experiments were performed using a Varian VNMR 400 MHz NMR.

6 References

1 A. Azizullah, M. N. K. Khattak, P. Richter and D. P. Häder, *Environ. Int.*, 2011, **37**, 479–497.

2 F. N. Chaudry and M. F. Malik, *J. Ecosyst. Ecography*, 2017, **7**, 1000225.

3 United Nations sustainable development goals, https://sdgs.un.org/goals, (accessed 28 November 2022).

4 Water pollution | Definition, Causes, Effects, Solutions, Examples, & Facts | Britannica, https://www.britannica.com/science/water-pollution, (accessed 31 October 2022).

5 M. Haseena, M. F. Malik, A. Javed, S. Arshad, N. Asif, S. Zulfiqar and J. Hanif, *Environ. Risk Assess. Remediat.,* 2017, **1**, 16-19.

6 D. H. Kumar Reddy and S. M. Lee, *J. Environ. Anal. Toxicol.*, 2012, **2**, 1000e103.

7 Point Source: Pollution Tutorial, https://oceanservice.noaa.gov/education/tutorial_pollution/03pointsource.html, (accessed 5 June 2023).

8 Point Source and Nonpoint Sources of Pollution | National Geographic Society, https://education.nationalgeographic.org/resource/point-source-and-nonpoint-sources-pollution, (accessed 31 October 2022).

9 United nations development goal 6, https://sdgs.un.org/goals/goal6, (accessed 28 November 2022).

10 Drinking-water, https://www.who.int/news-room/fact-sheets/detail/drinking-water, (accessed 31 October 2022).

11 V. R. Reddy and B. Behera, *Ecological Economics*, 2006, **58**, 520–537.

12 B. A. Anderson, J. H. Romani, H. Phillips, M. Wentzel and K. Tlabela, *Popul. Environ.*, 2007, **28**, 133–161.

13 Weathering | National Geographic Society, https://education.nationalgeographic.org/resource/weathering, (accessed 28 November 2022).

14 The Earth's crust - Chemistry LibreTexts, https://chem.libretexts.org/Bookshelves/Environmental_Chemistry/Geochemistry_(Lower)/The_Earth_and_its_Lithosphere/The_Earth's_crust, (accessed 28 November 2022).

15 J. Liu and G. Han, *Science of the Total Environment*, 2020, DOI:10.1016/j.scitotenv.2020.138208.

16 K. D. Coldsnow, W. D. Hintz, M. S. Schuler, A. B. Stoler and R. A. Relyea, *Biol. Invasions*, 2021, **23**, 1349–1366.

17 M. Ponikvar, in *Fluorine and Health: Molecular Imaging, Biomedical Materials and Pharmaceuticals*, ed. A. Tressaud and G. Haufe, Elsevier, Amsterdam, 1st edn, 2008, ch. 12, pp. 487–549.

18 P. Li, D. Karunanidhi, T. Subramani and K. Srinivasamoorthy, *Arch. Environ. Contam. Toxicol.*, 2021, DOI:0.1007/s00244-020-00805-z.

19 Decomposition: Types and Process of Decomposition, https://collegedunia.com/exams/decomposition-types-and-process-of-decomposition-biology-articleid-2728, (accessed 24 May 2023).

20 D. Lan, H. Zhu, J. Zhang, S. Li, Q. Chen, C. Wang, T. Wu and M. Xu, *Chemosphere*, 2022, DOI:10.1016/j.chemosphere.2021.133464.

21 V. K. Gupta, R. Kumar, A. Nayak, T. A. Saleh and M. A. Barakat, *Adv. Colloid Interface Sci.*, 2013, **193–194**, 24–34.

22 M. S. Haque, N. Nahar and S. M. Sayem, *Water Resour. Ind.*, 2021, DOI:10.1016/j.wri.2021.100145.

23 G. M. Ziarani, R. Moradi, N. Lashgari and H. G. Kruger, in *Metal-Free Synthetic Organic Dyes*, ed. E. M. McCloskey and K. Zaliva, Elsevier, Amsterdam, 2018, 1st edn, ch. 4, pp. 47–93.

24 S. A. Avlonitis, I. Poulios, D. Sotiriou, M. Pappas and K. Moutesidis, *Desalination*, 2008, **221**, 259–267.

25 C. R. Holkar, A. J. Jadhav, D. V. Pinjari, N. M. Mahamuni and A. B. Pandit, *J. Environ. Manage.*, 2016, **182**, 351–366.

26 P. J. Wakelyn, in *Cotton: Science and technology*, ed. S. Gordon and Y-L. Hsieh, Woodhead Publishing Limited, Cambridge, 2007, 1st edn, ch. 14, pp. 460-483.

27 R. T. Kapoor, M. Danish, R. S. Singh, M. Rafatullah and A. K. Abdul, *Journal of Water Process Engineering*, 2021, DOI:10.1016/j.jwpe.2021.102255.

28 S. Sarkar, A. Banerjee, U. Halder, R. Biswas and R. Bandopadhyay, *Water Conservation Science and Engineering*, 2017, **2**, 121–131.

29 S. Benkhaya, S. M'rabet and A. El Harfi, *Heliyon*, 2020, **6**, e03271.

30 M. Shahnawaz Khan, M. Khalid and M. Shahid, *Mater. Adv.*, 2020, **1**, 1575–1601.

31 B. Lellis, C. Z. Fávaro-Polonio, J. A. Pamphile and J. C. Polonio, *Biotechnology Research and Innovation*, 2019, **3**, 275–290.

32 M. A. M. Salleh, D. K. Mahmoud, W. A. W. A. Karim and A. Idris, *Desalination*, 2011, **280**, 1–13.

33 V. Selvaraj, T. Swarna Karthika, C. Mansiya and M. Alagar, *J. Mol. Struct.*, 2021, **1224**, 129195.

34 M. Balakrishnan, S. Arul Antony, S. Gunasekaran and R. K. Natarajan, *Indian J. Sci. Technol.*, 2008, **1,** 1-8.

35 S. Wong, N. A. N. Yac'cob, N. Ngadi, O. Hassan and I. M. Inuwa, *Chin. J. Chem. Eng.*, 2018, **26**, 870–878.

36 Bangladesh's Polluted Waters: Rivers Dying Due to Dyeing, https://www.iamrenew.com/environment/bangladeshs-polluted-waters-rivers-dying-due-to-dyeing/, (accessed 31 October 2022).

37 M. M. Islam, A. M. Khan and M. M. Islam, *Res. J. Engineering Sci.*, 2013, **2**, 31-37.

38 M. Sakamoto, T. Ahmed, S. Begum and H. Huq, *Sustainability (Switzerland)*, 2019, DOI:10.3390/su11071951.

39 Wastewater management in the garment industry - WIN - Water Integrity Network, https://www.waterintegritynetwork.net/2017/07/27/wastewater-management-garment-industry/, (accessed 7 December 2022).

40 L. Hossain, S. K. Sarker and M. S. Khan, *Environ. Dev.*, 2018, **26**, 23–33.

41 D. A. Yaseen and M. Scholz, *Int. J. Environ. Sci. Technol.*, 2019, **16**, 1193–1226.

42 S.M. Imtiazuddin, Majid Mumtaz and Khalil A. Mallick, *J. Basic Appl. Sci.*, 2012, **8**, 554–556.

43 M. A. Zoroddu, J. Aaseth, G. Crisponi, S. Medici, M. Peana and V. M. Nurchi, *J. Inorg. Biochem.*, 2019, **195**, 120–129.

44 J. H. Duffus, *Pure Appl. Chem.,* 2002, **74**, 793-807

45 J. Briffa, E. Sinagra and R. Blundell, *Heliyon*, 2020, **6**, e04691.

46 Heavy Metals - Lenntech, https://www.lenntech.com/processes/heavy/heavy-metals/heavy-metals.htm, (accessed 31 October 2022).

47 Z. Fu and S. Xi, *Toxicol. Mech. Methods*, 2020, **30**, 167–176.

48 N. K. Asare-Donkor and A. A. Adimado, *Environ. Earth Sci.*, 2020, **79**, 205.

49 M. Z. A. Zaimee, M. S. Sarjadi and M. L. Rahman, *Water (Switzerland)*, 2021, **13**, w13192659.

50 Chromium (Cr) Toxicity: Where Is Chromium Found? | Environmental Medicine | ATSDR, https://www.atsdr.cdc.gov/csem/chromium/where_is_chromium_found.html, (accessed 31 October 2022).

51 A. Pohl, *Water Air Soil Pollut.*, 2020, **231**, 503.

52 P. B. Tchounwou, C. G. Yedjou, A. K. Patlolla and D. J. Sutton, *EXS*, 2012, **101**, 133–164.

53 R. Turksoy, G. Terzioglu, I. E. Yalcin, O. T. Terzioglu and G. Demir, *Frontiers in Life Sciences and Related Technologies*, 2021, **2**, 44-50.

54 F. Li, Z. Zhong, C. Gu, C. Shen, C. Ma, Y. Liu, S. Yin and C. Xu, *Environ. Sci. Pollut. Res.*, 2021, **28**, 38689-38697.

55 A. C. Jadhav and N. C. Jadhav, in *Sustainable Technologies for Textile Wastewater Treatments*, ed. S. Muthu, Elsevier, Amsterdam, 1st edn, 2021, ch. 10, pp. 235–273.

56 T. M. Adyel, S. H. Rahman, M. Khan and S. M. Nazrul Islam, *Metals (Basel)*, 2012, **2**, 478–487.

57 A. Gürses, K. Güneş and E. Şahin, in *Green Chemistry and Water Remediation: Research and Applications*, ed. S. K. Sharma, Elsevier, Amsterdam, 1st edn, 2020, ch. 5, pp. 135–187.

58 A. Srivastava and S. Bandhu, *Case Stud. Chem. Environ. Eng.*, 2022, **5**, 100186.

59 D. Dahiya and P. S. Nigam, *Applied Sciences (Switzerland)*, 2020, **10**, 2958.

60 K. P. Mishra and P. R. Gogate, *Sep. Purif. Technol.*, 2010, **75**, 385–391.

61 V. K. Saharan, M. P. Badve and A. B. Pandit, *Chem. Eng. J.*, 2011, **178**, 100–107.

62 I. Eichlerová, L. Homolka, L. Lisá and F. Nerud, *Chemosphere*, 2005, **60**, 398–404.

63 A. Singh, D. B. Pal, A. Mohammad, A. Alhazmi, S. Haque, T. Yoon, N. Srivastava and V. K. Gupta, *Bioresour. Technol.*, 2022, **343**, 126154.

64 C. R. Holkar, A. J. Jadhav, D. v. Pinjari, N. M. Mahamuni and A. B. Pandit, *J. Environ. Manage.*, 2016, **182**, 351–366.

65 G. Bal and A. Thakur, *Materials Today: Proceedings*, 2022, **50**, 1575–1579.

66 T. Robinson, G. Mcmullan, R. Marchant and P. Nigam, *Bioresour. Technol.,* 2001, **77**, 247-255.

67 V. Katheresan, J. Kansedo and S. Y. Lau, *J. Environ. Chem. Eng.*, 2018, **6**, 4676–4697.

68 Y. Zheng, S. Yu, S. Shuai, Q. Zhou, Q. Cheng, M. Liu and C. Gao, *Desalination*, 2013, **314**, 89–95.

69 A. Ahmad, S. H. Mohd-Setapar, C. S. Chuong, A. Khatoon, W. A. Wani, R. Kumar and M. Rafatullah, *RSC Adv.*, 2015, **5**, 30801–30818.

70 S. Wang, W. Chen, C. Zhang and H. Pan, *Chem. Phys. Lett.*, 2021, **784**, 139104.

71 S. S. Ray, R. Gusain and N. Kumar, in *Carbon Nanomaterial-Based Adsorbents for Water Purification*, ed. S. Holt and M. C. Henriques, Elsevier, Amsterdam, 1st edn, 2020, ch. 4, pp. 67–100.

72 Momina, M. Shahadat and S. Isamil, *RSC Adv.*, 2018, **8**, 24571–24587.

73 V. K. Gupta and Suhas, *J. Environ. Manage.*, 2009, **90**, 2313–2342.

74 S. Madhav, A. Ahamad, P. Singh and P. K. Mishra, *Environmental Quality Management*, 2018, **27**, 31–41.

75 S. Moosavi, C. W. Lai, S. Gan, G. Zamiri, O. Akbarzadeh Pivehzhani and M. R. Johan, *ACS Omega*, 2020, **5**, 20684–20697.

76 C. Namasivayam, D. Prabha and M. Kumutha, *Bioresour. Technol.*, 1998, **64**, 77-79.

77 R-S. Juang, F-C. Wu and R-L. Tseng, *Colloids Surf., A*, 2002, **201**, 191-199.

78 A. El Nemr, O. Abdelwahab, A. El-Sikaily and A. Khaled, *J. Hazard. Mater.*, 2009, **161**, 102–110.

79 A. M. Aljeboree, A. N. Alshirifi and A. F. Alkaim, *Arabian J. Chem.*, 2017, **10**, S3381–S3393.

80 K. Philippou, I. Anastopoulos, I. Pashalidis, A. Hosseini-Bandegharaei, M. Usman, M. Kornaros, M. Omirou, D. Kalderis, J. v. Milojković, Z. R. Lopičić and M. Abatal, in *Sorbents Materials for Controlling Environmental Pollution: Current State and Trends*, ed. A. Nunez-Delgado, Elsevier, Amsterdam, 1st edn, 2021, ch. 6, pp. 113–133.

81 Q. Sun, B. Aguila, Y. Song and S. Ma, *Acc. Chem. Res.*, 2020, **53**, 812–821.

82 S. Ravi, Y. Choi and J. K. Choe, *Chemical Engineering Journal*, 2020, **379**, 122290.

83 M. Thommes, K. Kaneko, A. V. Neimark, J. P. Olivier, F. Rodriguez-Reinoso, J. Rouquerol and K. S. W. Sing, *Pure and Applied Chemistry*, 2015, **87**, 1051–1069.

84 S. Kandambeth, K. Dey and R. Banerjee, *J. Am. Chem. Soc.*, 2019, **141**, 1807–1822.

85 L. Bois, A. Bonhommé, A. Ribes, B. Pais, G. Raffin and F. Tessier, *Colloids Surf. A Physicochem. Eng. Asp.*, 2003, **221**, 221–230.

86 B. Smit and T. L. M. Maesen, *Chem. Rev.*, 2008, **108**, 4125–4184.

87 M. Djebbar, F. Djafri, M. Bouchekara and A. Djafri, *Appl. Water Sci.*, 2012, **2**, 77–86.

88 P. J. Lu, H. C. Lin, W. Te Yu and J. M. Chern, *J. Taiwan Inst. Chem. Eng.*, 2011, **42**, 305–311.

89 P. A. Kobielska, A. J. Howarth, O. K. Farha and S. Nayak, *Coord. Chem. Rev.*, 2018, **358**, 92–107.

90 L. Huang, R. Liu, J. Yang, Q. Shuai, B. Yuliarto, Y. V. Kaneti and Y. Yamauchi, *Chemical Engineering Journal*, 2021, **408**, 127991.

91 J. S. M. Lee and A. I. Cooper, *Chem. Rev.*, 2020, **120**, 2171–2214.

92 N. B. McKeown, *Polymer (Guildf)*, 2020, **202**, 122736.

93 Y. Tian and G. Zhu, *Chem. Rev.*, 2020, **120**, 8934–8986.

94 H. Wang, D. Jiang, D. Huang, G. Zeng, P. Xu, C. Lai, M. Chen, M. Cheng, C. Zhang and Z. Wang, *J. Mater. Chem. A Mater.*, 2019, **7**, 22848–22870.

95 A. Yadav and N. Sinha, *Encyclopaedia of Materials: Plastics and Polymers*, 2021, DOI:10.1016/B978-0-12-820352-1.00140-1.

96 G. Singh, J. Lee, A. Karakoti, R. Bahadur, J. Yi, D. Zhao, K. Albahily and A. Vinu, *Chem. Soc. Rev.*, 2020, **49**, 4360–4404.

97 T. Zhang, G. Xing, W. Chen and L. Chen, *Mater. Chem. Front.*, 2020, **4**, 332–353.

98 S. Haldar, D. Kaleeswaran, D. Rase, K. Roy, S. Ogale and R. Vaidhyanathan, *Nanoscale Horiz.*, 2020, **5**, 1264–1273.

99 J. X. Jiang, F. Su, A. Trewin, C. D. Wood, N. L. Campbell, H. Niu, C. Dickinson, A. Y. Ganin, M. J. Rosseinsky, Y. Z. Khimyak and A. I. Cooper, *Angewandte Chemie - International Edition*, 2007, **46**, 8574–8578.

100 Y. Kou, Y. Xu, Z. Guo and D. Jiang, *Angewandte Chemie - International Edition*, 2011, **50**, 8753–8757.

101 Y. Liao, H. Wang, M. Zhu and A. Thomas, *Adv. Mater.*, 2018, **30**, 1705710.

102 J. Liu, J. M. Tobin, Z. Xu and F. Vilela, *Polym. Chem.*, 2015, **6**, 7251–7255.

103 L. Chen, Y. Honsho, S. Seki and D. Jiang, *J. Am. Chem. Soc.*, 2010, **132**, 6742–6748.

104 L. Sun, Z. Liang, J. Yu and R. Xu, *Polym. Chem.*, 2013, **4**, 1932–1938.

105 Y. Xu, S. Jin, H. Xu, A. Nagai and D. Jiang, *Chem. Soc. Rev.*, 2013, **42**, 8012–8031.

106 Y. Liu, Y. Cui, C. Zhang, J. Du, S. Wang, Y. Bai, Z. Liang and X. Song, *Chemistry - A European Journal*, 2018, **24**, 7480–7488.

107 J. X. Jiang, F. Su, A. Trewin, C. D. Wood, H. Niu, J. T. A. Jones, Y. Z. Khimyak and A. I. Cooper, *J. Am. Chem. Soc.*, 2008, **130**, 7710–7720.

108 R. Dawson, A. Laybourn, Y. Z. Khimyak, D. J. Adams and A. I. Cooper, *Macromolecules*, 2010, **43**, 8524–8530.

109 J. Chen, W. Yan, E. J. Townsend, J. Feng, L. Pan, V. del Angel Hernandez and C. F. J. Faul, *Angewandte Chemie*, 2019, **131**, 11841–11845.

110 Y. Nailwal, M. Devi and S. K. Pal, *ACS Appl. Polym. Mater.*, 2022, **4**, 2648–2655.

111 J. Kim, C. M. Moisanu, C. N. Gannett, A. Halder, J. J. Fuentes-Rivera, S. H. Majer, K. M. Lancaster, A. C. Forse, H. D. Abruña and P. J. Milner, *Chemistry of Materials*, 2021, **33**, 8334–8342.

112 S. Wang, Y. Liu, Y. Yu, J. Du, Y. Cui, X. Song and Z. Liang, *New J. Chem.*, 2018, **42**, 9482–9487.

113 S. Gan, Y. Zeng, J. Liu, J. Nie, C. Lu, C. Ma, F. Wang and G. Yang, *Catal. Sci. Technol.*, 2022, **12**, 1202–1210.

114 Y. B. Zhou and Z. P. Zhan, *Chem. Asian J.*, 2018, **13**, 9–19.

115 F. Xu, X. Chen, Z. Tang, D. Wu, R. Fu and D. Jiang, *Chem. Commun.*, 2014, **50**, 4788–4790.

116 R. S. Sprick, B. Bonillo, M. Sachs, R. Clowes, J. R. Durrant, D. J. Adams and A. I. Cooper, *Chem. Commun.*, 2016, **52**, 10008–10011.

117 L. Pan, Z. Liu, M. Tian, B. C. Schroeder, A. E. Aliev and C. F. J. Faul, *ACS Appl. Mater. Interfaces*, 2019, **11**, 48352–48362.

118 A. Li, H. X. Sun, D. Z. Tan, W. J. Fan, S. H. Wen, X. J. Qing, G. X. Li, S. Y. Li and W. Q. Deng, *Energy Environ. Sci.*, 2011, **4**, 2062–2065.

119 W. Zhao, Y. Jiao, R. Gao, L. Wu, S. Cheng, Q. Zhuang, A. Xie and W. Dong, *Chemical Engineering Journal*, 2020, **319**, 123591.

120 R. X. Yang, T. T. Wang and W. Q. Deng, *Sci. Rep.*, 2015, **5**, 10155.

121 X. Sheng, X. Ding, D. You, M. Peng, Z. Dai, X. Hu, H. Shi, L. Yang, P. Shao and X. Luo, *Environ. Res.*, 2022, **211**, 113007.

122 S. Wang, X. Meng, H. Luo, L. Yao, X. Song and Z. Liang, *Sep. Purif. Technol.*, 2022, **284**, 120245.

123 Subodh, K. Prakash, K. Chaudhary and D. T. Masram, *Appl. Catal. A Gen.*, 2020, **593**, 117411.

124 B. Wang, L. S. Lee, C. Wei, H. Fu, S. Zheng, Z. Xu and D. Zhu, *Environmental Pollution*, 2016, **216**, 884–892.

125 P. Kuhn, M. Antonietti and A. Thomas, *Angewandte Chemie - International Edition*, 2008, **47**, 3450–3453.

126 X. Zhu, C. Tian, S. M. Mahurin, S. H. Chai, C. Wang, S. Brown, G. M. Veith, H. Luo, H. Liu and S. Dai, *J. Am. Chem. Soc.*, 2012, **134**, 10478–10484.

127 S. Yu, J. Mahmood, H. Noh, J. Seo, S. Jung, S. Shin, Y. Im, I. Jeon and J. Baek, *Angewandte Chemie*, 2018, **130**, 8574–8578.

128 P. Puthiaraj, S. S. Kim and W. S. Ahn, *Chemical Engineering Journal*, 2016, **283**, 184–192.

129 K. Wang, L.-M. Yang, X. Wang, L. Guo, G. Cheng, C. Zhang, S. Jin, B. Tan and A. Cooper, *Angewandte Chemie*, 2017, **129**, 14337–14341.

130 C. Krishnaraj, H. S. Jena, K. Leus and P. van der Voort, *Green Chem.*, 2020, **22**, 1038–1071.

131 C. E. Chan-Thaw, A. Villa, P. Katekomol, D. Su, A. Thomas and L. Prati, *Nano. Lett.*, 2010, **10**, 537–541.

132 M. Liu, L. Guo, S. Jin and B. Tan, *J. Mater. Chem. A Mater.*, 2019, **7**, 5153–5172.

133 F. Xu, S. Yang, G. Jiang, Q. Ye, B. Wei and H. Wang, *ACS Appl. Mater. Interfaces*, 2017, **9**, 37731–37738.

134 S. Chang, W. Xie, C. Yao, G. Xu, S. Zhang and Y. Xu, *Eur. Polym. J.*, 2021, **159**, 110753.

135 P. Kuhn, M. Antonietti and A. Thomas, *Angewandte Chemie - International Edition*, 2008, **47**, 3450–3453.

136 Z. A. Ghazi, A. M. Khattak, R. Iqbal, R. Ahmad, A. A. Khan, M. Usman, F. Nawaz, W. Ali, Z. Felegari, S. U. Jan, A. Iqbal and A. Ahmad, *New J. Chem.*, 2018, **42**, 10234–10242.

137 F. An, J. Liu, Z. Xu and S. Zheng, *Water Sci. Technol.*, 2020, **82**, 3023–3031.

138 J. Liu, D. Zhou, Z. Xu and S. Zheng, *Environmental Pollution*, 2017, **226**, 379–384.

139 C. Ayed, W. Huang and K. A. I. Zhang, *Front. Chem. Sci. Eng.*, 2020, **14**, 397–404.

140 S. R. Zhu, Q. Qi, Y. Fang, W. N. Zhao, M. K. Wu and L. Han, *Cryst. Growth Des.*, 2018, **18**, 883–891.

141 P. Puthiaraj, Y. R. Lee, S. Zhang and W. S. Ahn, *J. Mater. Chem. A Mater.*, 2016, **4**, 16288–16311.

142 P. Puthiaraj, S. S. Kim and W. S. Ahn, *Chemical Engineering Journal*, 2016, **283**, 184–192.

143 V. S. Vyas, F. Haase, L. Stegbauer, G. Savasci, F. Podjaski, C. Ochsenfeld and B. v. Lotsch, *Nat. Commun.*, 2015, DOI:10.1038/ncomms9508.

144 M. Zhang, Y. Du and H. Liu, *ACS Appl. Polym. Mater.*, 2023, **5**, 654-661.

145 M. Afshari, M. Dinari, K. Zargoosh and H. Moradi, *Ind. Eng. Chem. Res.*, 2020, **59**, 9116–9126.

146 M. Dinari, N. Mokhtari and M. Hatami, *Journal of Polymer Research*, 2021, DOI:10.1007/s10965-021-02463-8.

147 T. Xu, L. Zhou, Y. He, S. An, C. Peng, J. Hu and H. Liu, *Ind. Eng. Chem. Res.*, 2019, **58**, 19642–19648.

148 S. Pourebrahimi and M. Pirooz, *Cleaner Chemical Engineering*, 2022, **2**, 100012.

149 T. Xu, S. An, C. Peng, J. Hu and H. Liu, *Ind. Eng. Chem. Res.*, 2020, **59**, 8315–8322.

150 X. Sheng, H. Shi, L. Yang, P. Shao, K. Yu and X. Luo, *Science of the Total Environment*, 2021, 750, 141683.

151 N. Mokhtari, M. Afshari and M. Dinari, *Polymer (Guildf)*, 2020, **195**, 122430.

152 S. Ren, R. Dawson, A. Laybourn, J. X. Jiang, Y. Khimyak, D. J. Adams and A. I. Cooper, *Polym. Chem.*, 2012, **3**, 928–934.

153 T. Geng, S. Ye, Z. Zhu and W. Zhang, *J. Mater. Chem. A Mater.*, 2018, **6**, 2808–2816.

154 B. T. Ingoglia, C. C. Wagen and S. L. Buchwald, *Tetrahedron*, 2019, **75**, 4199–4211.

155 D. S. Surry and S. L. Buchwald, *Chem. Sci.*, 2011, **2**, 27–50.

156 Y. Sunesson, E. Limé, S. O. Nilsson Lill, R. E. Meadows and P. O. Norrby, *J. Org. Chem.*, 2014, **79**, 11961–11969.

157 A. Poater, F. Ragone, A. Correa and L. Cavallo, *Dalton Trans.*, 2011, **40**, 11066–11069.

158 J. Sherwood, J. H. Clark, I. J. S. Fairlamb and J. M. Slattery, *Green Chem.*, 2019, **21**, 2164–2213.

159 M. M. Heravi, Z. Kheilkordi, V. Zadsirjan, M. Heydari and M. Malmir, *J. Organomet. Chem.*, 2018, **861**, 17–104.

160 H. C. Tu, L. X. Zhao, L. Liu, X. X. Wang, J. M. Lin, X. Wang and R. S. Zhao, *Colloids Surf. A Physicochem. Eng. Asp.*, 2023, DOI:10.1016/j.colsurfa.2022.130393.

161 S. Zulfiqar, M. I. Sarwar and C. T. Yavuz, *RSC Adv.*, 2014, **4**, 52263–52269.

162 R. Peng, G. Chen, F. Zhou, R. Man and J. Huang, *Chemical Engineering Journal*, 2019, **371**, 260–266.

163 L. Shao, M. Liu, Y. Sang and J. Huang, *Microporous Mesoporous Mater.*, 2019, **285**, 105–111.

164 M. R. Liebl and J. Senker, *Chem. Mater.*, 2013, **25**, 970–980.

165 Z. Qian, Z. J. Wang and K. A. I. Zhang, *Chem. Mater.*, 2021, **33**, 1909–1926.

166 Y. Liao, J. Weber and C. F. J. Faul, *Chemical Communications*, 2014, **50**, 8002–8005.

167 J. C. Maxwell, B. C. Baker and C. F. J. Faul, *ACS Appl. Polym. Mater.*, 2023, **5**, 662-671.

168 N. H. Park, E. V. Vinogradova, D. S. Surry and S. L. Buchwald, *Angewandte Chemie - International Edition*, 2015, **54**, 8259–8262.

169 IR Spectrum Table, https://www.sigmaaldrich.com/GB/en/technical-documents/technical-article/analytical-chemistry/photometry-and-reflectometry/ir-spectrum-table, (accessed 3 April 2023).

170 M. Mu, Y. Wang, Y. Qin, X. Yan, Y. Li and L. Chen, *ACS Appl. Mater. Interfaces*, 2017, **9**, 22856–22863.

171 M. Thommes, K. Kaneko, A. V. Neimark, J. P. Olivier, F. Rodriguez-Reinoso, J. Rouquerol and K. S. W. Sing, *Pure Appl. Chem.*, 2015, **87**, 1051–1069.

172 Q. Yang, M. Sheng, X. Li, C. Tucker, S. Vásquez Céspedes, N. J. Webb, G. T. Whiteker and J. Yu, *Org. Process. Res. Dev.*, 2020, **24**, 916–939.

173 X. Hu, *J. Appl. Polym. Sci.*, 2017, DOI:10.1002/app.44505.

174 F. Ambroz, T. J. Macdonald, V. Martis and I. P. Parkin, *Small Methods*, 2018, **2**, 1800173.

175 S. Brunauer, P. H. Emmett and E. Teller, *J. Am. Chem. Soc.*, 1938, **60**, 309-319.

176 K. S. W. Sing, *Pure Appl. Chem.,* 1982, **54**, 2201-2218.

177 J. W. M. Osterrieth, J. Rampersad, D. Madden, N. Rampal, L. Skoric, B. Connolly, M. D. Allendorf, V. Stavila, J. L. Snider, R. Ameloot, J. Marreiros, C. Ania, D. Azevedo, E. Vilarrasa-Garcia, B. F. Santos, X. H. Bu, Z. Chang, H. Bunzen, N. R. Champness, S. L. Griffin, B. Chen, R. B. Lin, B. Coasne, S. Cohen, J. C. Moreton, Y. J. Colón, L. Chen, R. Clowes, F. X. Coudert, Y. Cui, B. Hou, D. M. D'Alessandro, P. W. Doheny, M. Dincă, C. Sun, C. Doonan, M. T. Huxley, J. D. Evans, P. Falcaro, R. Ricco, O. Farha, K. B. Idrees, T. Islamoglu, P. Feng, H. Yang, R. S. Forgan, D. Bara, S. Furukawa, E. Sanchez, J. Gascon, S. Telalović, S. K. Ghosh, S. Mukherjee, M. R. Hill, M. M. Sadiq, P. Horcajada, P. Salcedo-Abraira, K. Kaneko, R. Kukobat, J. Kenvin, S. Keskin, S. Kitagawa, K. ichi Otake, R. P. Lively, S. J. A. DeWitt, P. Llewellyn, B. v. Lotsch, S. T. Emmerling, A. M. Pütz, C. Martí-Gastaldo, N. M. Padial, J. García-Martínez, N. Linares, D. Maspoch, J. A. Suárez del Pino, P. Moghadam, R. Oktavian, R. E. Morris, P. S. Wheatley, J. Navarro, C. Petit, D. Danaci, M. J. Rosseinsky, A. P. Katsoulidis, M. Schröder, X. Han, S. Yang, C. Serre, G. Mouchaham, D. S. Sholl, R. Thyagarajan, D. Siderius, R. Q. Snurr, R. B. Goncalves, S. Telfer, S. J. Lee, V. P. Ting, J. L. Rowlandson, T. Uemura, T. Iiyuka, M. A. van der Veen, D. Rega, V. van Speybroeck, S. M. J. Rogge, A. Lamaire, K. S. Walton, L. W. Bingel, S. Wuttke, J. Andreo, O. Yaghi, B. Zhang, C. T. Yavuz, T. S. Nguyen, F. Zamora, C. Montoro, H. Zhou, A. Kirchon and D. Fairen-Jimenez, *Adv. Mater.*, 2022, **34**, 2201502.

178 C. Kang, Z. Zhang, A. K. Usadi, D. C. Calabro, L. S. Baugh, K. Chai, Y. Wang and D. Zhao, *J. Am. Chem. Soc.*, 2022, **144**, 20363–20371.

179 B. M. Amos-Tautua, O. J. Fakayode, S. P. Songca and O. S. Oluwafemi, *Nano-Structures and Nano-Objects*, 2020, **23**, 100480.

180 S. J. T. Pollard, G. D. Fowler, C. J. Sollars and R. Perry, *The Science of the Total Environment*, 1992, **116**, 31-52.

181 S. Wong, N. A. Ghafar, N. Ngadi, F. A. Razmi, I. M. Inuwa, R. Mat and N. A. S. Amin, *Sci. Rep.*, 2020, **10**, 2928.

182 R. S. Hebbar, A. M. Isloor and A. F. Ismail, in *Membrane Characterization*, ed. N. Hilal, A. F. Ismail, T. Matsuura, D. Oatley-Radcliffe, Elsevier, Amsterdam, 1st edn, 2017, ch. 12, pp. 219–255.

183 T. M. G. Selva, J. S. G. Selva and R. B. Prata, in *Encyclopedia of Sensors and Biosensors*, ed. T. R. L. C. Paixao, Elsevier, Amsterdam, 1st edn, 2023, vol. 2, pp. 45–72.

184 B. W. Chieng, N. A. Ibrahim, N. A. Daud and Z. A. Talib, in *Synthesis, Technology and Applications of Carbon Nanomaterials*, ed. S. A. Rashid, R. N. I. R. Othman, M. Z. Hussein, Elsevier, Amsterdam, 1st edn, 2019, ch. 8, pp. 177–203.

185 S. Krainer and U. Hirn, *Colloids Surf. A Physicochem. Eng. Asp.*, 2021, **619**, 126503.

186 Water Quality and Hardness checker, https://www.bristolwater.co.uk/home/account-and-services/water-quality-checker?bw_wq_search_input=bs8+1ts, (accessed 5 June 2023).

187 K. Azoulay, I. Bencheikh, A. Moufti, A. Dahchour, J. Mabrouki and S. el Hajjaji, *Chem. Data Collect.,* 2020, **27**, 100385.

188 J. W. Heo, L. An, J. Chen, J. H. Bae and Y. S. Kim, *Chemosphere*, 2022, **295**, 133815.

189 J. Liu, T. W. Chen, Y. L. Yang, Z. C. Bai, L. R. Xia, M. Wang, X. L. Lv and L. Li, *Carbohydr. Polym.*, 2020, **230**, 115619.

190 Y. S. Ho and G. Mckay, *Process Biochemistry*, 1999, **34**, 451-465.

191 J. P. Simonin, *Chemical Engineering Journal*, 2016, **300**, 254–263.

192 Z. Aly, A. Graulet, N. Scales and T. Hanley, *Environ. Sci. Pollut. Res.*, 2014, **21**, 3972–3986.

193 Y. Wu, in *Periphyton*, ed. L. S. Kelleher, E. Thomson, Elsevier, Amsterdam, 1st edn, 2017, ch. 16, pp. 367–387.

194 E. D. Revellame, D. L. Fortela, W. Sharp, R. Hernandez and M. E. Zappi, *Clean. Eng. Technol.*, 2020, **1**, 100032.

195 Y. He, W. Bao, Y. Hua, Z. Guo, X. Fu, B. Na, D. Yuan, C. Peng and H. Liu, *RSC Adv*, 2022, **12**, 5587–5594.

196 D. Bartholomew, *Comprehensive Heterocyclic Chemistry II,* 1996, **6**, 575-636.

197 E. M. Espinoza, J. A. Clark, J. B. Derr, D. Bao, B. Georgieva, F. H. Quina and V. I. Vullev, *ACS Omega*, 2018, **3**, 12857–12867.

198 K. Sharma, S. Sharma, V. Sharma, P. K. Mishra, A. Ekielski, V. Sharma and V. Kumar, *Nanomaterials*, 2021, **11**, 1403 .

199 Y. H. Jang, S. Hwang, S. B. Chang, J. Ku and D. S. Chung, *Journal of Physical Chemistry A*, 2009, **113**, 13036–13040.

200 T. Baati, P. Horcajada, R. Gref, P. Couvreur and C. Serre, J Chromatogr B Analyt *Technol. Biomed. Life Sci.*, 2011, **879**, 2311–2314.

201 21.4: Acidity and Basicity of Amines - Chemistry LibreTexts, https://chem.libretexts.org/Bookshelves/Organic_Chemistry/Map%3A_Organic_Chemistry_(Vollhardt_and_Schore)/21%3A_Amines_and_Their_Derivatives/21.04%3A_Acidity__and__Basicity__of_Amines, (accessed 30 May 2023).

202 A. Bensedira, N. Haddaoui, R. Doufnoune, O. Meziane and N. S. Labidi, *Polymers and Polymer Composites*, 2022, DOI:10.1177/09673911221141747.

203 B. Samiey and F. Ashoori, *Chem. Cent. J.*, 2012, DOI:10.1186/1752-153X-6-14.

204 R. S. Razmara, A. Daneshfar and R. Sahrai, *Journal of Industrial and Engineering Chemistry*, 2011, **17**, 533–536.

205 A. A. Shalaby and A. A. Mohamed, *RSC Adv.*, 2020, **10**, 11311–11316.

206 X. Chen, M. F. Hossain, C. Duan, J. Lu, Y. F. Tsang, M. S. Islam and Y. Zhou, *Chemosphere*, 2022, **307**, 135545.

207 O. A. Attallah, M. A. Al-Ghobashy, M. Nebsen and M. Y. Salem, *RSC Adv.*, 2016, **6**, 11461–11480.

208 A. Ayub, Z. A. Raza, M. I. Majeed, M. R. Tariq and A. Irfan, *Int. J. Biol. Macromol.*, 2020, **163**, 603–617.

209 X. Gao, I. Hassan, Y. Peng, S. Huo and L. Ling, *J. Clean Prod.*, 2021, **319**, 128777.

210 M. Mozaffari Majd, V. Kordzadeh-Kermani, V. Ghalandari, A. Askari and M. Sillanpää, *Sci. Total Environ.*, 2022, **812**, 151334.

211 N. Jarrah, *J. Environ. Chem. Eng.*, 2017, **5**, 4319–4326.

212 Y. Zhang, X. Hong, X. M. Cao, X. Q. Huang, B. Hu, S. Y. Ding and H. Lin, *ACS Appl. Mater. Interfaces*, 2021, **13**, 6359–6366.

213 R. O. Cristóvão, A. P. M. Tavares, J. M. Loureiro, R. A. R. Boaventura and E. A. Macedo, *Bioresour. Technol.*, 2009, **100**, 6236–6242.

214 S. Velusamy, A. Roy, S. Sundaram and T. Kumar Mallick, *Chem. Rec.*, 2021, **21**, 1570–1610.

215 Z. Yang, Y. Gu, B. Yuan, Y. Tian, J. Shang, D. C. W. Tsang, M. Liu, L. Gan, S. Mao and L. Li, *J. Hazard. Mater.*, 2021, 403, 123702.

216 B. N. Sulastri, S. Apriyani, H. Zu'Amah, A. N. Ardiwinata and W. Purbalisa, *IOP Conf. Ser.: Earth Environ. Sci.*, 2021, **648**, 012210.

217 H. Shan, S. Li, Z. Yang, X. Zhang, Y. Zhuang, Q. Zhu, D. Cai, P. Qin and J. Baeyens, *Chemical Engineering Journal*, 2021, **426**, 130757.

218 K. Zhao, L. Kong, W. Yang, Y. Huang, H. Li, S. Ma, W. Lv, J. Hu, H. Wang and H. Liu, *ACS Appl. Mater. Interfaces*, 2019, **11**, 44751-44757.

219 C. Liu, R. Bai, L. Hong and T. Liu, *J. Colloid Interface Sci.*, 2010, **345**, 454–460.

220 H. Choi, T. Kim and S. Y. Kim, *Gels*, 2021, **7**, 121.

221 N. Ariffin, M. Mustafa, A. B. Abdullah, M. Remy, R. Mohd, A. Zainol, M. F. Murshed, H.- Zain, M. A. Faris and R. Bayuaji, *MATEC Web of Conferences*, 2017, **97**, 01023.

222 J. Yu, C. Chi, B. Zhu, K. Qiao, X. Cai, Y. Cheng and S. Yan, *Sci. Total Environ.*, 2020, **700**, 134412.

223 R. Gomes, P. Bhanja and A. Bhaumik, *Chemical Communications*, 2015, **51**, 10050–10053.

224 Water Pollution | FilterWater.com, https://www.filterwater.com/t-articles.water-pollution.aspx, (accessed 31 October 2022).

225 D. Bingol, N. Tekin and M. Alkan, *Appl. Clay Sci.*, 2010, **50**, 315–321.

226 A. Waheed, N. Baig, N. Ullah and W. Falath, *J. Environ. Manage.*, 2021, **287**, 112360.

227 M. G. Mohamed, A. F. M. El-Mahdy, M. G. Kotp and S. W. Kuo, *Mater. Adv.*, 2022, **3**, 707–733.

228 X. Pan, X. Qin, Q. Zhang, Y. Ge, H. Ke and G. Cheng, *Microporous and Mesoporous Mater.*, 2010, **296**, 109990.

229 Y. He, Z. Guo, M. Chen, S. Wan, N. Peng, X. Fu, D. Yuan and B. Na, *Journal of Porous Materials*, 2023, **30**, 1439–1448.

230 P. Jamshidi and F. Shemirani, *Research on Chemical Intermediates*, 2020, **46**, 4403–4422.

231 M. Harja, G. Buema and D. Bucur, *Sci. Rep.*, 2022, DOI:10.1038/s41598-022-10093-3.

232 Acid-base properties of amides, http://www.qorganica.es/qot/T11/acido_base_amidas_e_exported/, (accessed 12 May 2023).

233 HSAB Principle-Applications-Pearson's Hard Soft Acid Base Concept, http://www.adichemistry.com/inorganic/cochem/hsab/hard-soft-acid-base-theory.html, (accessed 30 November 2022).

7 Appendix

7.1 POP-1 & POP-2

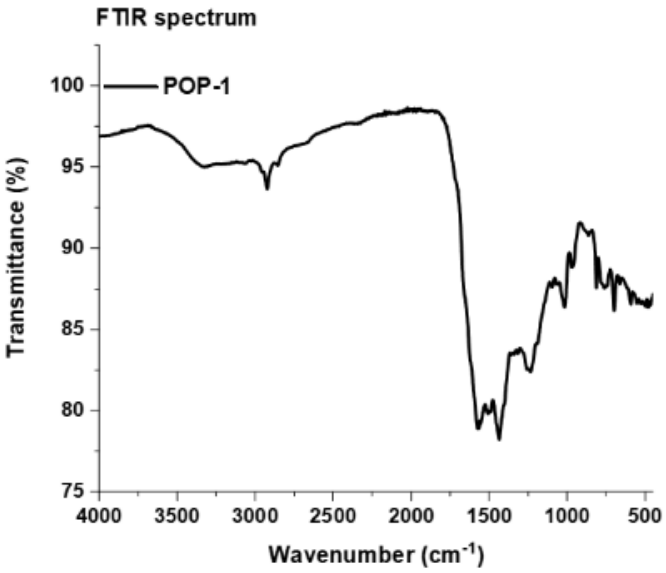

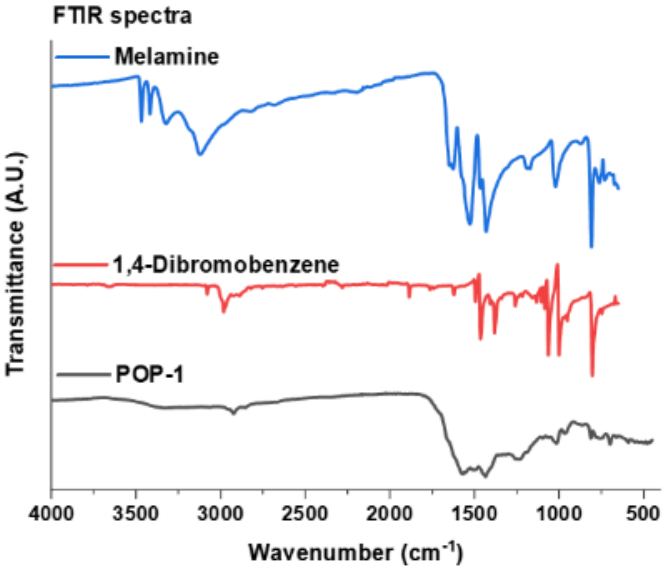

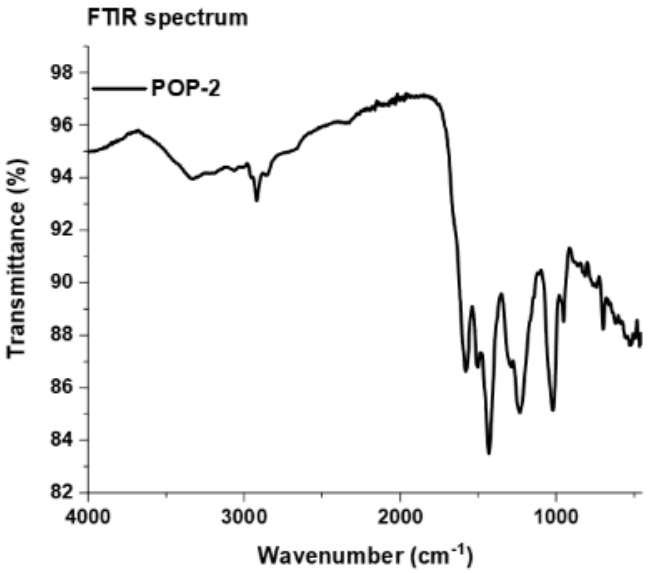

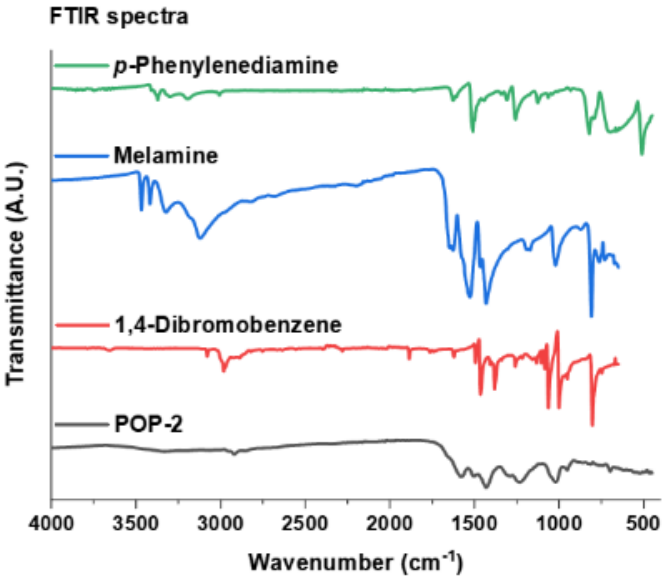

7.2 TAPT

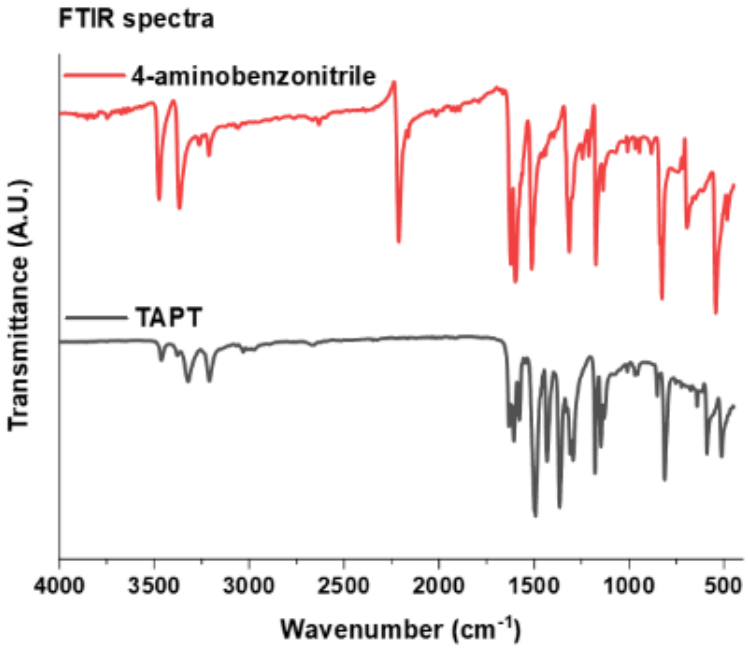
FTIR spectra
4-aminobenzonitrile
TAPT
Transmittance (A.U.)
4000
3500
3000
2500
2000
1500
1000
500
Wavenumber (cm-1)

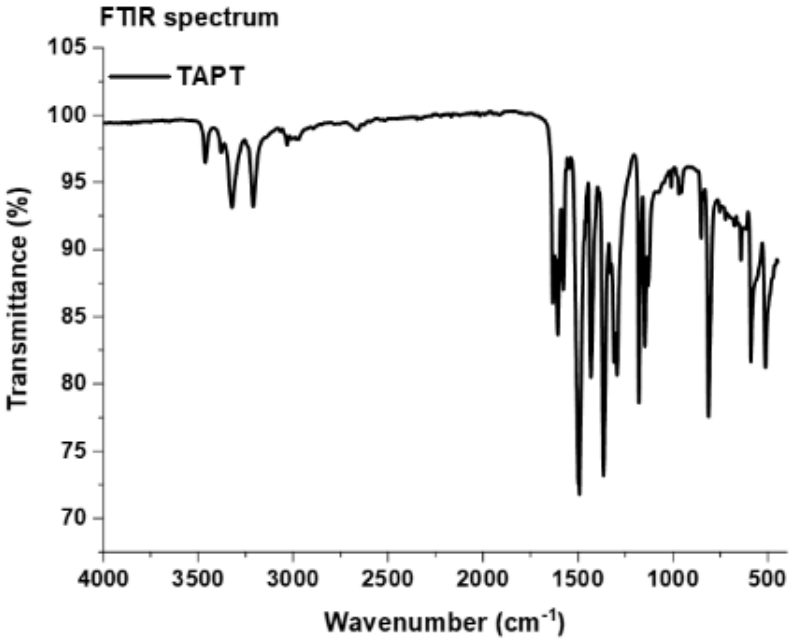
FTIR spectrum
TAPT
Transmittance (%)
105
100
95
90
85
80
75
70
4000
3500
3000
2500
2000
1500
1000
500
Wavenumber (cm-1)

6-Aminobenzonitrile H^1 NMR

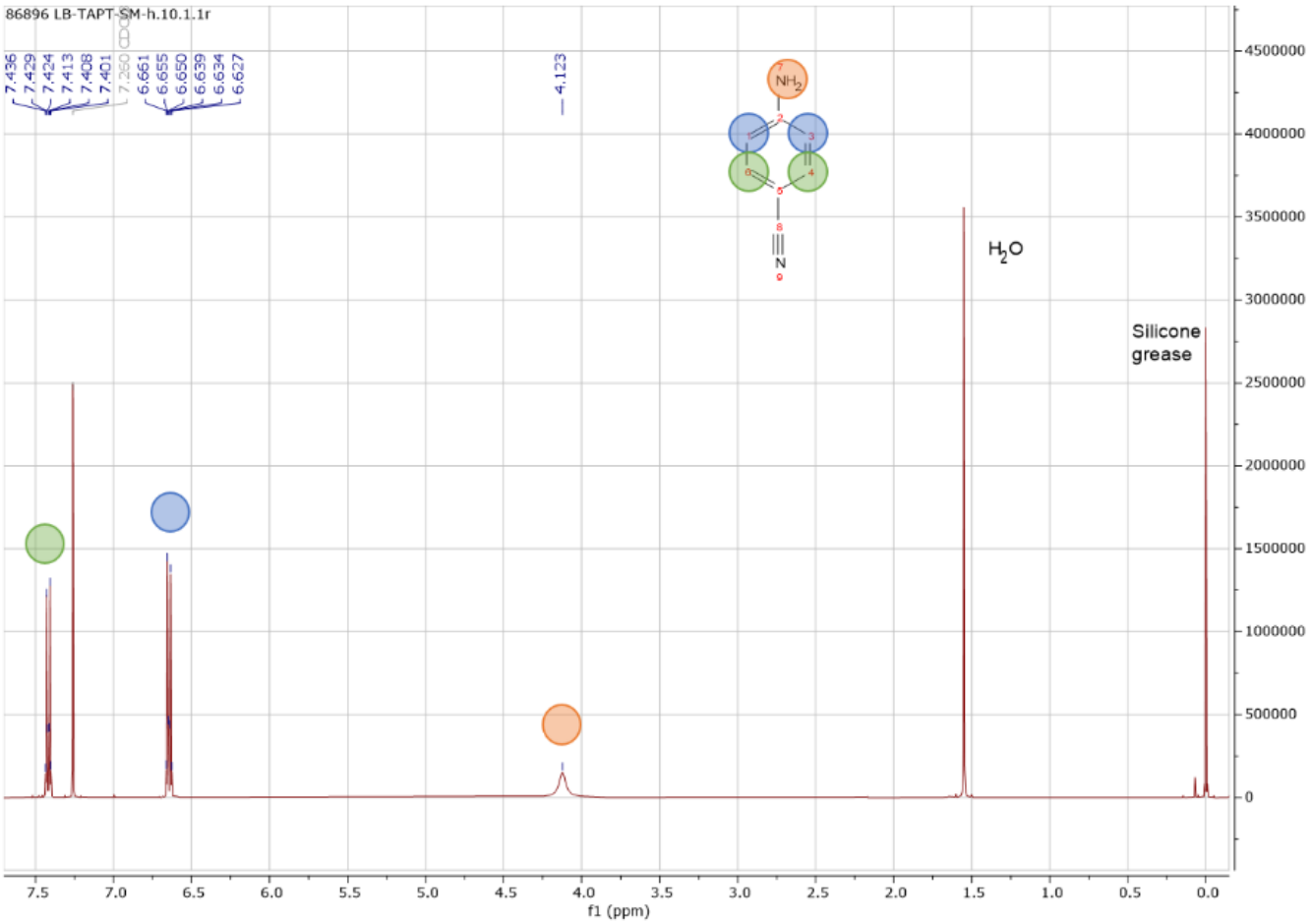

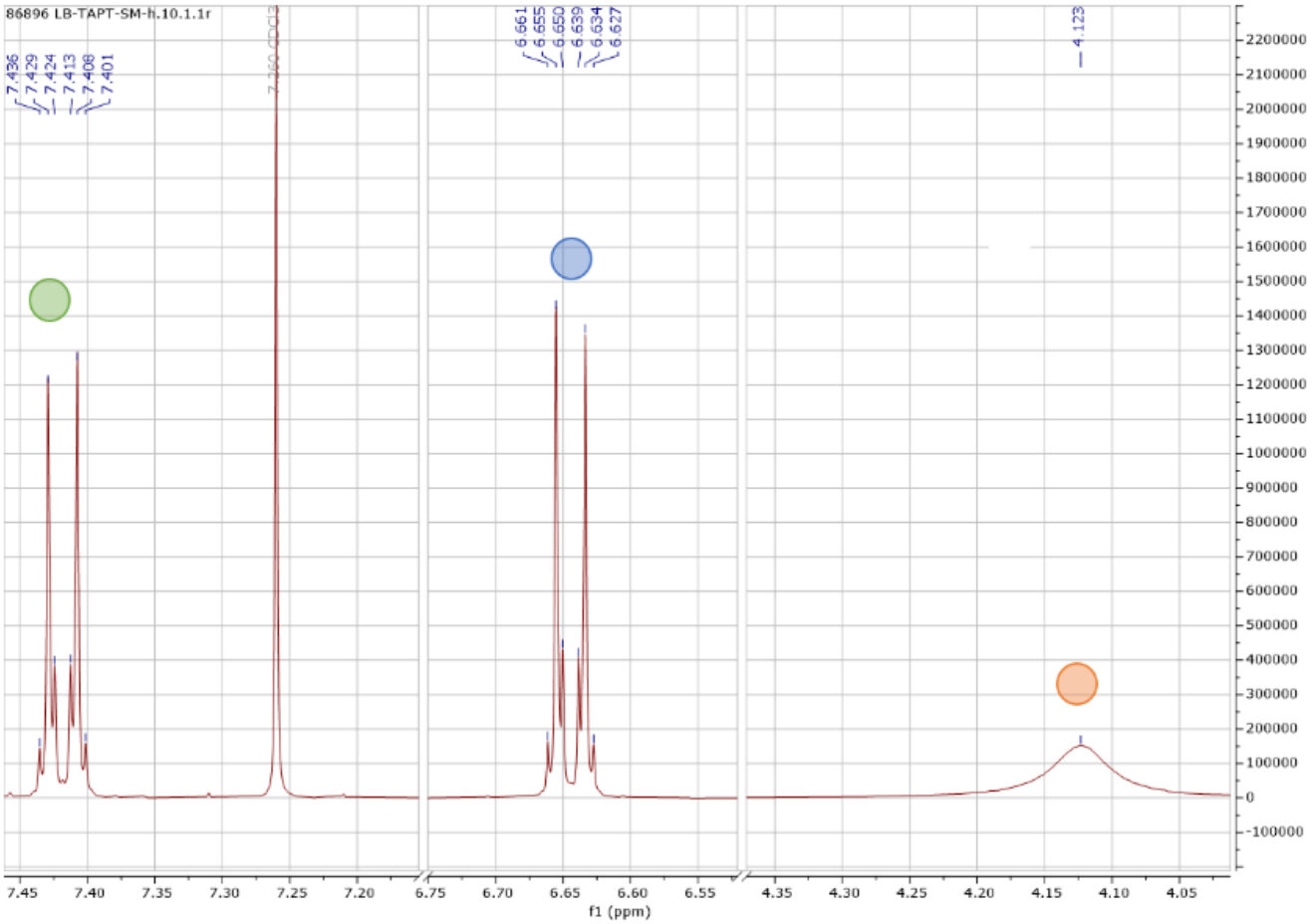

TAPT H^1 NMR

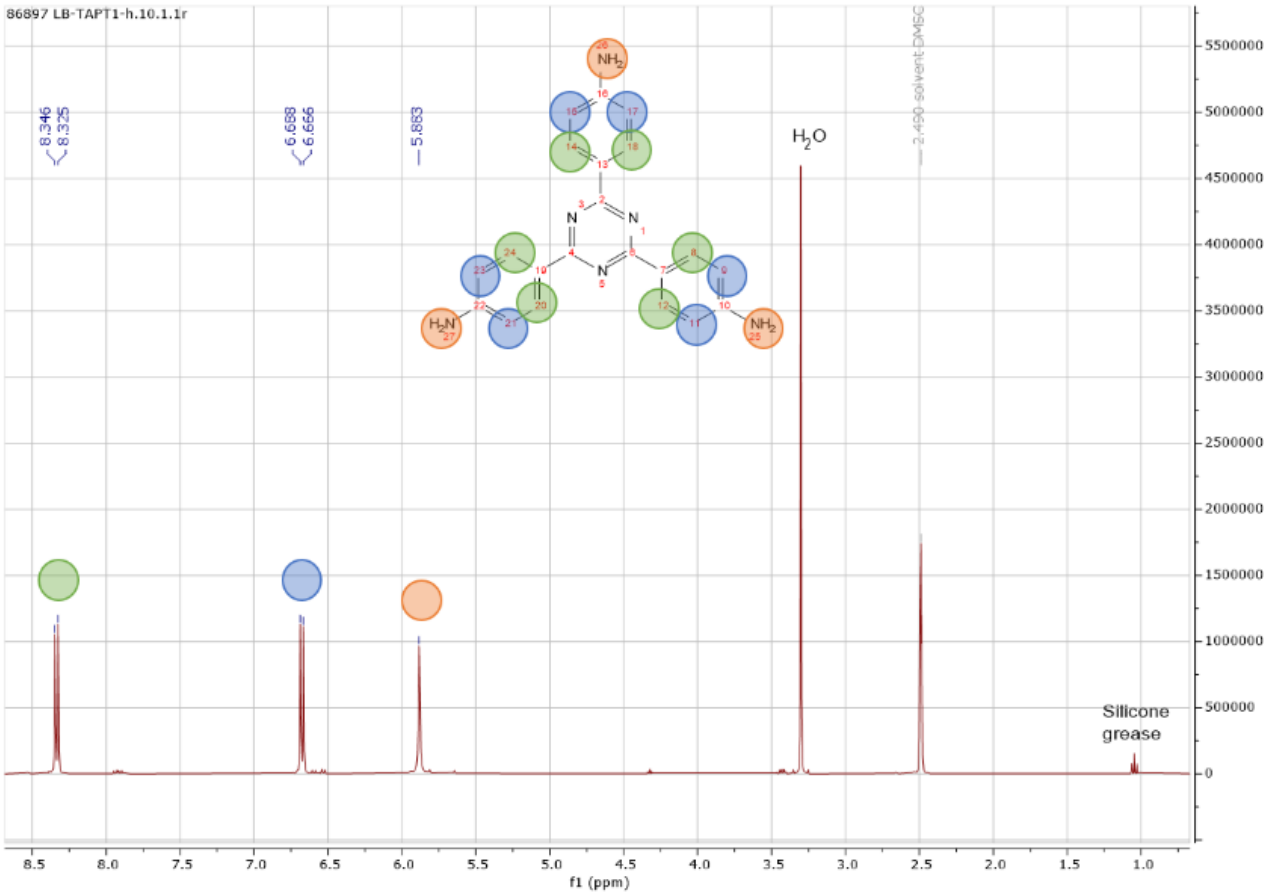
86897 LB-TAPT1-h.10.1.1r
8.346
8.325
6.688
6.666
5.883
H2O
2.490 solvent DMSO
Silicone grease
f1 (ppm)

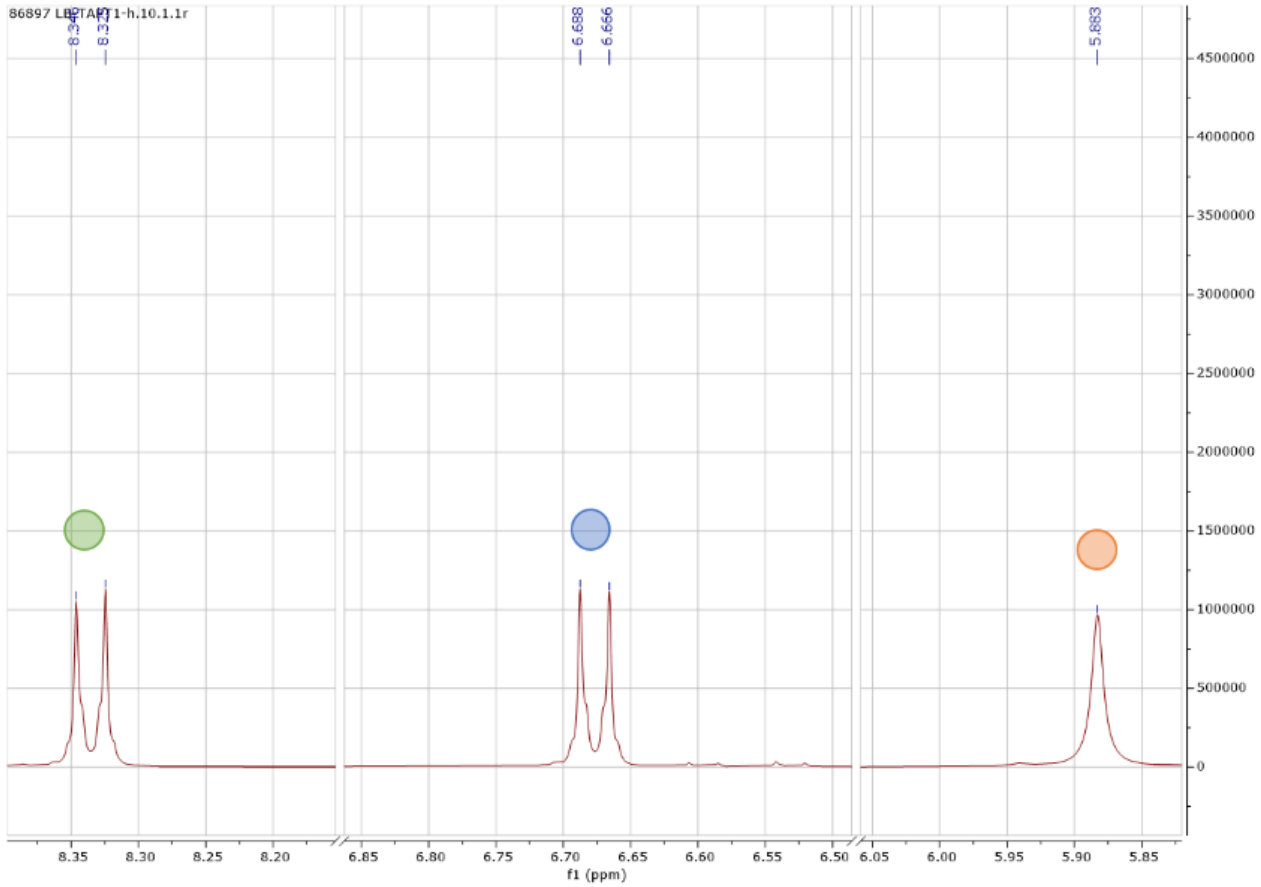
86897 LB-TAPT1-h.10.1.1r
6.688
6.666
5.883
f1 (ppm)

7.3 POP-3

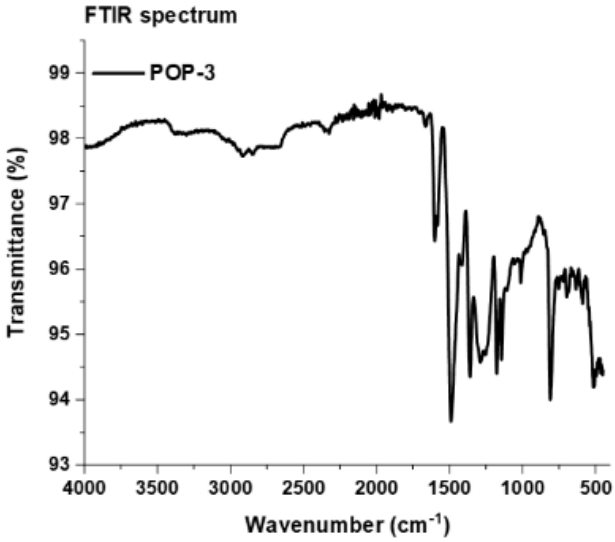
FTIR spectrum
POP-3
Transmittance (%)
Wavenumber (cm-1)

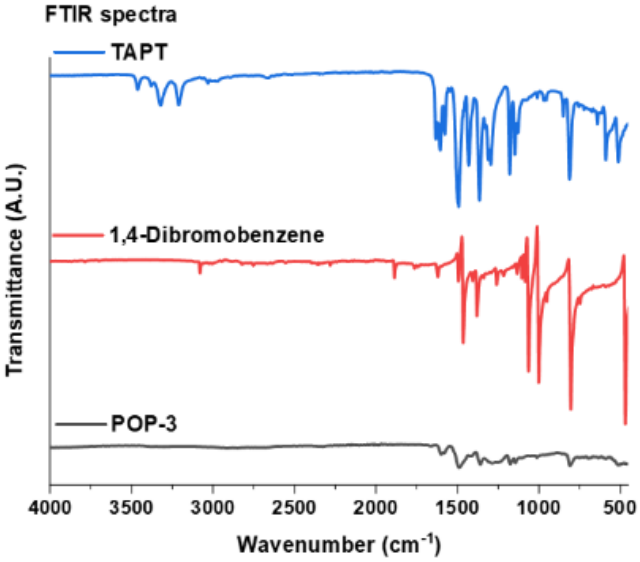
FTIR spectra
TAPT
1,4-Dibromobenzene
POP-3
Transmittance (A.U.)
Wavenumber (cm-1)

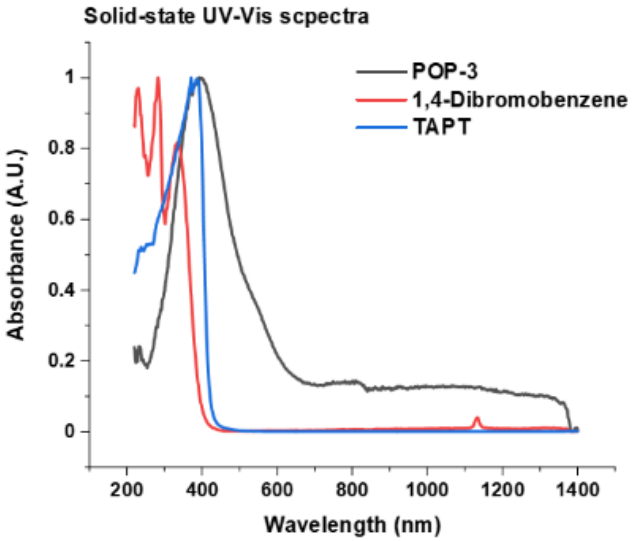
Solid-state UV-Vis scpectra
POP-3
1,4-Dibromobenzene
TAPT
Absorbance (A.U.)
Wavelength (nm)

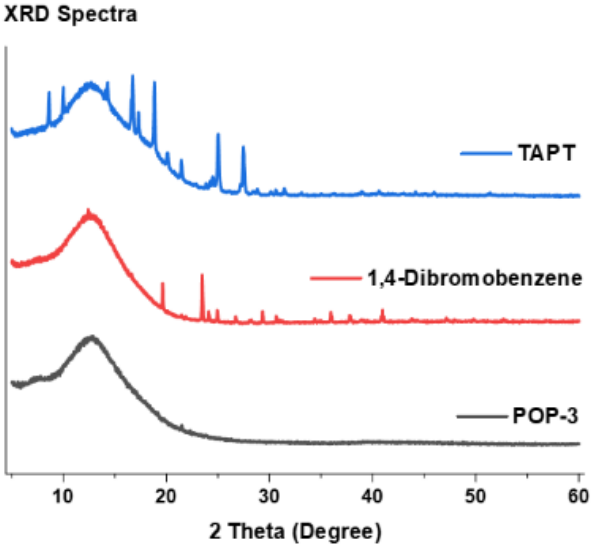
XRD Spectra
TAPT
1,4-Dibromobenzene
POP-3
2 Theta (Degree)

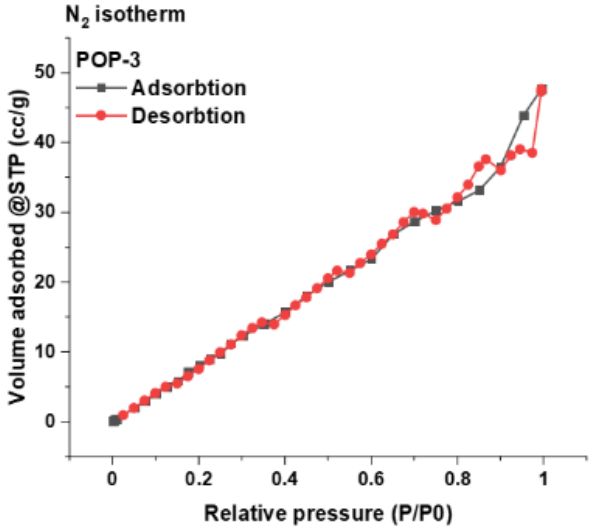
N2 isotherm
POP-3
Adsorbtion
Desorbtion
Volume adsorbed @STP (cc/g)
Relative pressure (P/P0)

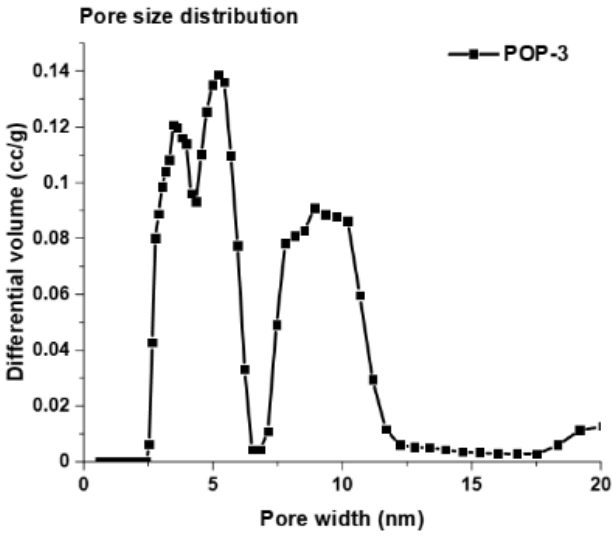
Pore size distribution
POP-3
Differential volume (cc/g)
Pore width (nm)

7.4 POP-4

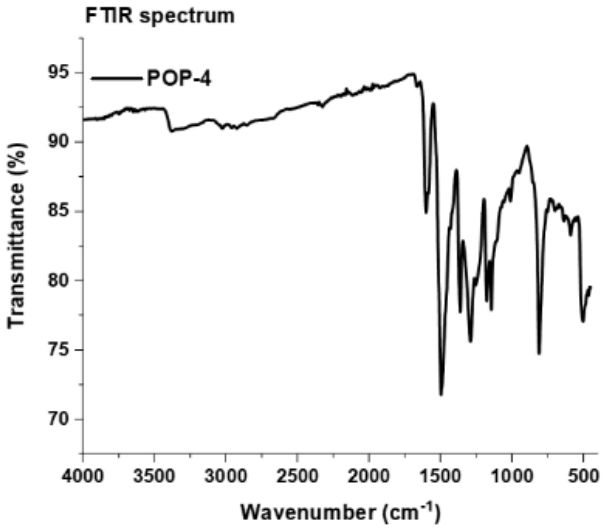
FTIR spectrum
POP-4
Transmittance (%)
Wavenumber (cm-1)

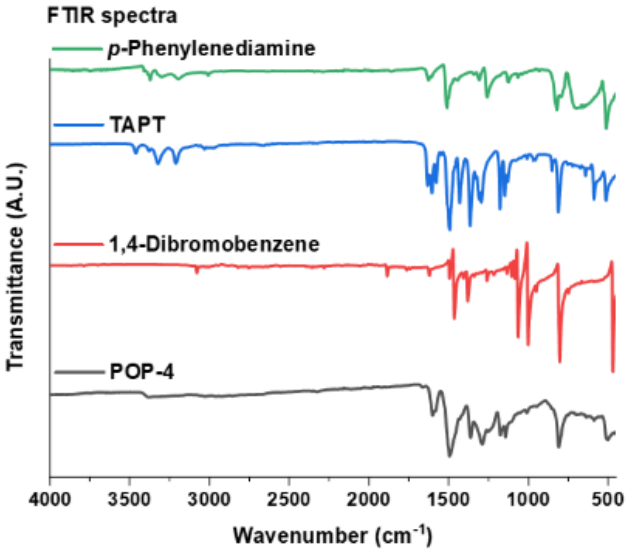
FTIR spectra
p-Phenylenediamine
TAPT
1,4-Dibromobenzene
POP-4
Transmittance (A.U.)
Wavenumber (cm-1)

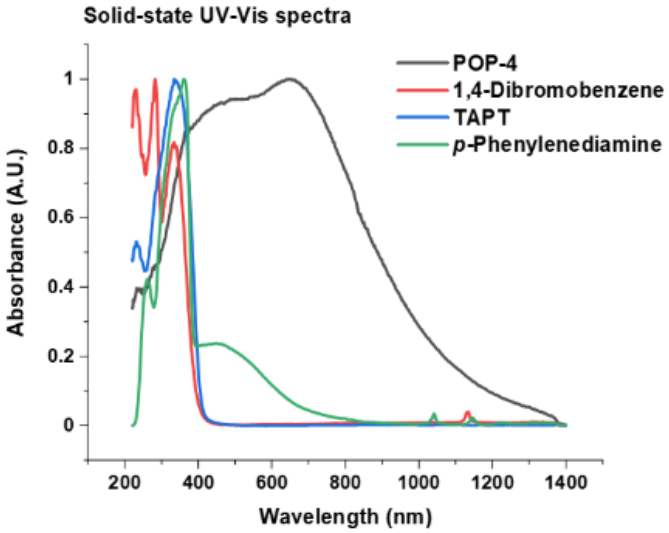
Solid-state UV-Vis spectra
POP-4
1,4-Dibromobenzene
TAPT
p-Phenylenediamine
Absorbance (A.U.)
Wavelength (nm)

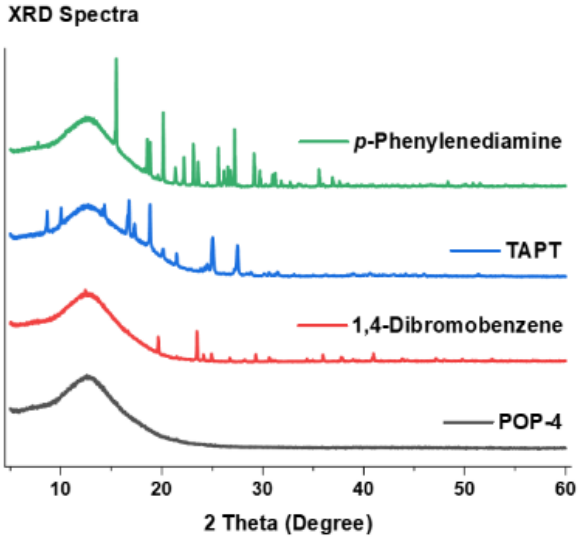
XRD Spectra
p-Phenylenediamine
TAPT
1,4-Dibromobenzene
POP-4
2 Theta (Degree)

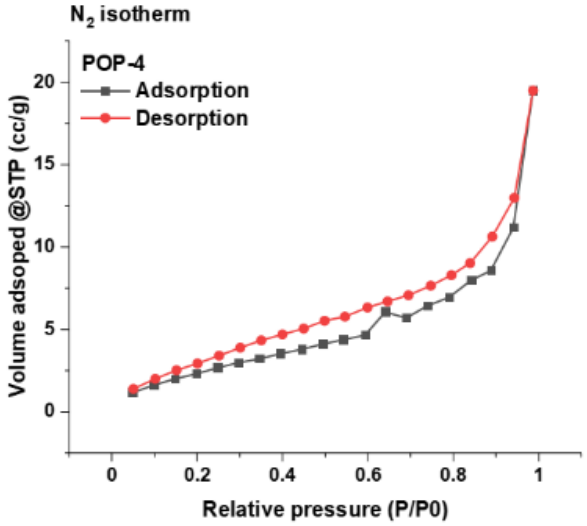
N2 isotherm
POP-4
Adsorption
Desorption
Volume adsoped @STP (cc/g)
Relative pressure (P/P0)

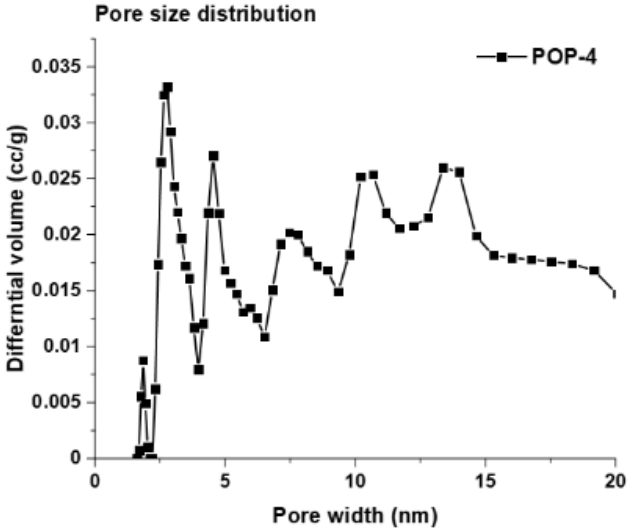
Pore size distribution
POP-4
Differntial volume (cc/g)
Pore width (nm)

7.5 POP-5

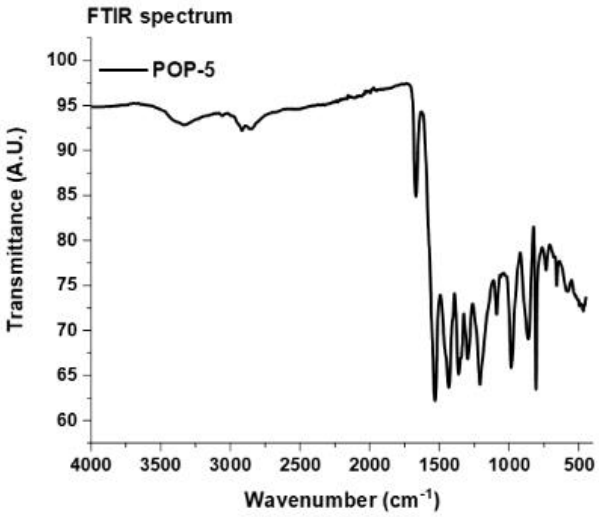
FTIR spectrum
POP-5
Transmittance (A.U.)
Wavenumber (cm-1)

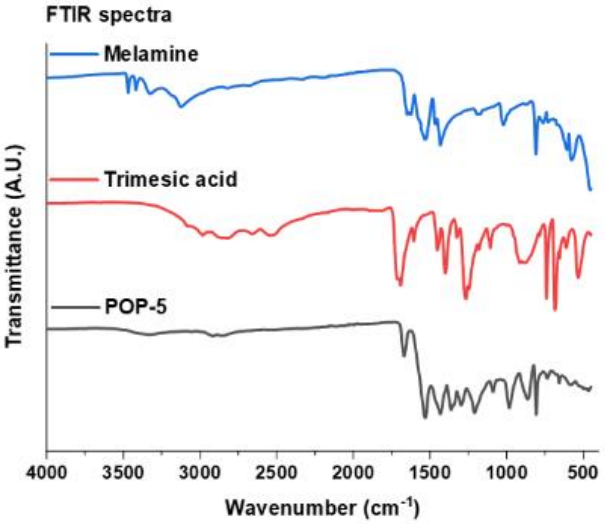
FTIR spectra
Melamine
Trimesic acid
POP-5
Transmittance (A.U.)
Wavenumber (cm-1)

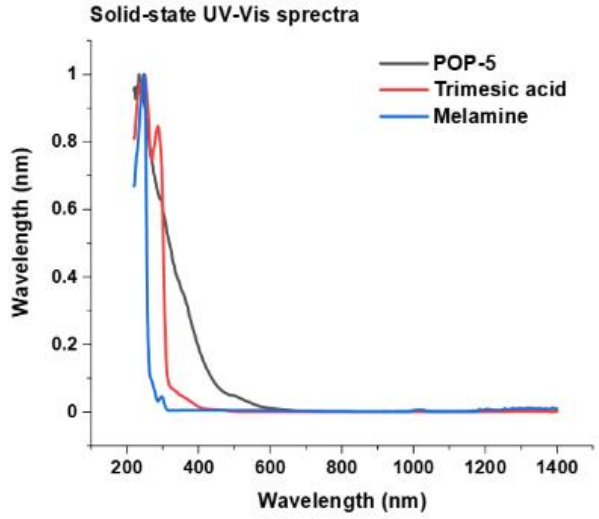
Solid-state UV-Vis sprectra
POP-5
Trimesic acid
Melamine
Wavelength (nm)
Wavelength (nm)

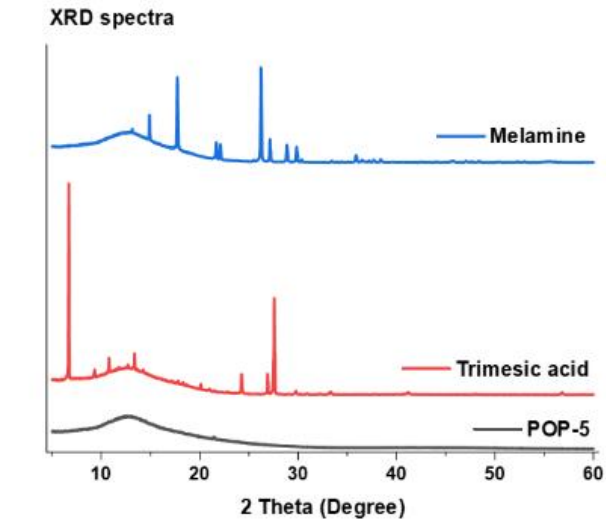
XRD spectra
Melamine
Trimesic acid
POP-5
2 Theta (Degree)

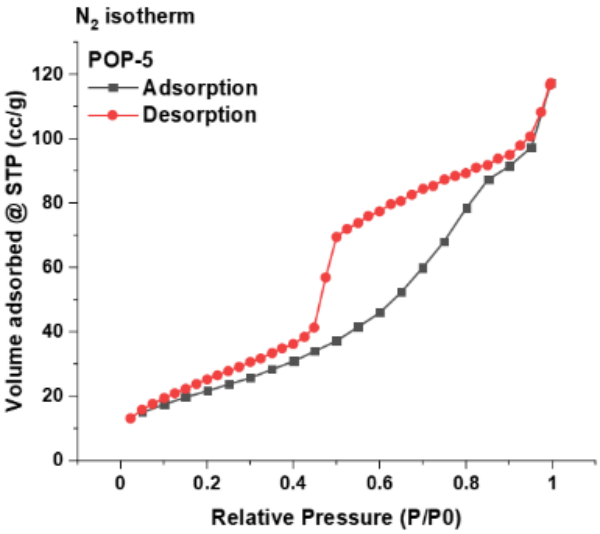
N2 isotherm
POP-5
Adsorption
Desorption
Volume adsorbed @ STP (cc/g)
Relative Pressure (P/P0)

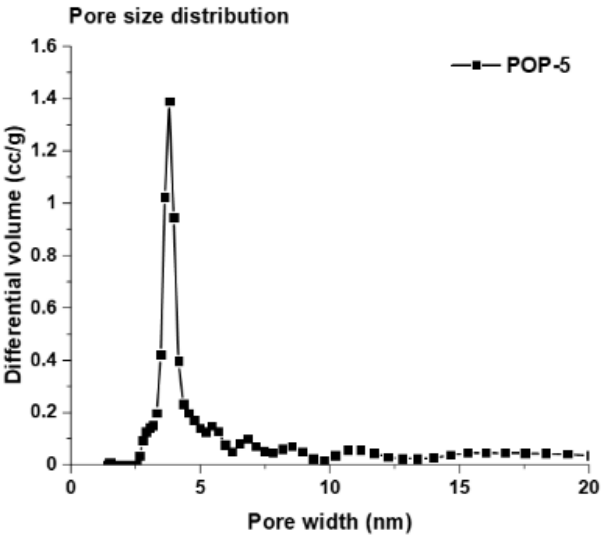
Pore size distribution
POP-5
Differential volume (cc/g)
Pore width (nm)

7.6 POP-6

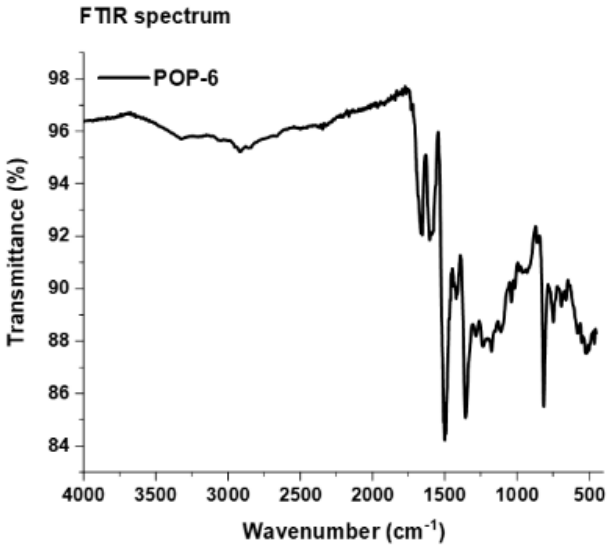
FTIR spectrum
POP-6
Transmittance (%)
Wavenumber (cm-1)

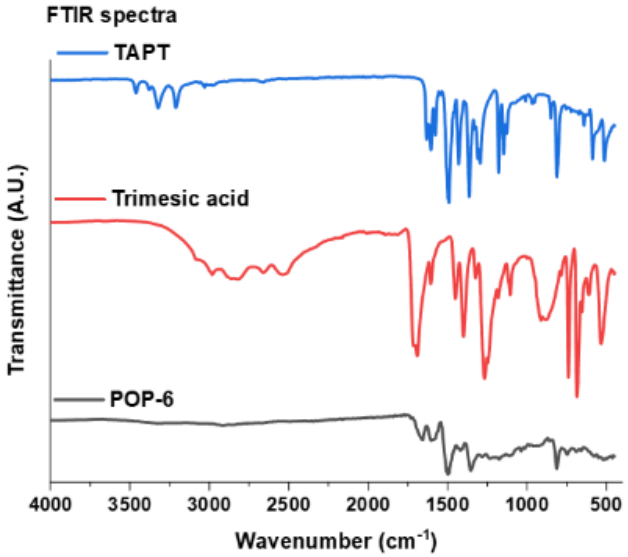
FTIR spectra
TAPT
Trimesic acid
POP-6
Transmittance (A.U.)
Wavenumber (cm-1)

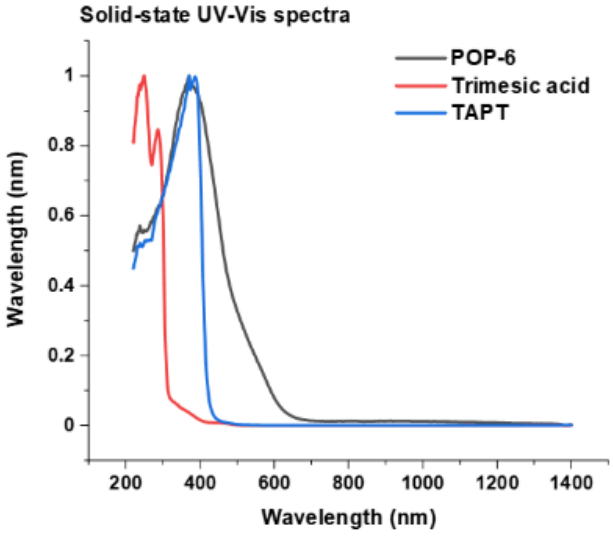
Solid-state UV-Vis spectra
POP-6
Trimesic acid
TAPT
Wavelength (nm)
Wavelength (nm)

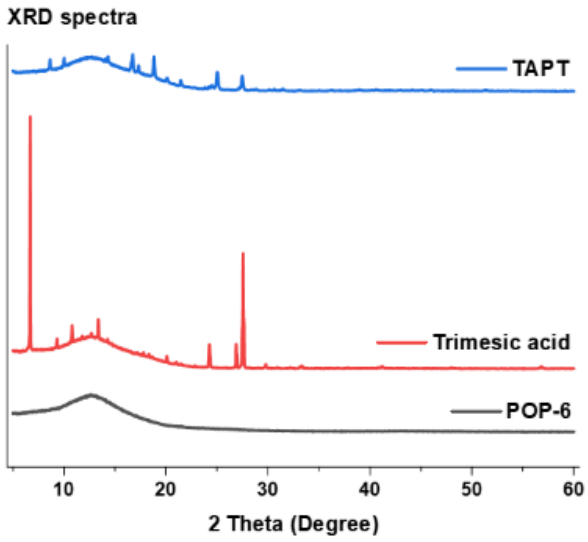
XRD spectra
TAPT
Trimesic acid
POP-6
2 Theta (Degree)

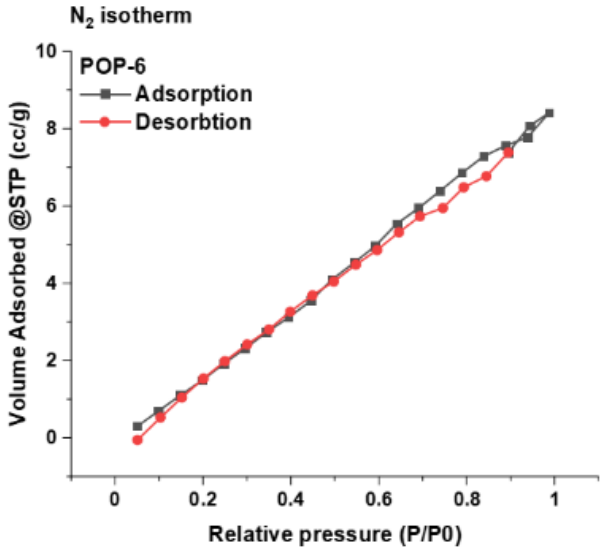
N2 isotherm
POP-6
Adsorption
Desorbtion
Volume Adsorbed @STP (cc/g)
Relative pressure (P/P0)

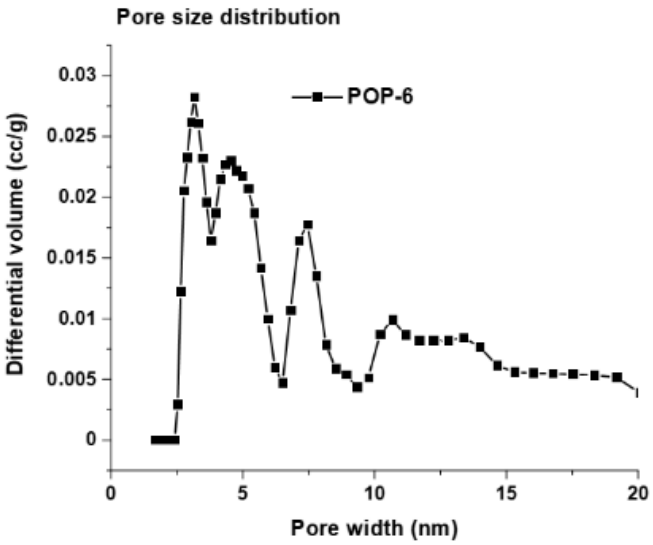
Pore size distribution
POP-6
Differential volume (cc/g)
Pore width (nm)

7.7 TAPT-N

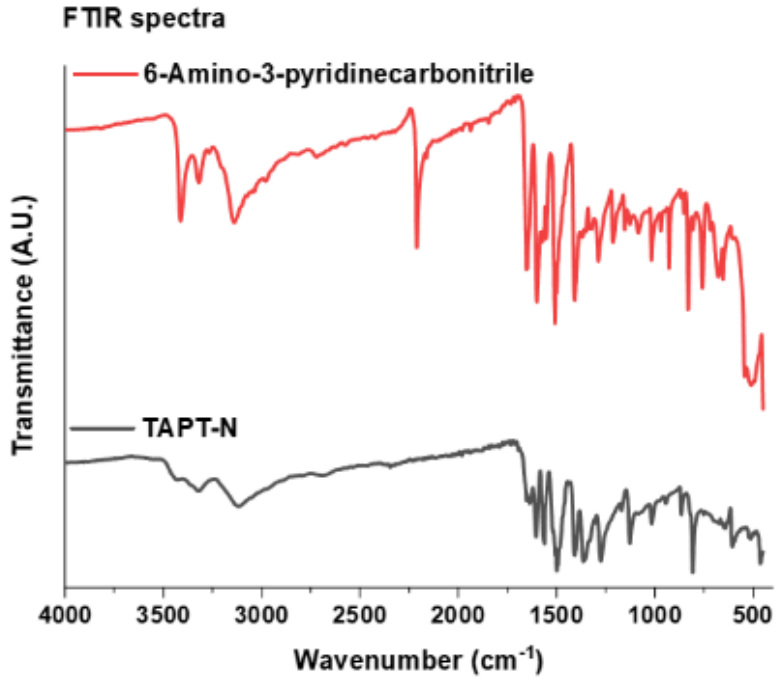
FTIR spectra
6-Amino-3-pyridinecarbonitrile
TAPT-N
Transmittance (A.U.)
4000
3500
3000
2500
2000
1500
1000
500
Wavenumber (cm-1)

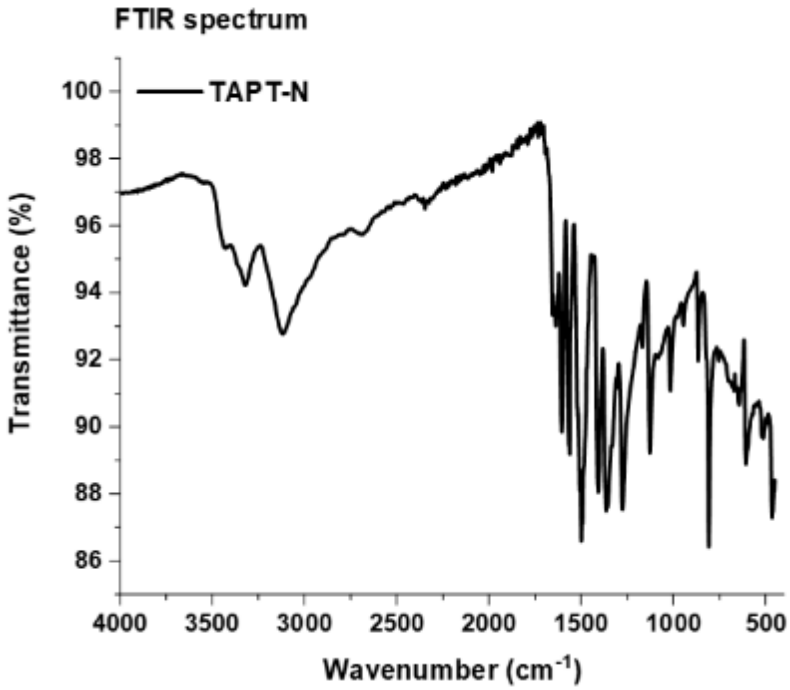
FTIR spectrum
TAPT-N
Transmittance (%)
100
98
96
94
92
90
88
86
4000
3500
3000
2500
2000
1500
1000
500
Wavenumber (cm-1)

6-Amino-3-pyridinecarbonitrile H^1 NMR

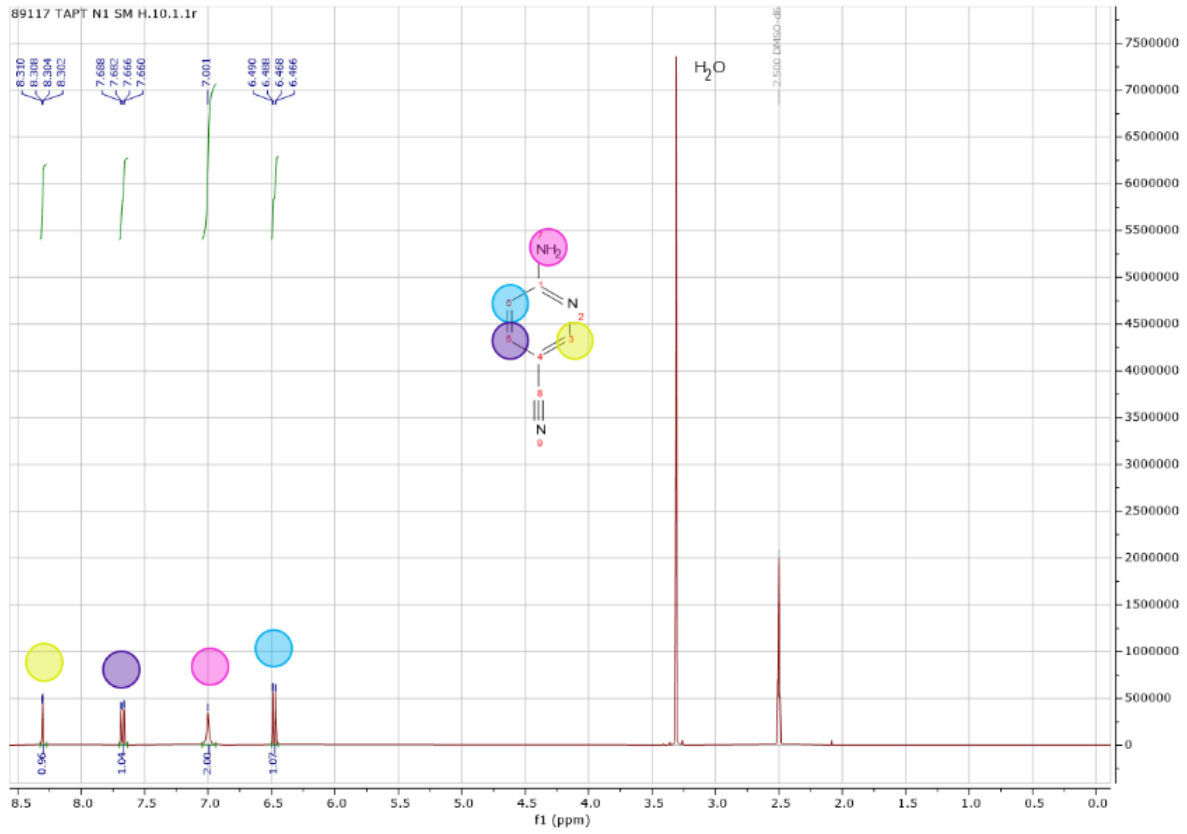

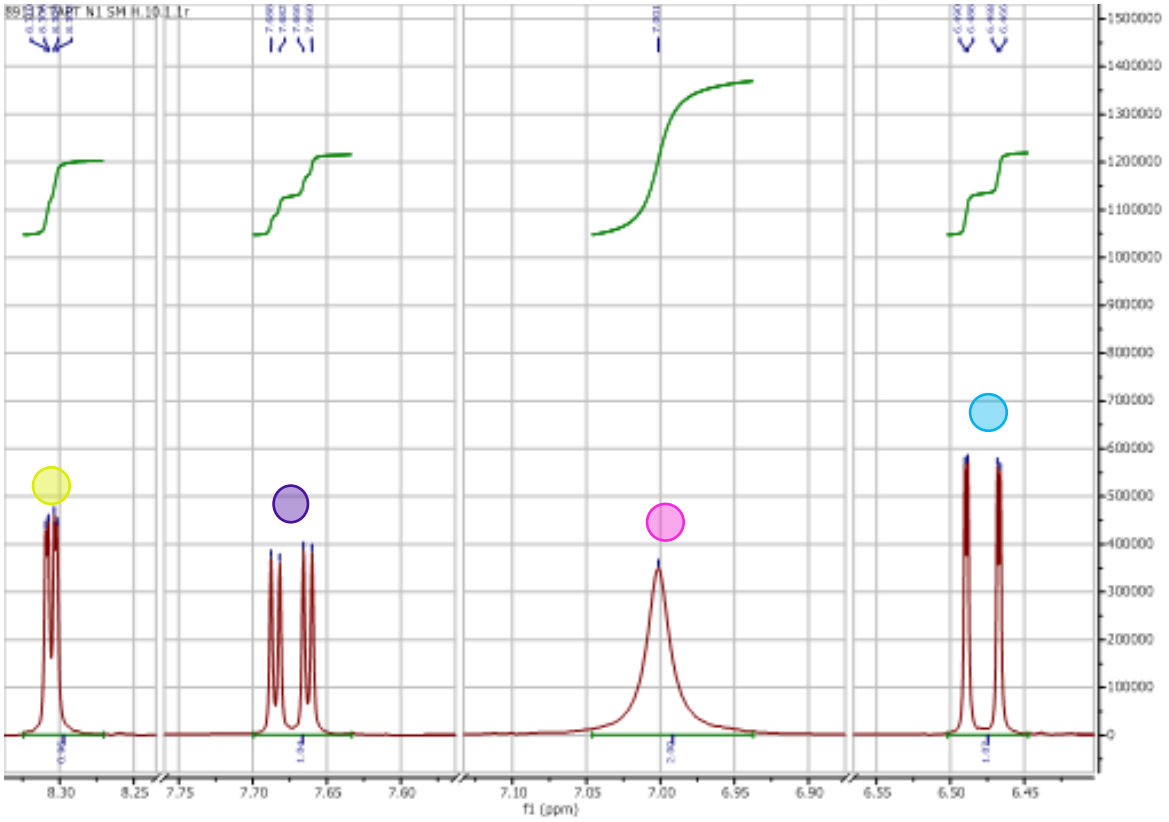

TAPT-N H^1 NMR

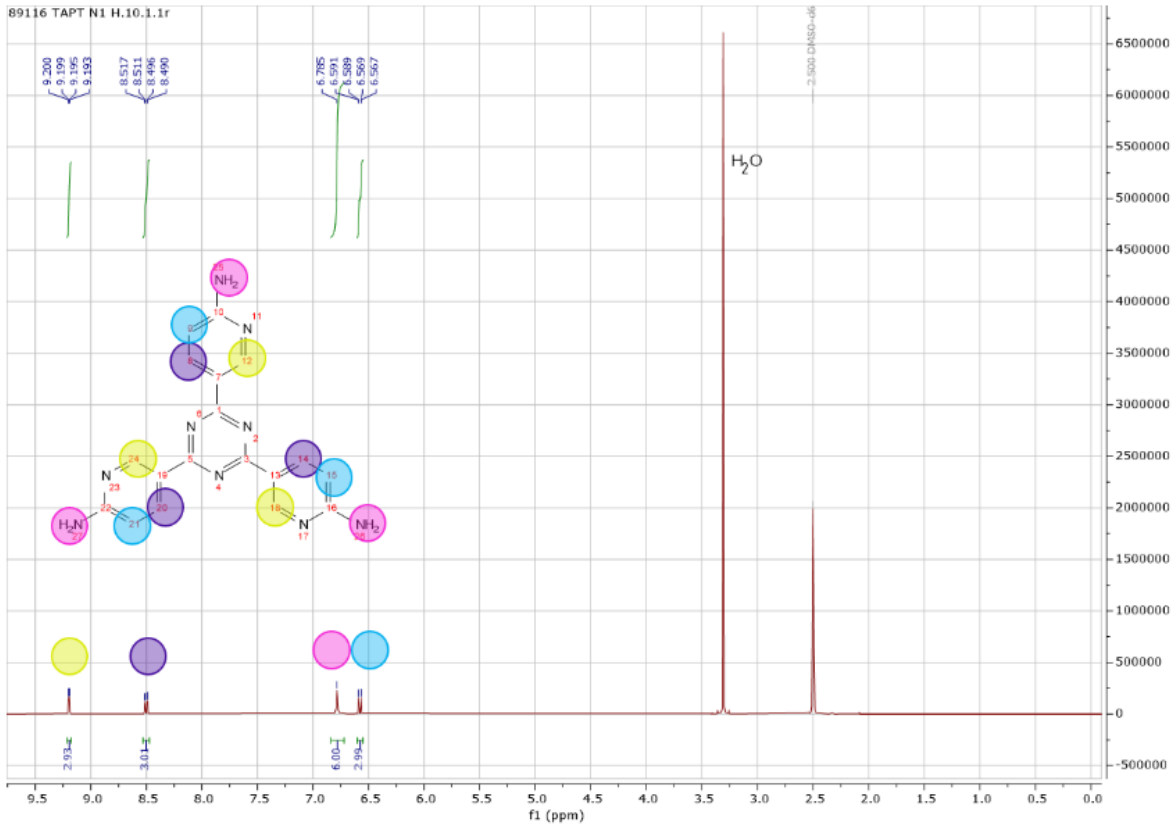

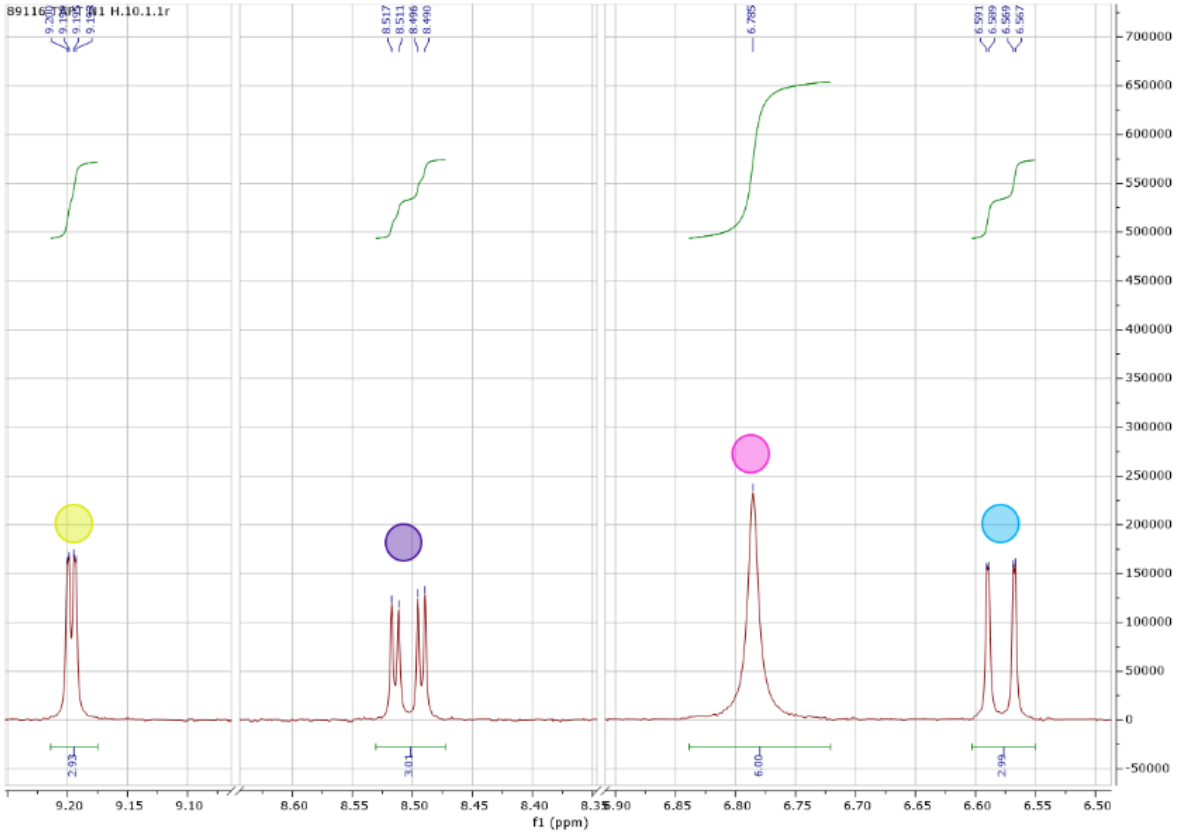

7.8 POP-7

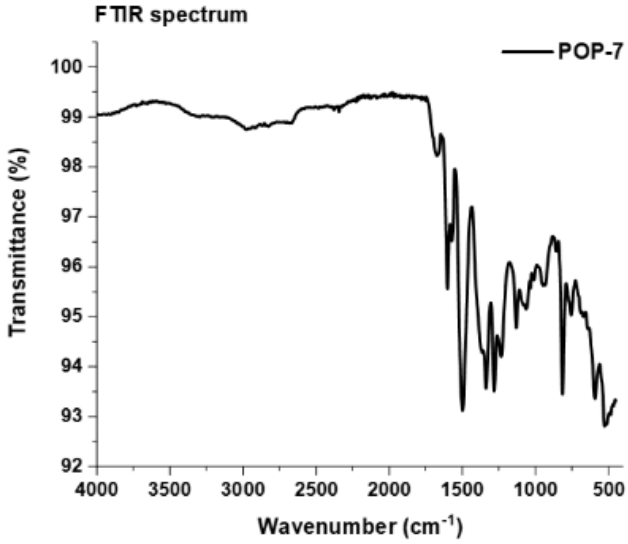
FTIR spectrum
POP-7
Transmittance (%)
Wavenumber (cm-1)

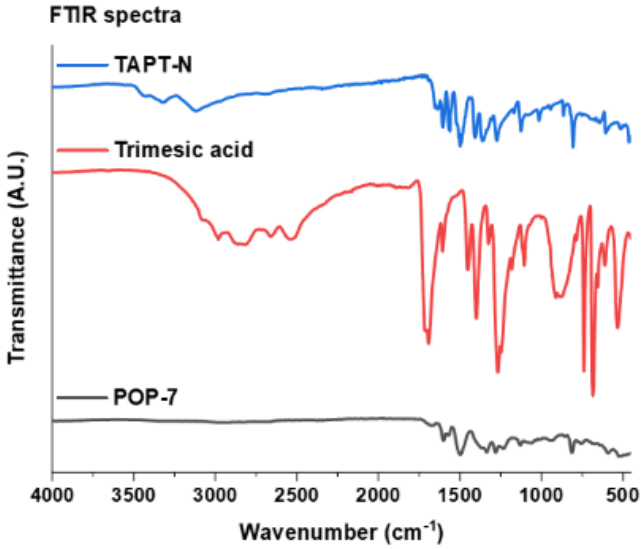
FTIR spectra
TAPT-N
Trimesic acid
POP-7
Transmittance (A.U.)
Wavenumber (cm-1)

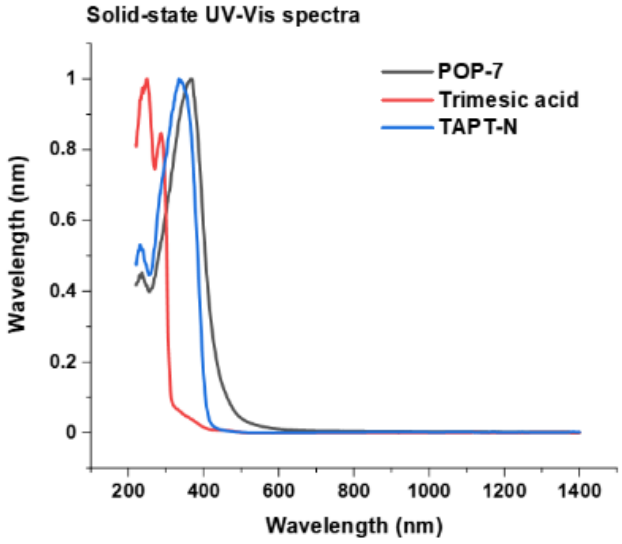
Solid-state UV-Vis spectra
POP-7
Trimesic acid
TAPT-N
Wavelength (nm)
Wavelength (nm)

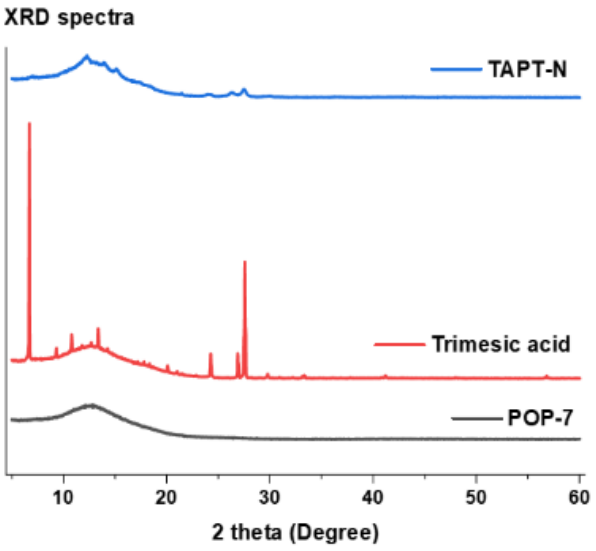
XRD spectra
TAPT-N
Trimesic acid
POP-7
2 theta (Degree)

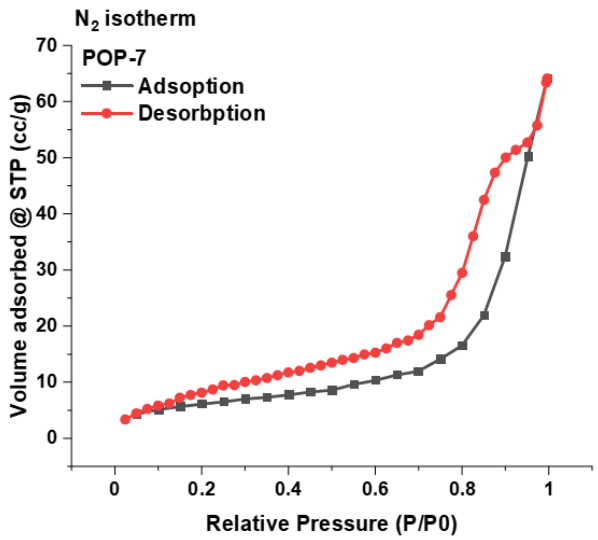
N2 isotherm
POP-7
Adsoption
Desorbption
Volume adsorbed @ STP (cc/g)
Relative Pressure (P/P0)

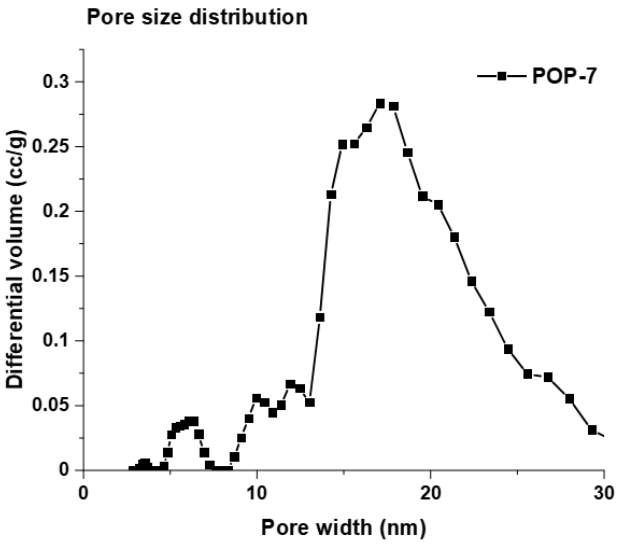
Pore size distribution
POP-7
Differential volume (cc/g)
Pore width (nm)

7.9 Standard dye adsorption experiments

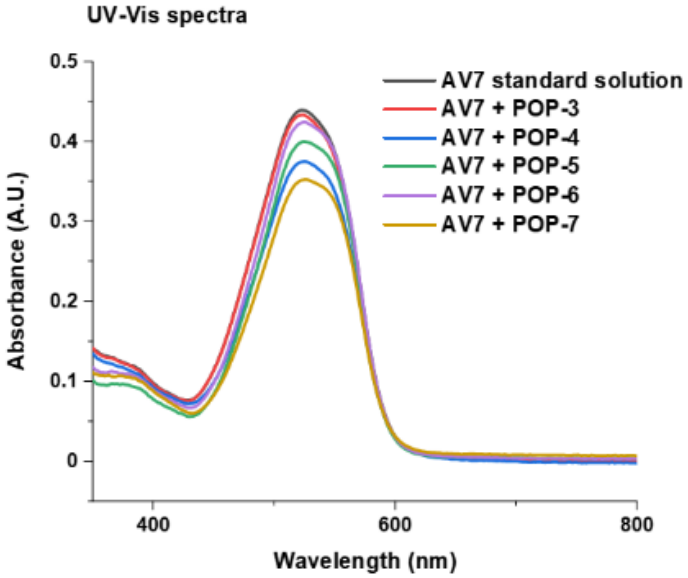

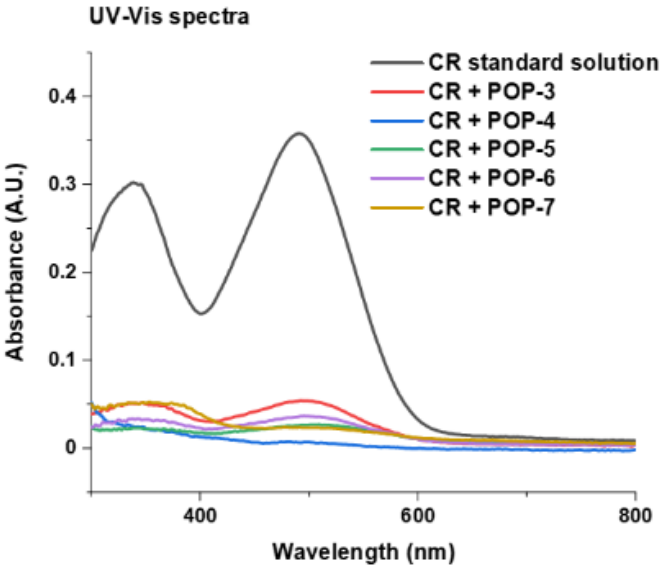

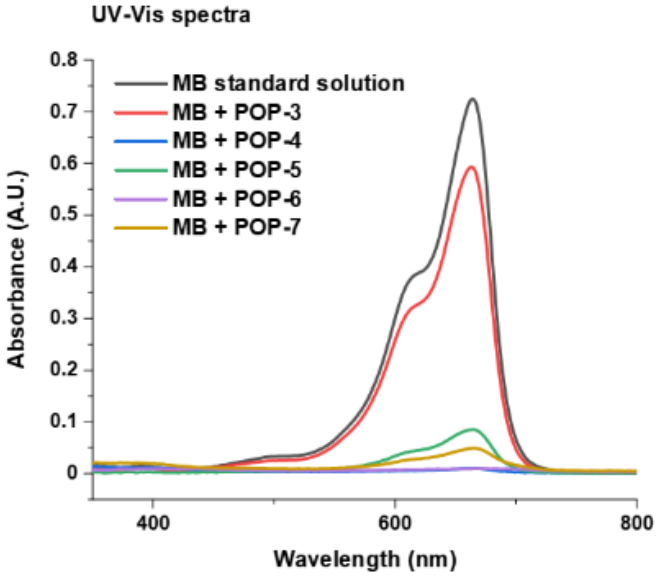

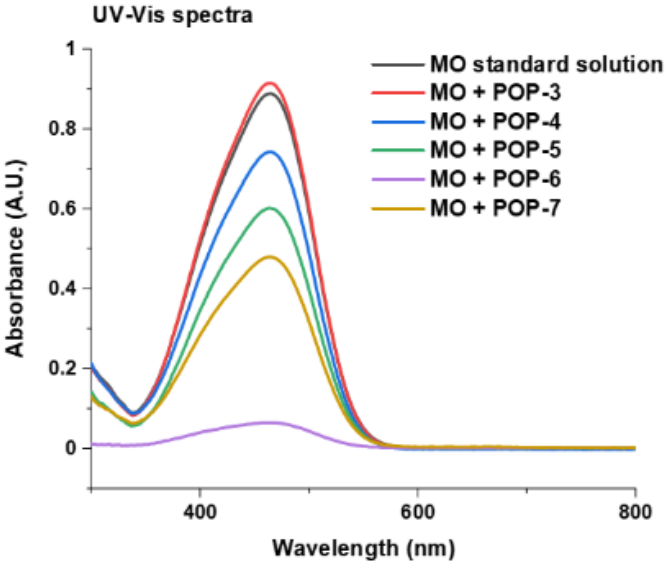

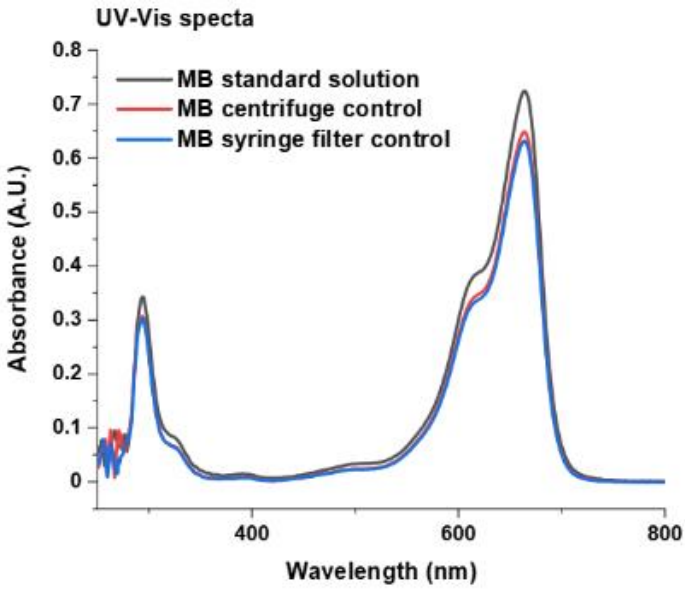

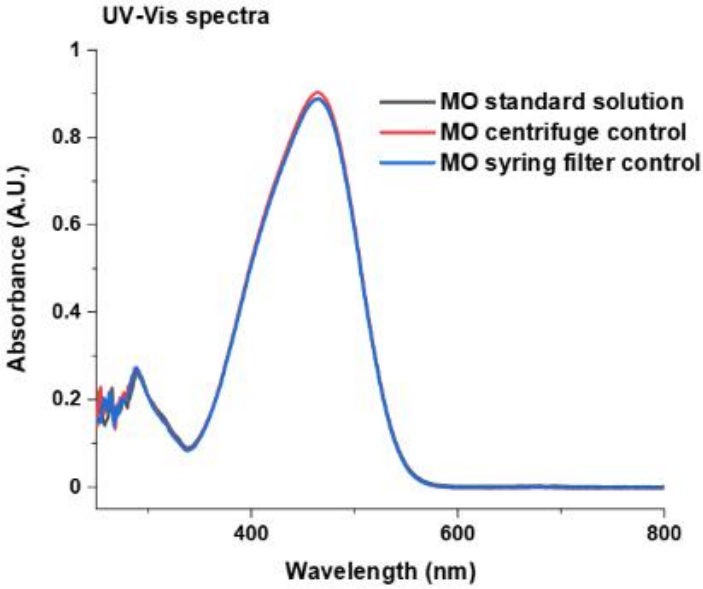

7.10 pH experiments of MB and MO with regards to POP-6

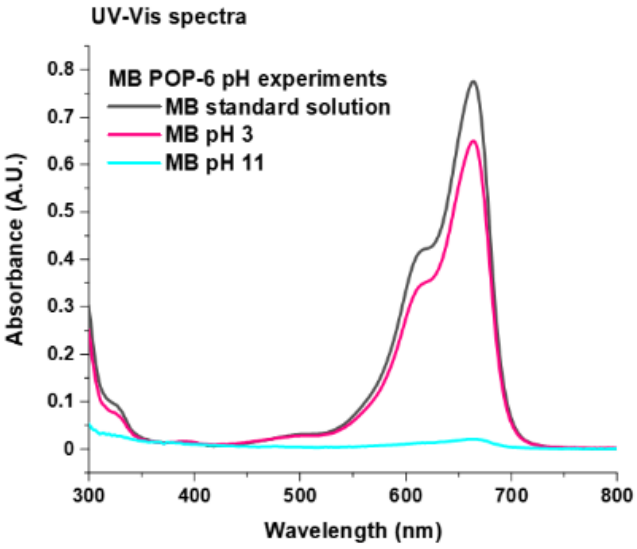

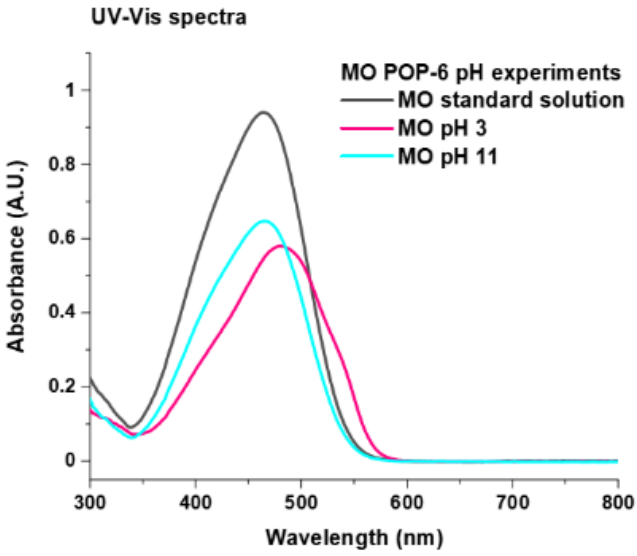

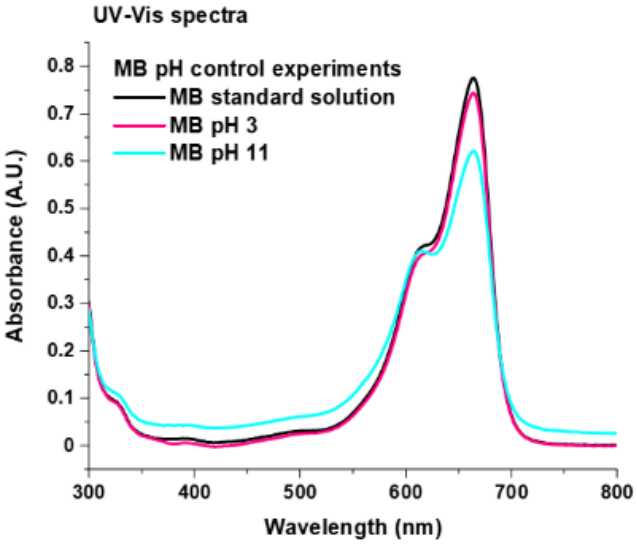

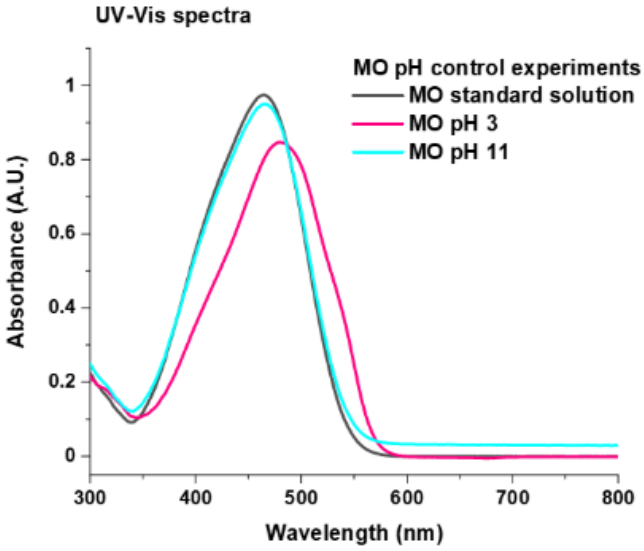

7.11 Rate of MB and MO adsorption with regards to POP-6

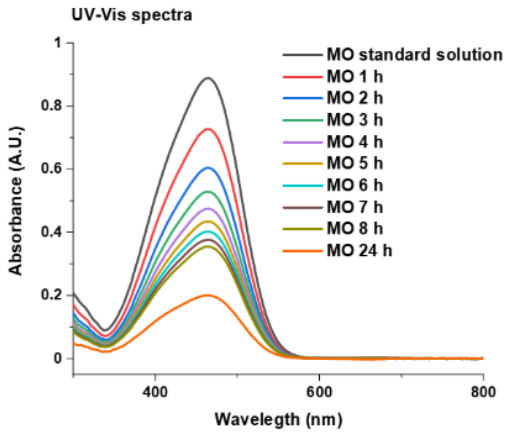

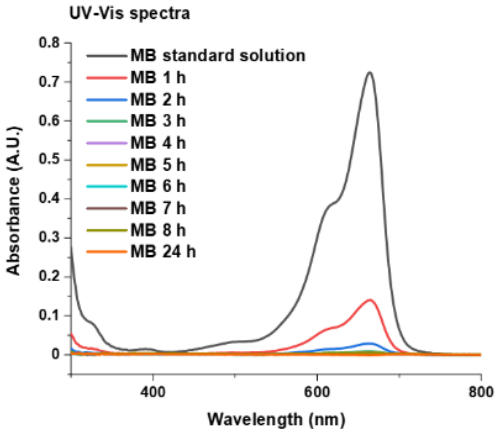

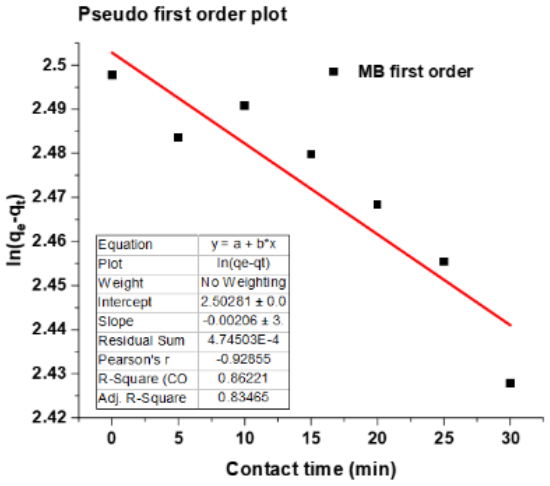

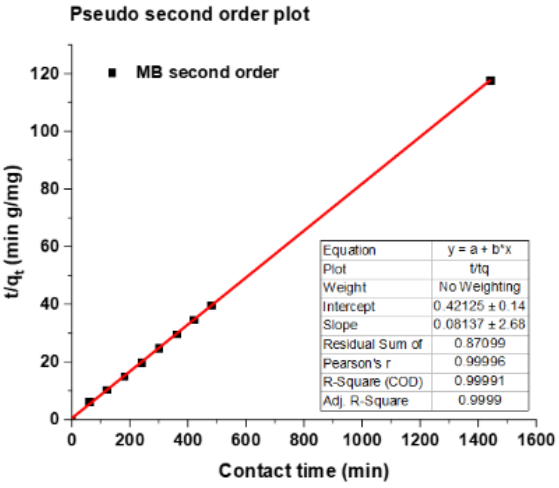

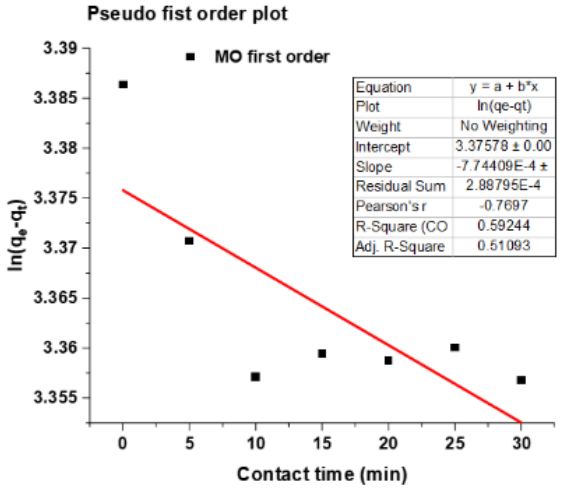

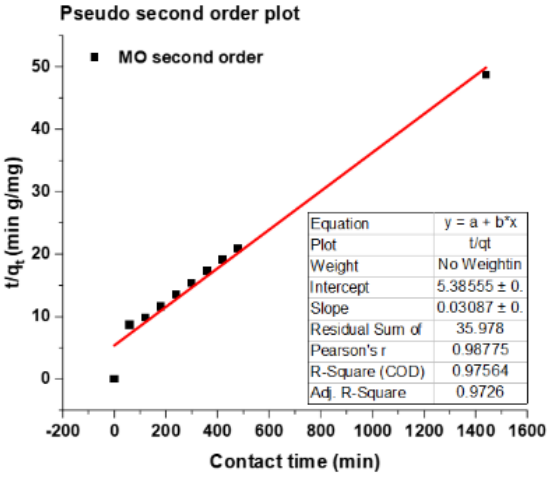

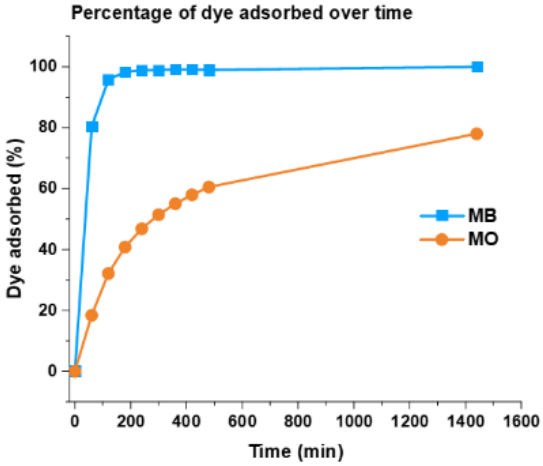

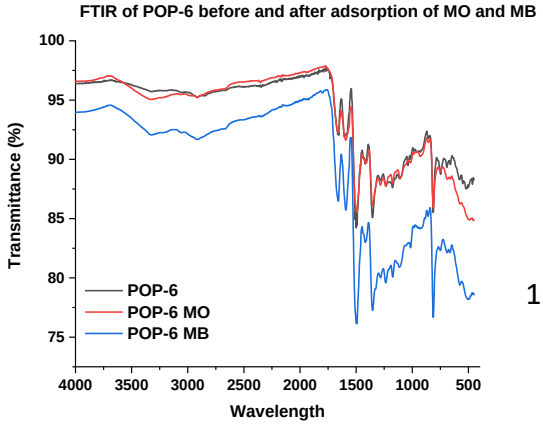

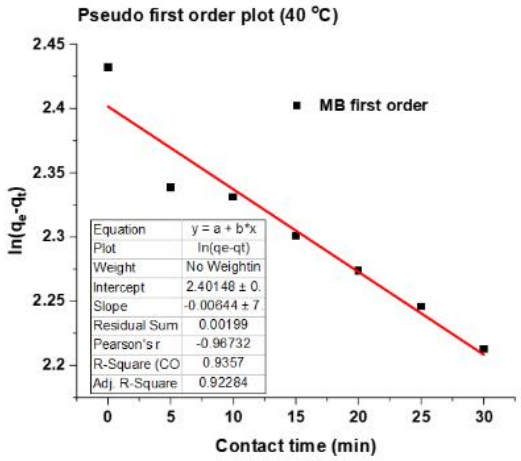
Pseudo first order plot (40 °C)
MB first order
ln(qe-qt)
Contact time (min)
Equation | y = a + b*x
Plot | ln(qe-qt)
Weight | No Weightin
Intercept | 2.40148 ± 0.
Slope | -0.00644 ± 7
Residual Sum | 0.00199
Pearson's r | -0.98732
R-Square (CO | 0.9357
Adj. R-Square | 0.92284

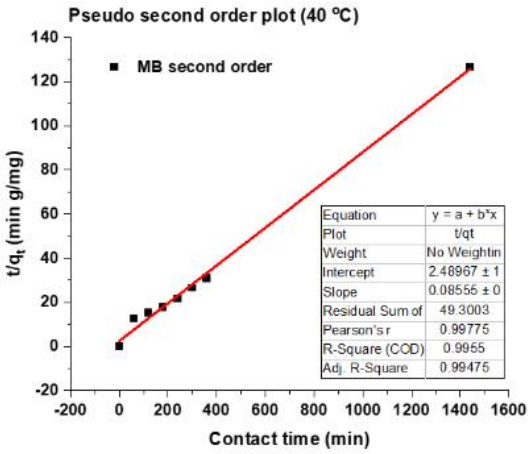
Pseudo second order plot (40 °C)
MB second order
t/qt (min g/mg)
Contact time (min)
Equation | y = a + b*x
Plot | t/qt
Weight | No Weightin
Intercept | 2.48967 ± 1
Slope | 0.08555 ± 0
Residual Sum of | 49.3003
Pearson's r | 0.99775
R-Square (COD) | 0.9955
Adj. R-Square | 0.99475

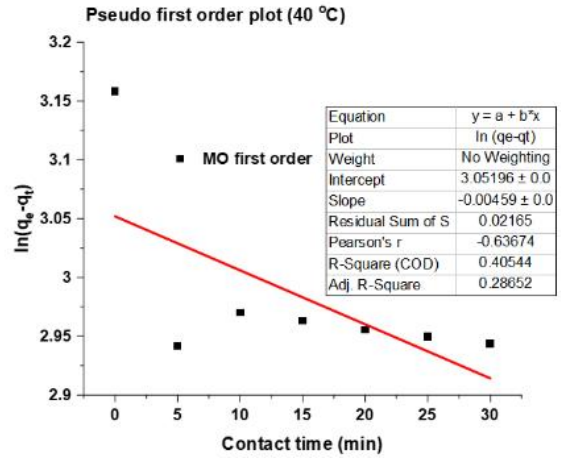
Pseudo first order plot (40 °C)
MO first order
ln(qe-qt)
Contact time (min)
Equation | y = a + b*x
Plot | ln (qe-qt)
Weight | No Weighting
Intercept | 3.05196 ± 0.0
Slope | -0.00459 ± 0.0
Residual Sum of S | 0.02165
Pearson's r | -0.63674
R-Square (COD) | 0.40544
Adj. R-Square | 0.28652

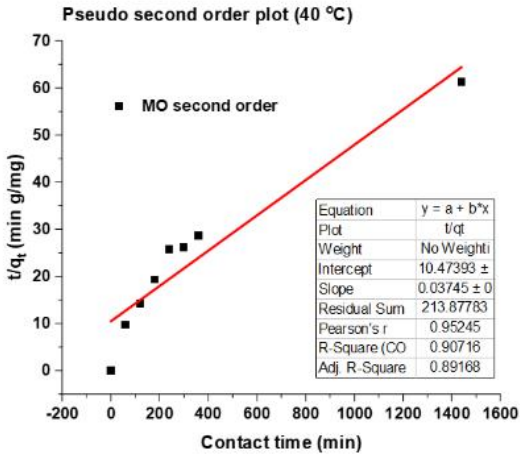
Pseudo second order plot (40 °C)
MO second order
t/qt (min g/mg)
Contact time (min)
Equation | y = a + b*x
Plot | t/qt
Weight | No Weightin
Intercept | 10.47393 ±
Slope | 0.03745 ± 0
Residual Sum | 213.87783
Pearson's r | 0.95245
R-Square (CO | 0.90716
Adj. R-Square | 0.89168

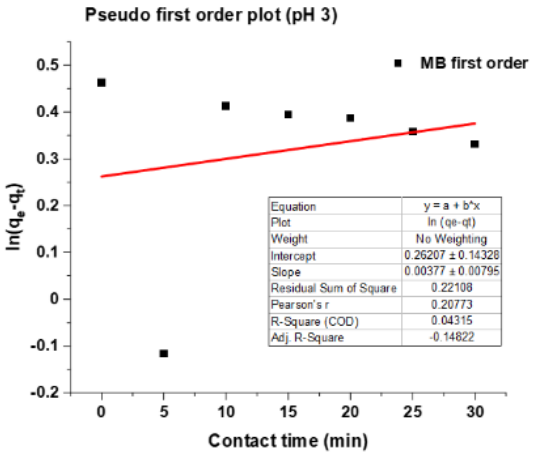
Pseudo first order plot (pH 3)
MB first order
ln(qe-qt)
Contact time (min)
Equation | y = a + b*x
Plot | ln (qe-qt)
Weight | No Weighting
Intercept | 0.26207 ± 0.14328
Slope | 0.00377 ± 0.00795
Residual Sum of Square | 0.22108
Pearson's r | 0.20773
R-Square (COD) | 0.04315
Adj. R-Square | -0.14822

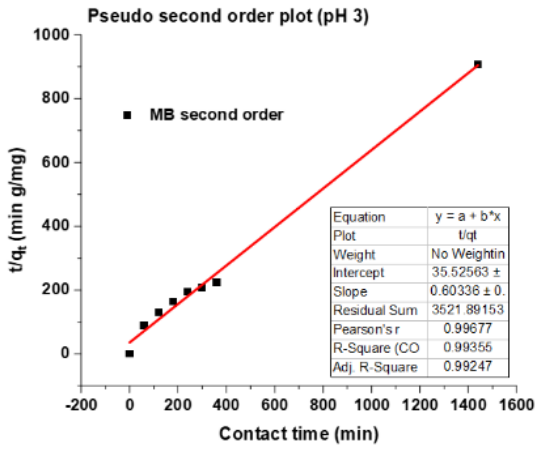
Pseudo second order plot (pH 3)
MB second order
t/qt (min g/mg)
Contact time (min)
Equation | y = a + b*x
Plot | t/qt
Weight | No Weightin
Intercept | 35.52563 ±
Slope | 0.60336 ± 0.
Residual Sum | 3521.89153
Pearson's r | 0.99677
R-Square (CO | 0.99355
Adj. R-Square | 0.99247

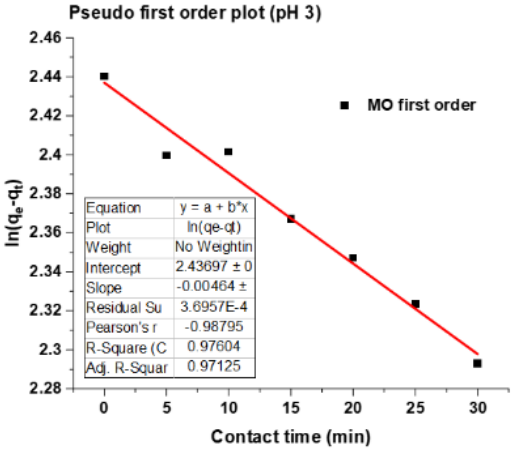
Pseudo first order plot (pH 3)
MO first order
ln(qe-qt)
Contact time (min)
Equation | y = a + b*x
Plot | ln(qe-qt)
Weight | No Weightin
Intercept | 2.43697 ± 0
Slope | -0.00464 ±
Residual Su | 3.6957E-4
Pearson's r | -0.98795
R-Square (C | 0.97604
Adj. R-Squar | 0.97125

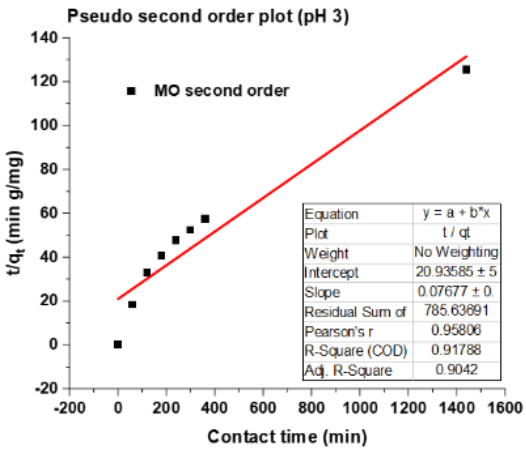
Pseudo second order plot (pH 3)
MO second order
t/qt (min g/mg)
Contact time (min)
Equation | y = a + b*x
Plot | t / qt
Weight | No Weighting
Intercept | 20.93585 ± 5
Slope | 0.07677 ± 0.
Residual Sum of | 785.63691
Pearson's r | 0.95806
R-Square (COD) | 0.91788
Adj. R-Square | 0.9042

Pseudo first order plot (pH 3)

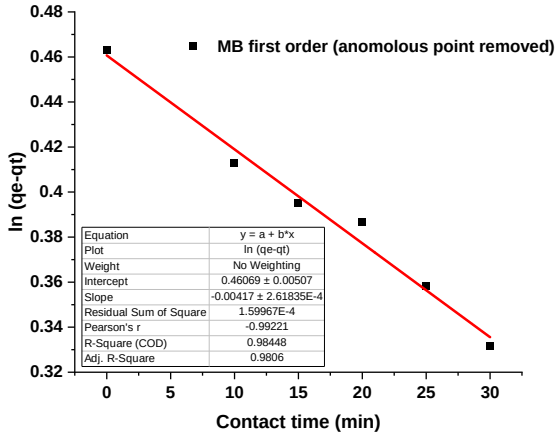

Pseudo first order plot (pH 11)

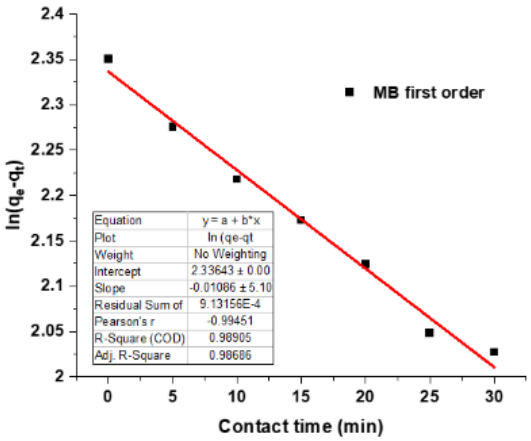

Pseudo second order plot (pH 11)

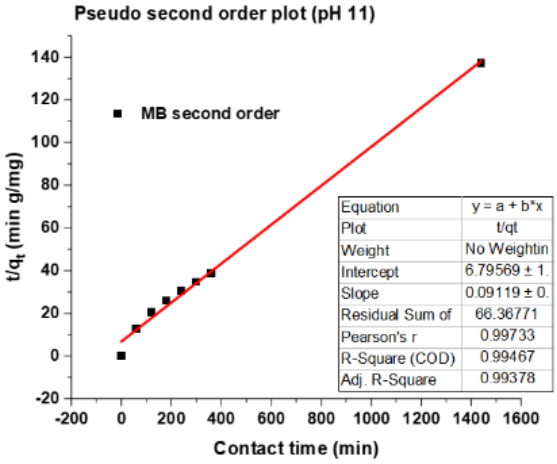

Pseudo first order plot (pH 11)

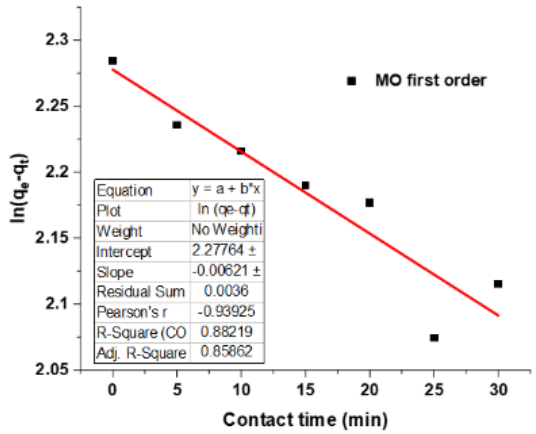

Pseudo second order plot (pH 11)

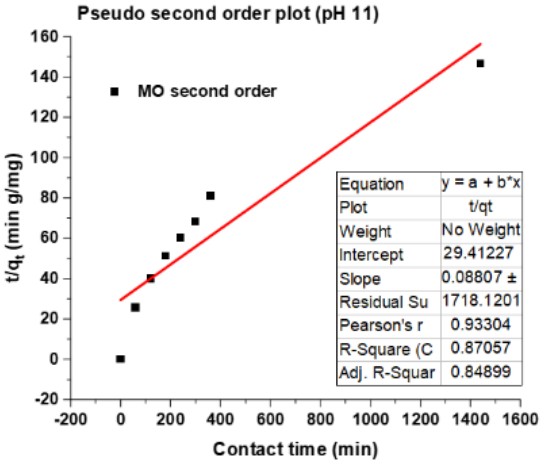

7.12 Adsorption isotherms of MB and MO with regards to POP-6

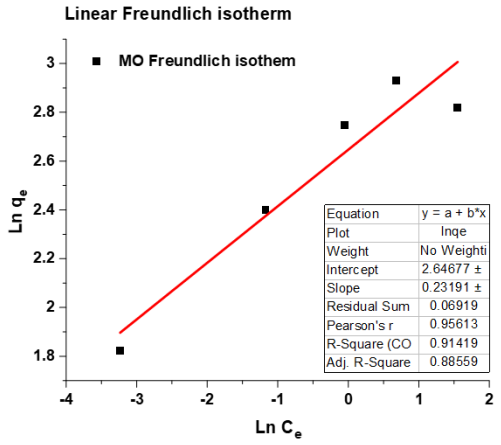

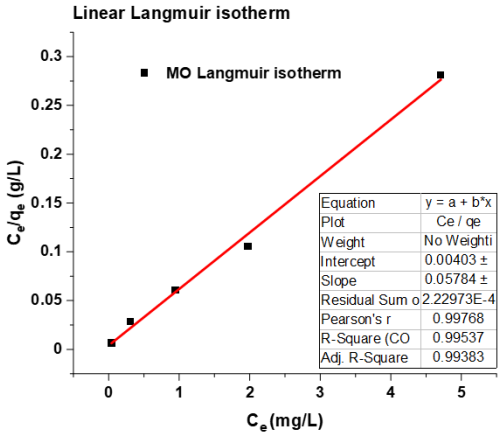

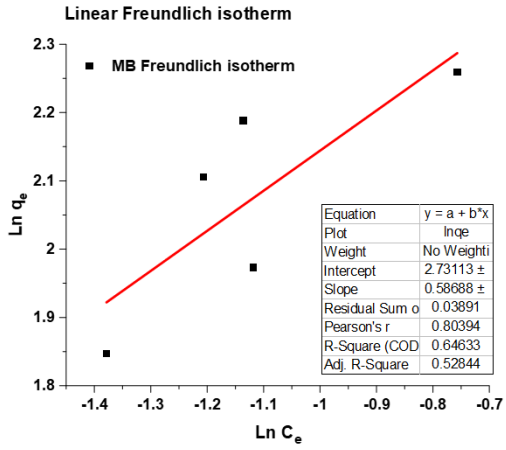

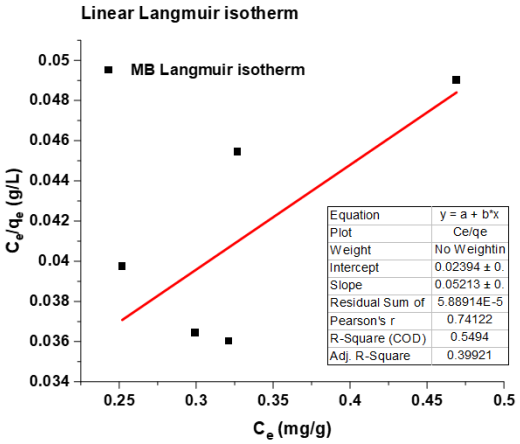

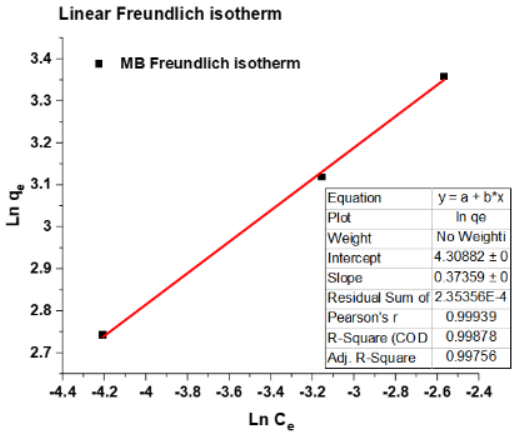

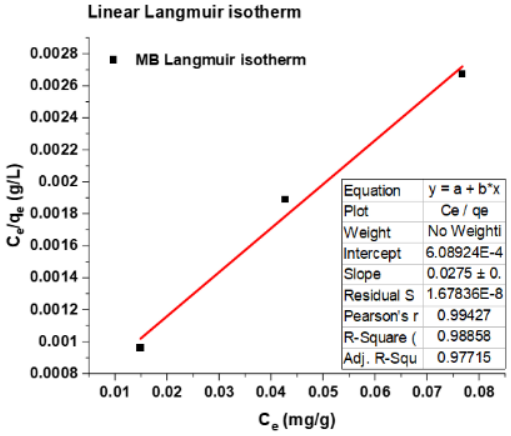

7.13 Recyclability of POP-6 with regards to MB and MO

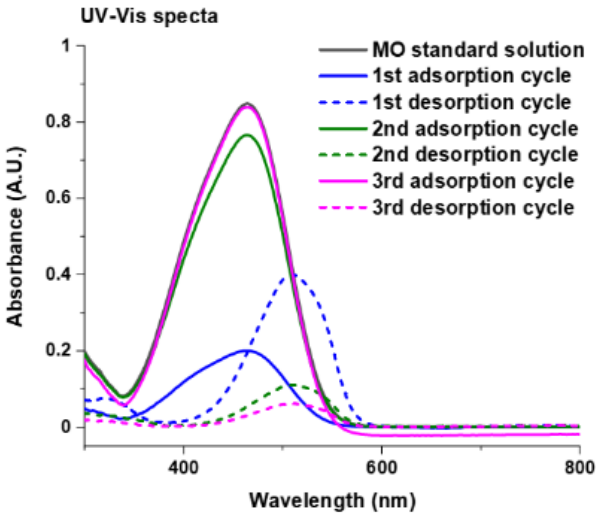

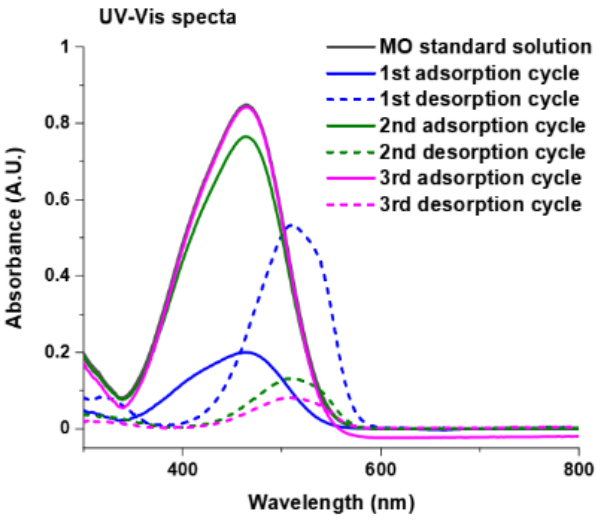

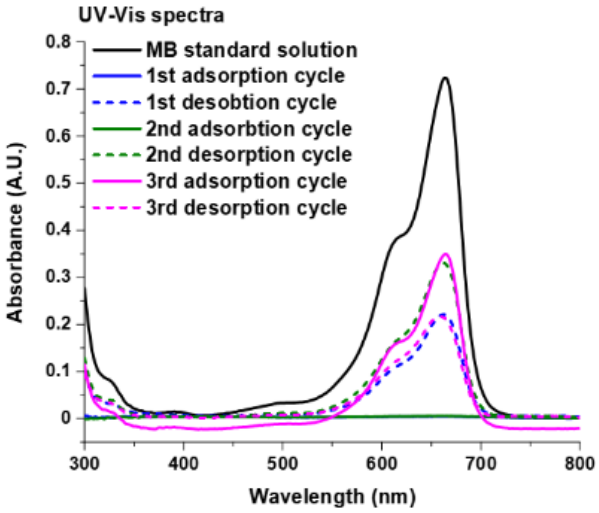

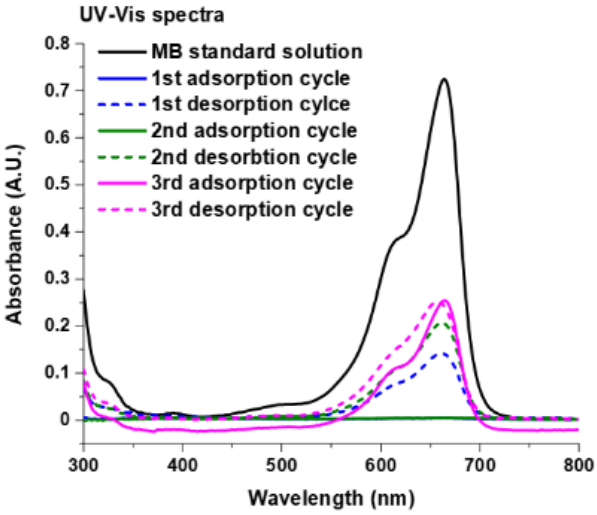

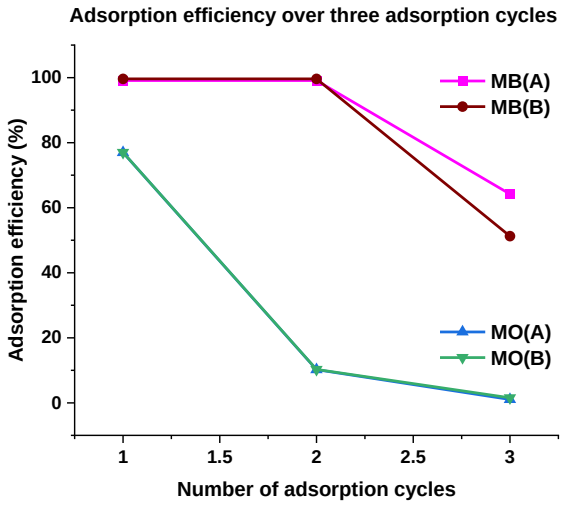

7.14 Textile wastewater simulated conditions

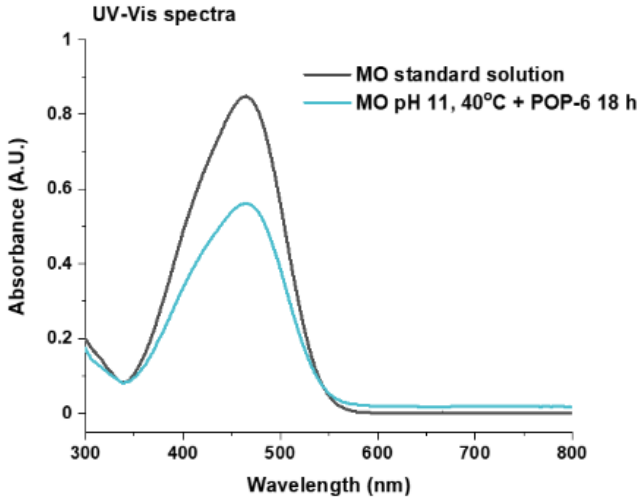

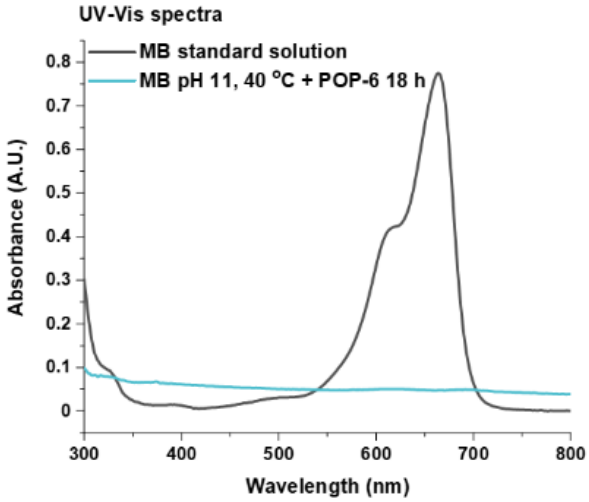

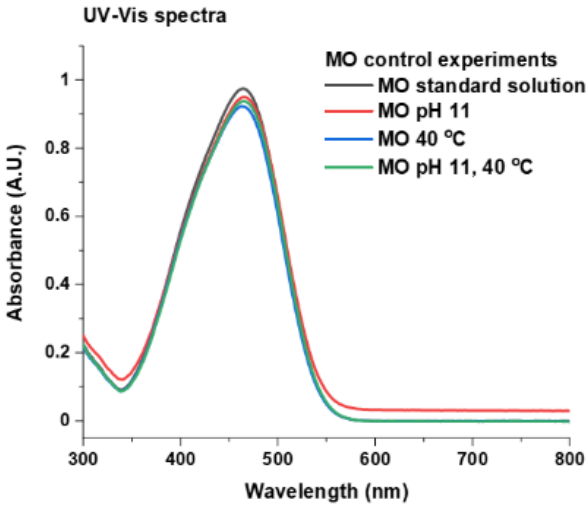

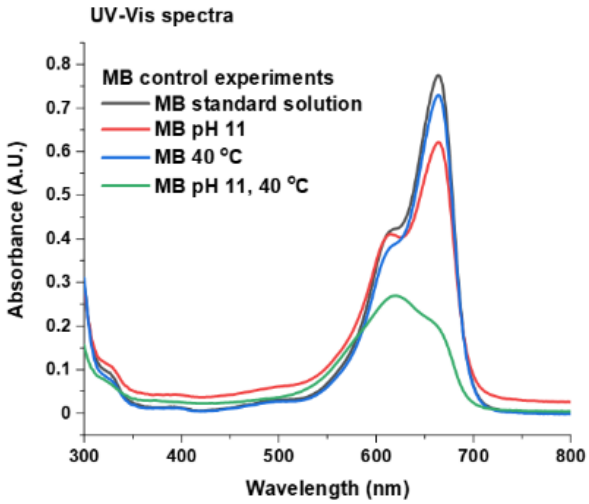

7.15 Standard metal adsorption experiments

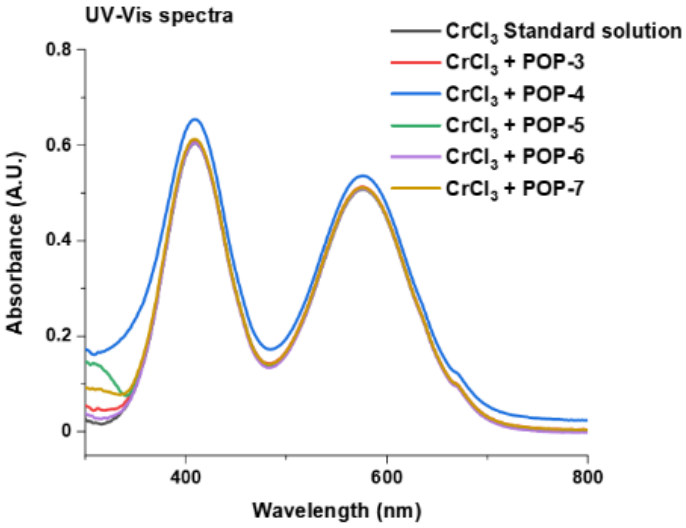

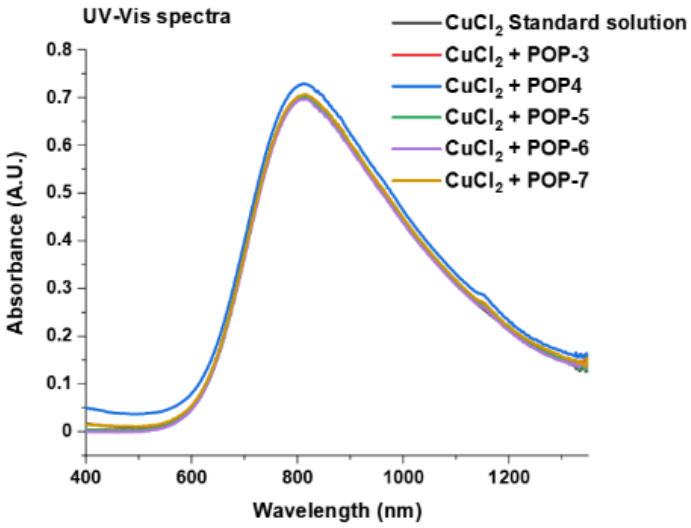

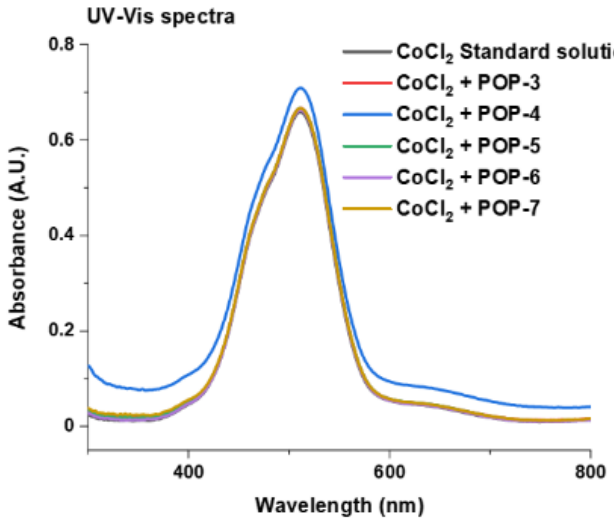

7.16 Calibration curves

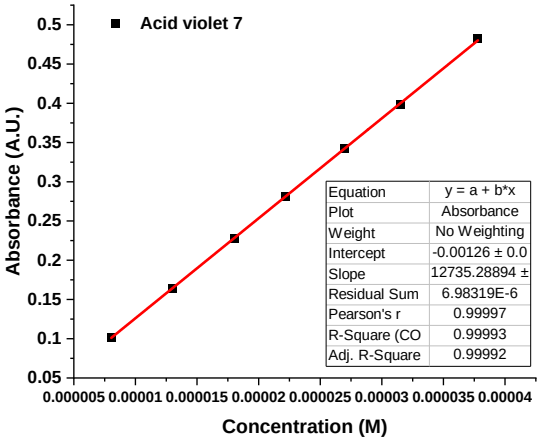

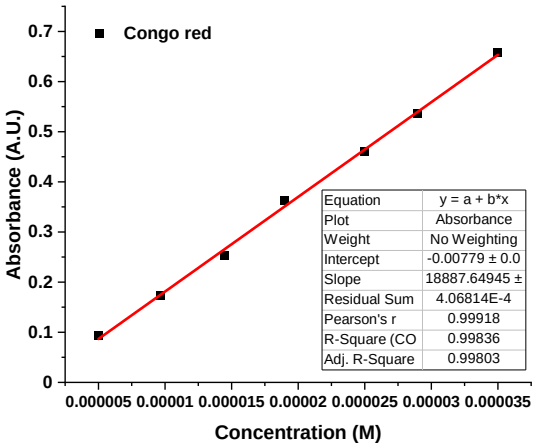

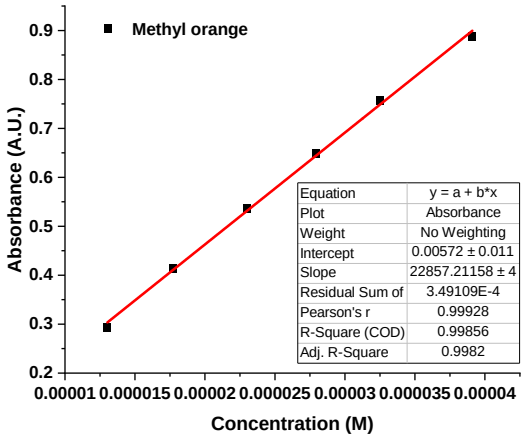

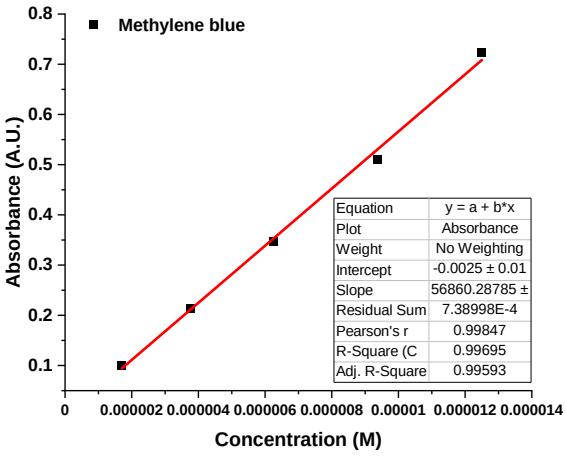

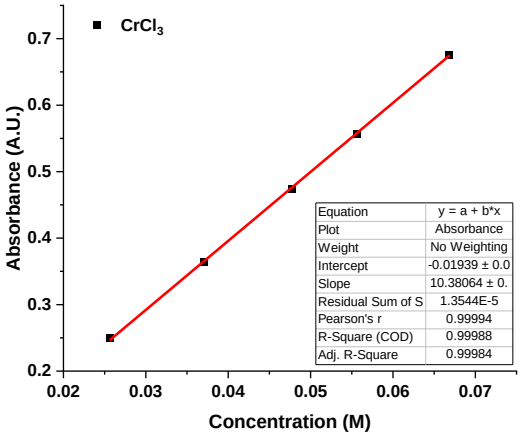

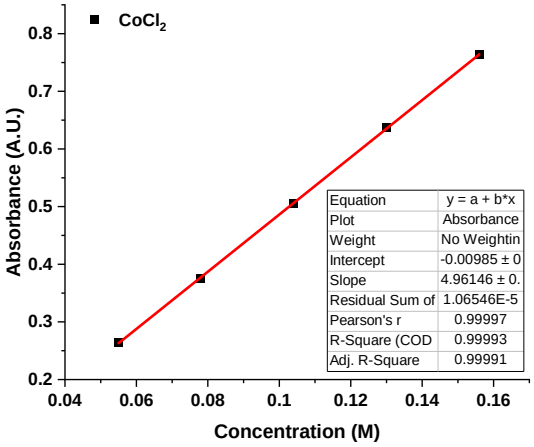

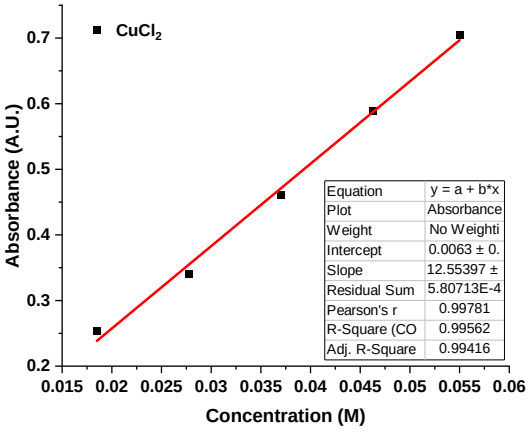

7.17 Contact angle

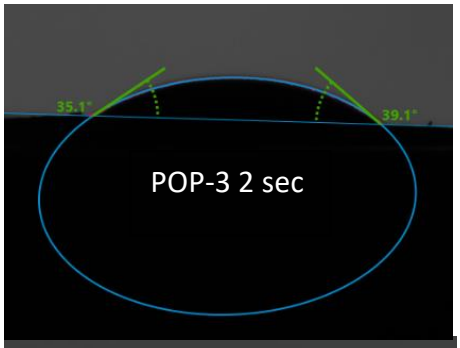

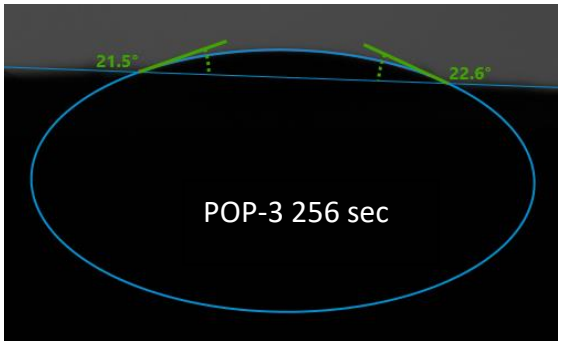

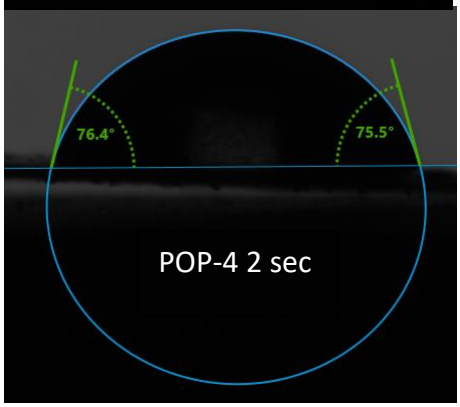

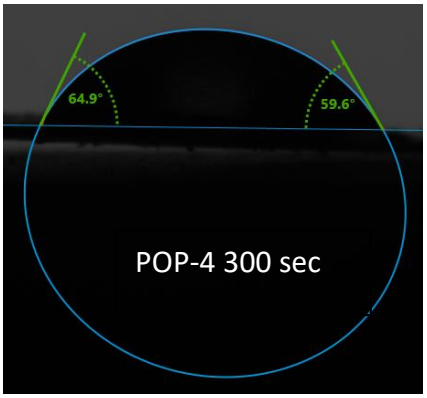

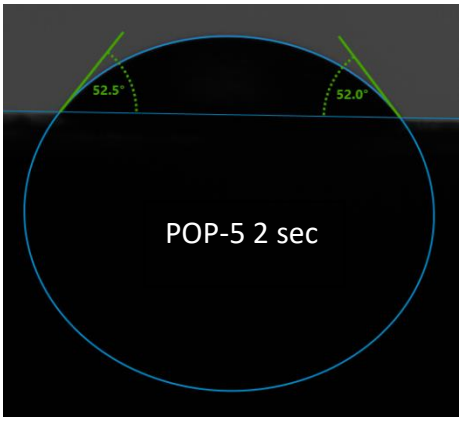

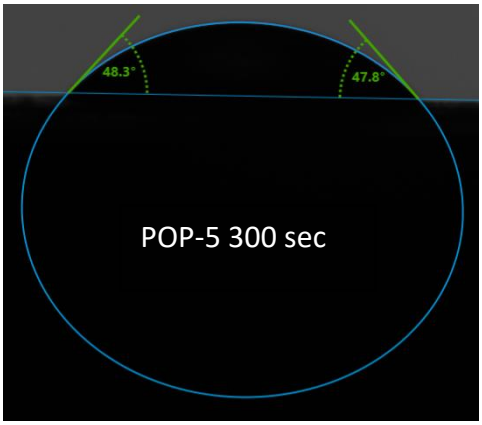

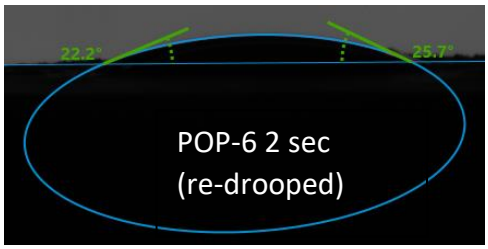

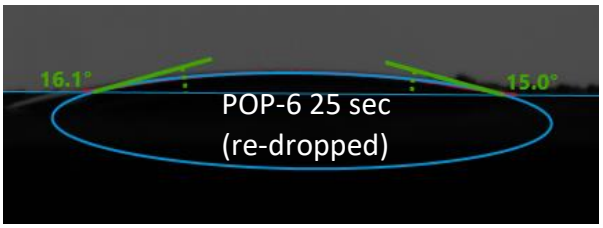

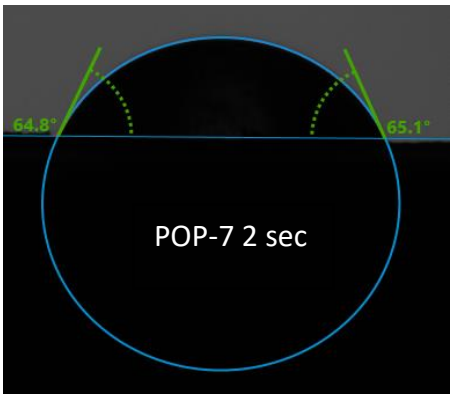

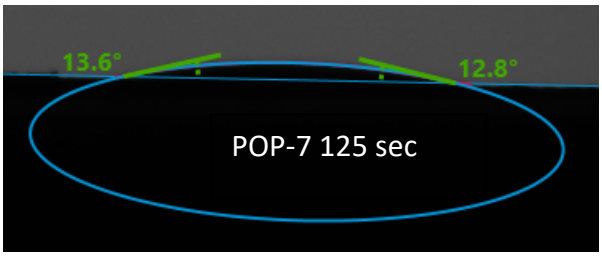

7.18 SEM images

7.18.1 POP-3

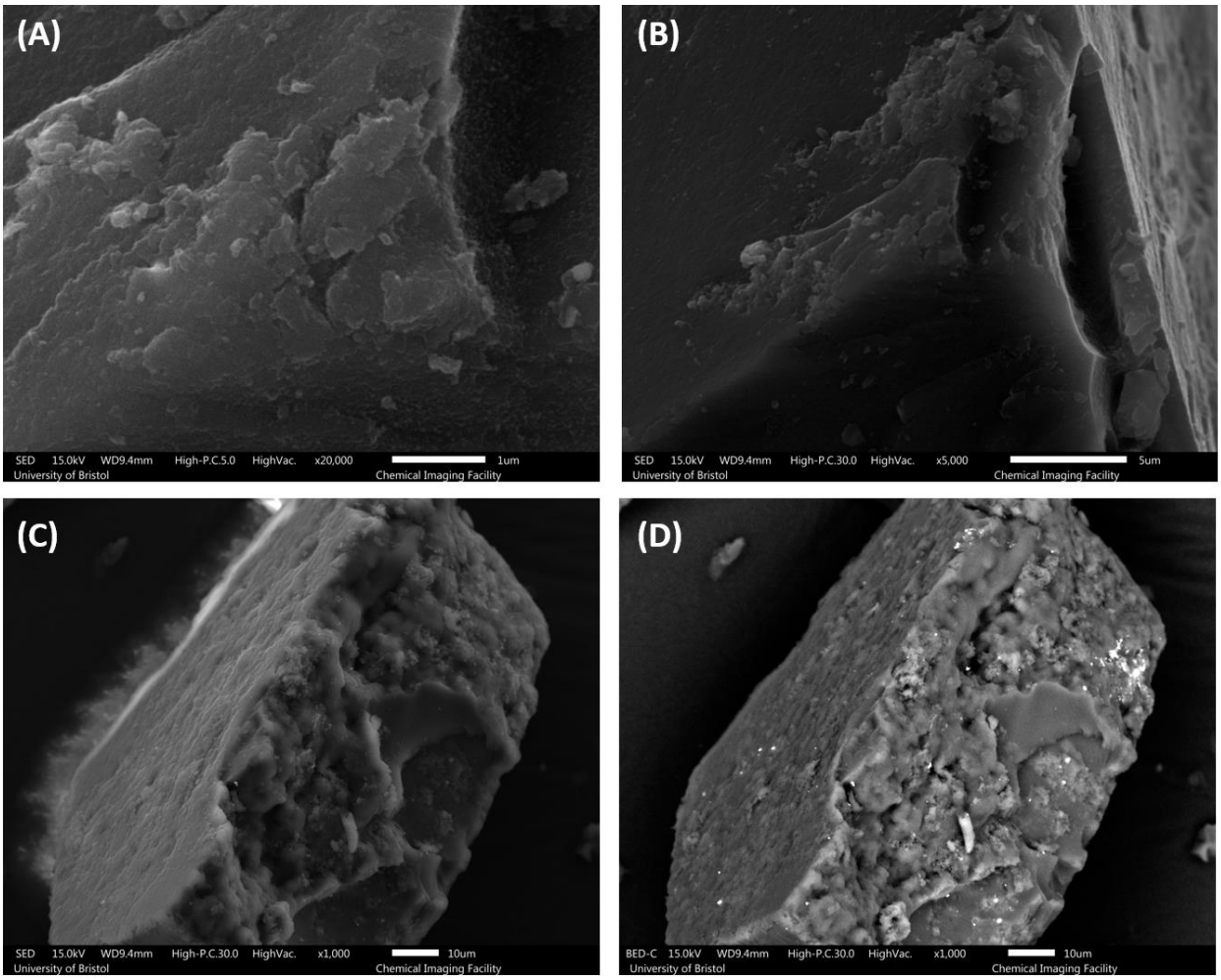

Magnification: (A) x20,000 at 1 µm (SED), (B) x5,000 at 5 µm (SED), (C) x1,000 at 10 µm (SED), (D) x1,000 at 10 µm (BED-C).

7.18.2 POP-4

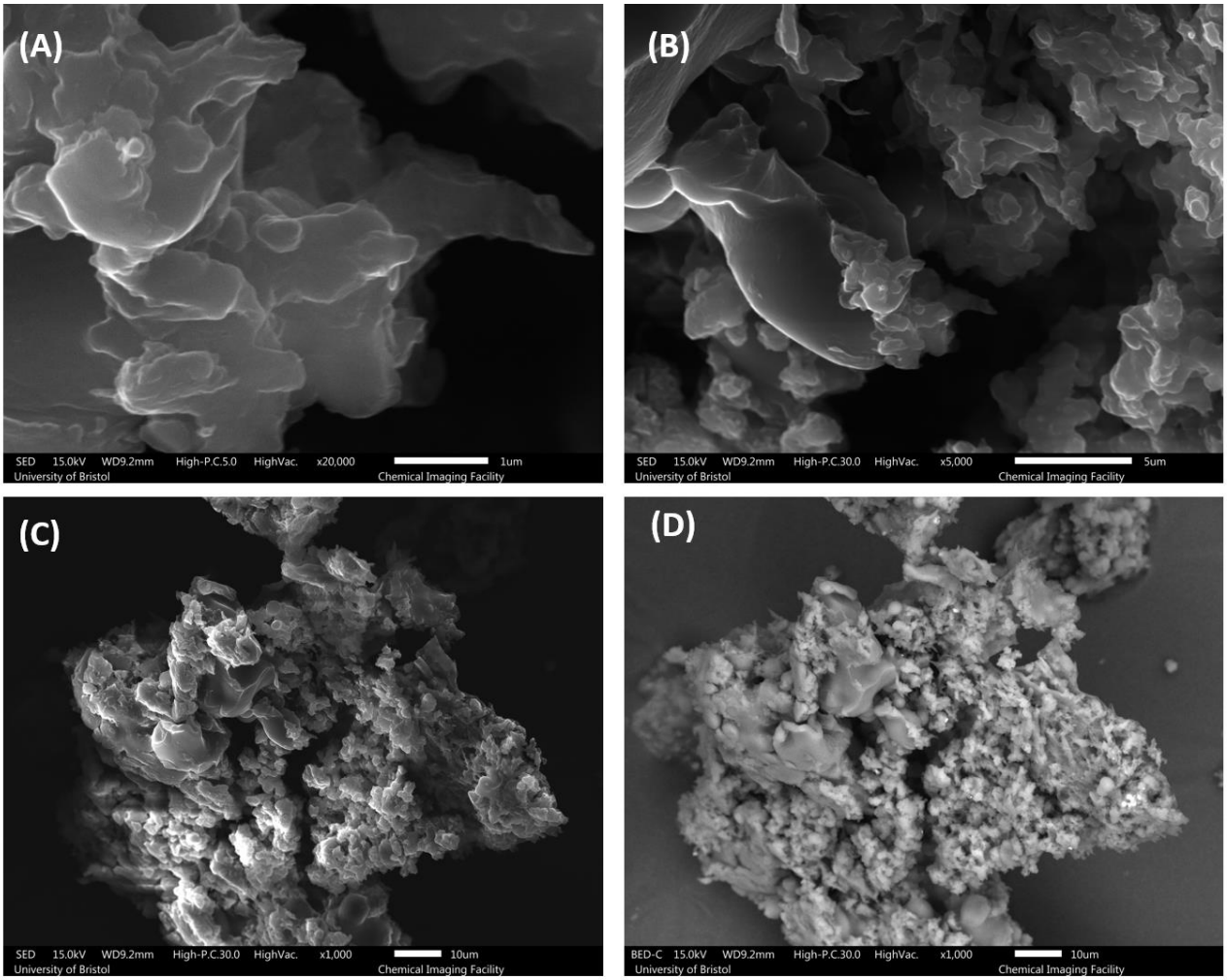

Magnification: (A) x20,000 at 1 µm (SED), (B) x5,000 at 5 µm (SED), (C) x1,000 at 10 µm (SED), (D) x1,000 at 10 µm (BED-C).

7.18.3 POP-5

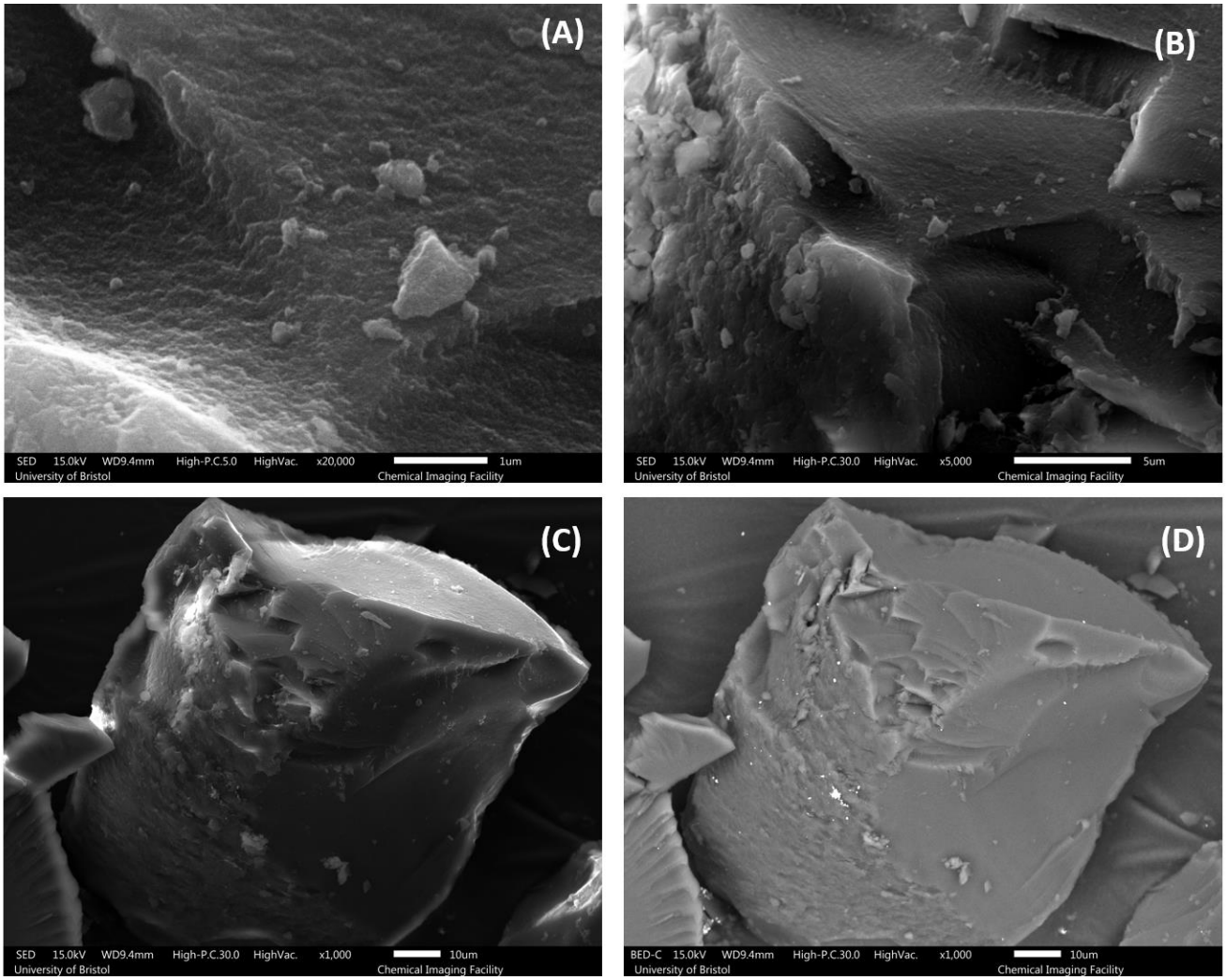

Magnification: (A) x20,000 at 1 µm (SED), (B) x5,000 at 5 µm (SED), (C) x1,000 at 10 µm (SED), (D) x1,000 at 10 µm (BED-C).

7.18.4 POP-6

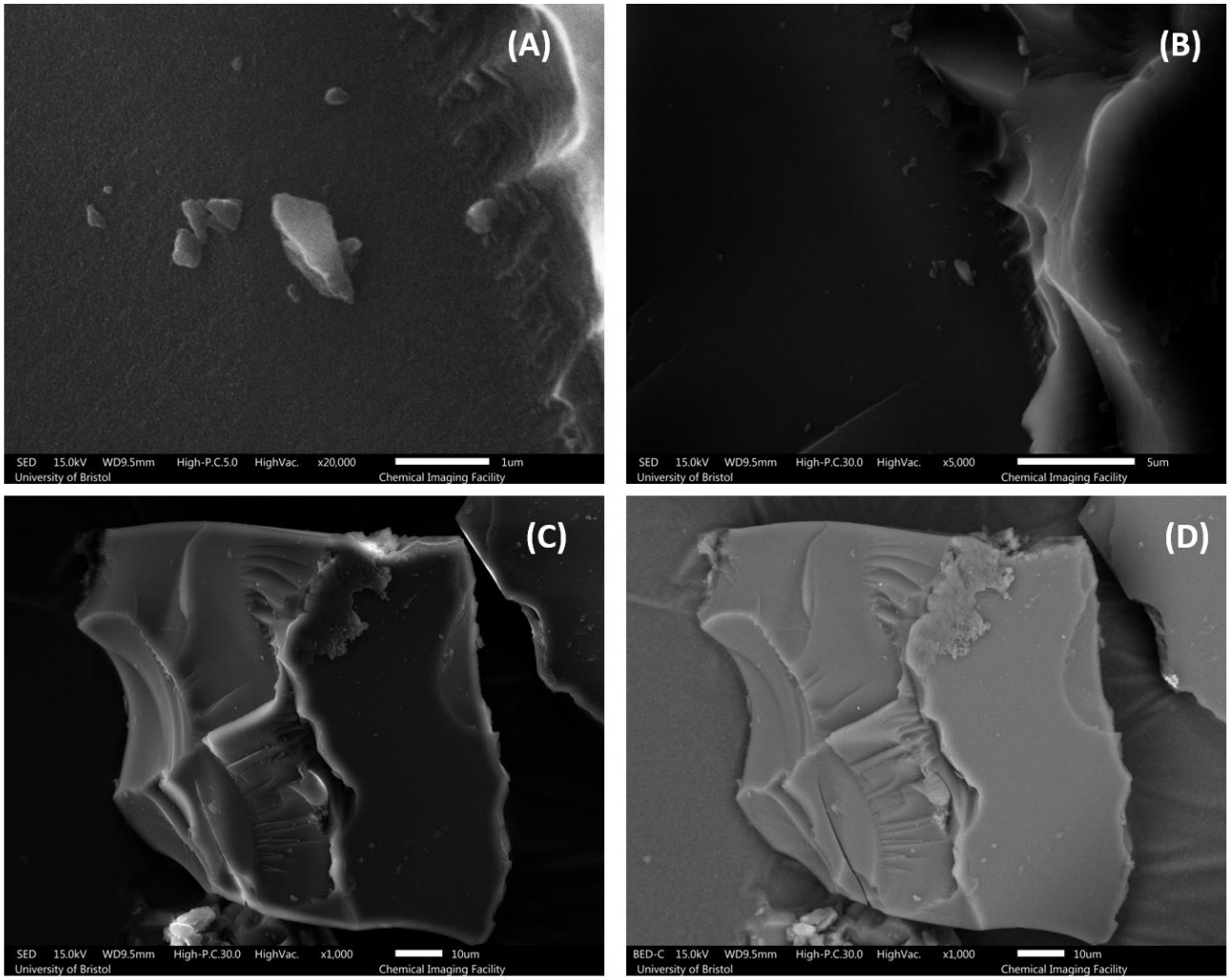

Magnification: (A) x20,000 at 1 µm (SED), (B) x5,000 at 5 µm (SED), (C) x1,000 at 10 µm (SED), (D) x1,000 at 10 µm (BED-C).

7.18.5 POP-7

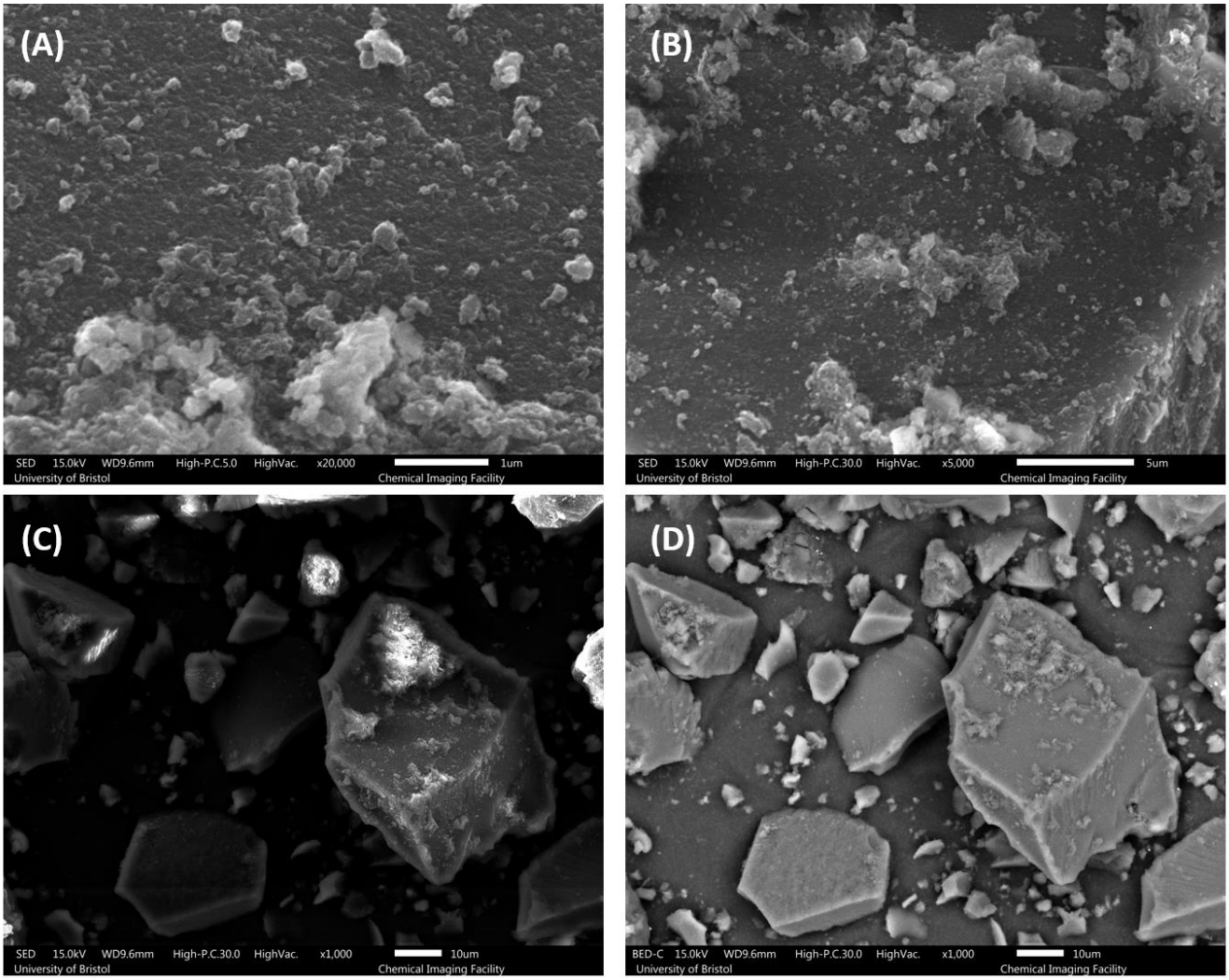

Magnification: (A) x20,000 at 1 µm (SED), (B) x5,000 at 5 µm (SED), (C) x1,000 at 10 µm (SED), (D) x1,000 at 10 µm (BED-C).